From slab rollback to orogenic plateau formation: a numerical modelling study of ocean-continent subduction systems

Master of Science Thesis

Sebastian G. Wolf

Department of Earth Science
University of Bergen

June 2016

Abstract

The crustal structures of overriding plates in subduction settings around the world can vary between a large variety of deformation styles, ranging from extensional structures and back arc opening induced by slab roll back, as e.g. in the Tonga-Kermadec subduction zone, to large, plateau-like orogens such as the central Andes. Several studies propose that the first order influence on the deformation style of the overriding plate is its movement away from or towards the trench and the 3D mantle flow pattern of the subduction zone. Other studies focussing on mountain building above subduction zones propose in addition that metamorphism of the lower continental crust is controlling orogeny, and that terrane accretion is a possibility for growth of active subduction margins.

I attempt to test the above presented concepts with numerical, 2D thermo-mechanically coupled models of ocean-continent subduction. The model domain is on the upper mantle scale and subduction is decoupled from the lower mantle. I consider first order parameters like plate velocities and mantle flow as the main drivers for subduction and associated deformation on Earth, and vary those parameters to find the main factors controlling deformation. In a second modelling step, the influence of metamorphic densification reactions of the lower continental crust and long-term development of margins with accreted terranes is investigated.

I find that every kind of deformation is preceded by corner flow induced thinning of the overriding plate. The corner flow velocity is proportional to the subduction velocity and thus a higher subduction velocity leads to faster thinning and deformation of the overriding plate. I find that return flow and overriding plate movement away from the trench are the main factors that lead to overriding plate extension and back-arc opening. Overriding plate movement towards the trench is the only factor which can lead to overriding plate shortening, but only if the movement rules out return flow induced trench retreat. These parameters are in accordance with a statistical analysis of the subduction zones on Earth, which shows that the models can reproduce first order subduction zone characteristics.

A comparison of my models with active back-arc spreading centres shows that corner flow induced weakening is probably an important mechanism for lithospheric thinning on Earth. My models with shortening of the overriding plate are dominated by ablative subduction, and do not reproduce structures as e.g. found in the Andes. This shows that further modelling is necessary, for instance integrating lower mantle - slab interaction and a more realistic subduction channel rheology.

Models investigating the influence of densification reactions and terrane accretion are also strongly influenced by ablative subduction, and further studies with more realistic subduction channel parameters are necessary. Yet the models show that densification of the lower continental crust can induce deformation and modifies shortening structures. Furthermore accretion of a weak terrane is possible, but subsequent subduction can modify the margin significantly.

Acknowledgments

My cordial thanks go to:

Prof. Ritske Huismans, for supervising this thesis. I'm very grateful for his intensive guidance and time from introduction to numerical modelling to general discussions about mantle flow and subduction systems and all kinds of science topics. Especially his fast response to questions was very help- and useful.

Prof. Stephane Rondenay, for co-supervising this thesis and some ideas about subduction systems from a seismological view. I'm also grateful to him for offering and sponsoring my first EGU-trip.

Thomas Theunissen and Romain Beucher, for always having an ear for my problems concerning code implementations or simple bash-scripting. Thomas is in special thanked for his discussions about subduction zones and his help with FANTOM-specific things. Romain is especially thanked for his almost ready made plotting software, which only had to be adapted to FANTOM and works brilliantly.

Leo Zijerveld for helping me with some implementations to make FANTOM ready for subduction zones.

Johannes Wiest and Felix Halpaap for nice every-day geological discussions, relaxing walks in the park and correcting parts of this thesis.

Last but not least Birte Myklebust, for taking care of some of my germanised English and simply for being there every day.

Contents

1 Introduction to plate tectonics and active convergent margins

Subduction zones - what are they - and why bother to get to know more about them?

Our planet is currently covered by 14 bigger and 38 smaller plates with oceanic or continental composition or a combination of both (Bird, 2003). Those plates are moving across the Earth with absolute velocities approximately ranging from $0 - 8\,\mathrm{cm/yr}$ (Schellart et al., 2011) and their spherical nature and differential velocities make them interact. Earthquake maps tell us that the interaction between plates induces tectonic activity and thus deformation at the plate boundaries, whereas intra-plate areas are tectonically relatively inactive (Fig. 1 A). The spatial distribution of earthquakes and their focal mechanisms give further information on the nature of plate boundaries, and a first order classification into divergent, conservative and convergent boundaries was developed (Fig. 1 B). Divergent boundaries are the sites of sea floor spreading, where new oceanic material is created and conservative boundaries are composed of transform faults, which allow plates to pass each other with little or no deformation. Boundaries of the third type, which I focus on in this thesis, are convergent boundaries, traditionally subdivided into collision zones and subduction zones. In collision zones, two continental plates or a continental plate and a magmatic arc collide and a mountain range forms, like e.g. the Himalayas. In subduction zones one oceanic plate sinks below an oceanic (e.g. Mariana subduction zone) or a continental plate (e.g. subduction below the Andes).

These simple geometrical and compositional subdivisions give a good first order description of how plates behave and are linked to each other. Nevertheless a short look at the geological map of the Earth and only considering convergent margins already shows, that there is a big variety of structures and deformation styles at active convergent margins. If following the traditional perception of collision zones as being sites of a big mountain range, the Andes, as the longest mountain range on Earth, are a collisional mountain belt. However, the Andes forms on top of the South American subduction zone and are thus no collision zone in the traditional sense. Additionally, and in contrast to the high mountain range of the Andes, a lot of subduction zones show extensional deformation in the overriding plate. This behaviour is coupled to trench retreat and back arc spreading. Textbook examples of mature subduction zones which induce back-arc opening are the Tonga-Kermadec and the Scotia subduction zones. Furthermore, convergent margins are no static systems as for example when a piece of continent is attached to a subducting plate, a subduction zone can transform into a collision zone. That is generally thought to have happened in the Alpine-Himalayan belt, when the Adriatic promontory, the Indian and the Arabian plate collided with the Eurasian continent.

Dewey and Bird (1970) came up with a first classification of mountain building processes by proposing two types of mountain chains: Cordilleran type orogens, which grow due to thermal processes related to the rise of magma above a subducting oceanic slab, and Collision type orogens, which grow by physical processes like faulting and folding due to the collision of two continental pieces. According to their model, the Andes and North American Cordilleras are Cordilleran type orogens whereas the Alpine-Himalayan belt is of Collision type. More recent

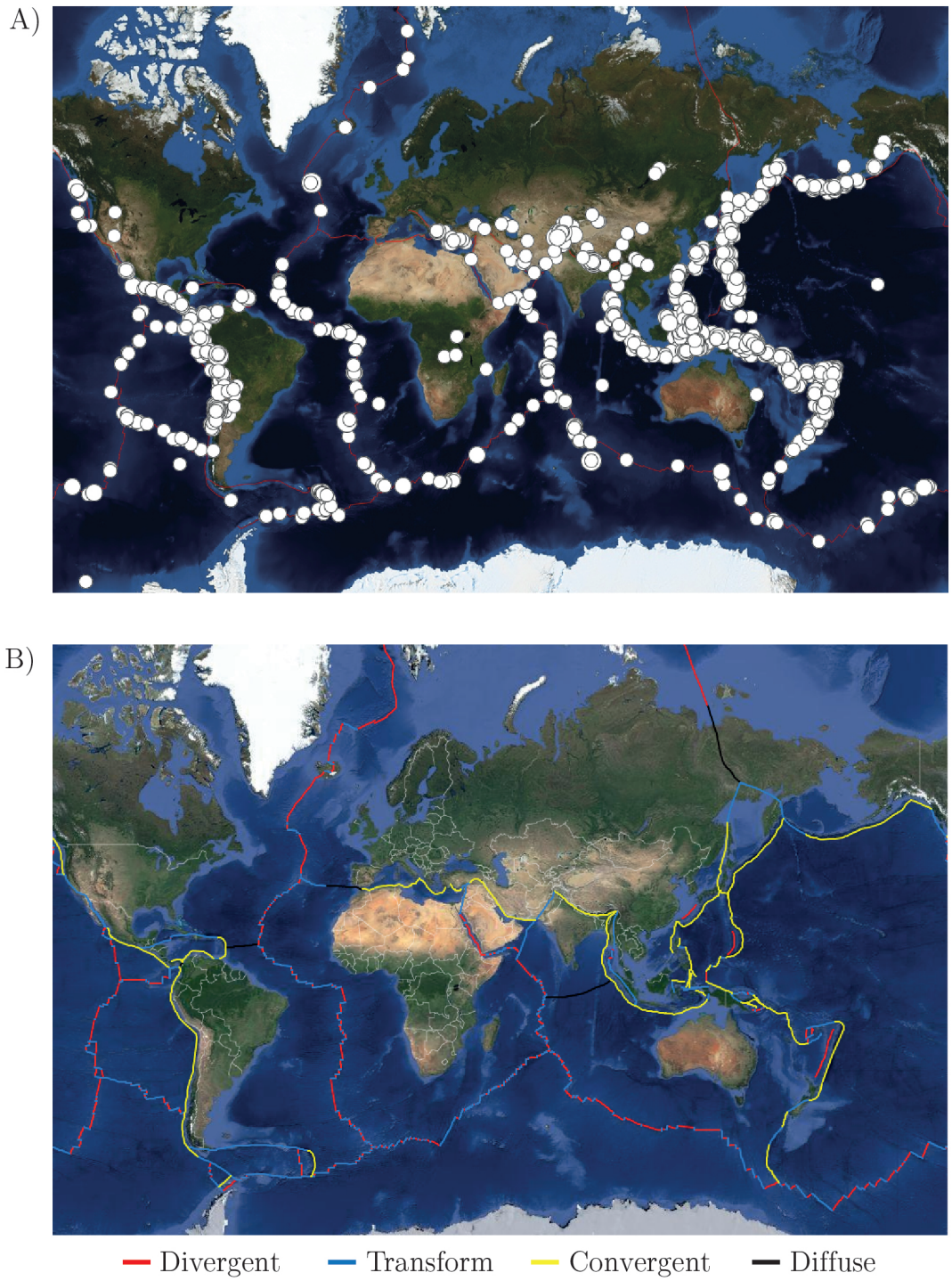

Figure 1: A) Satellite image of the Earth with all ~1600 earthquakes with magnitude greater 5.0 recorded in 2015 (white circles) and plate boundaries (red lines). Earthquakes are plotted with the youngest on top and the size of a circle is proportional to magnitude. Thus areas with high earthquake density will appear under-represented. Almost all of the earthquakes occur at plate boundaries whereof the vast amount happens at convergent plate boundaries. B) Satellite image of the Earth with simplified plate boundaries colour coded after type. Note that a diffuse boundary is included for cases where margins cannot be clearly classified. A) was generated from the website of the US geological survey earthquake catalogue. The satellite image in B) is from google maps with a plot of the plate boundaries from the US geological survey.

work, however, suggests that the formation and crustal thickening of Cordilleran type orogens, like the Andes, is probably not only a result of thermal processes but that crustal shortening also played a significant role. Estimations for crustal shortening in the Andes range from 250-350 km (Oncken et al., 2006) up to over 400 km (Arriagada et al., 2008). Hence there is a wide variety of structural styles in the vicinity of convergent margins and neither the classical division into subduction zones and collision zones nor Dewey and Bird (1970)'s classification do sufficiently describe their dynamic behaviour.

In course of the different observations related to subduction systems, different geoscientific fields started to develop ideas and investigate how subduction zones behave. Thereby one of the striking questions was and still remains, why and how the overriding plate in subduction zones deforms and thickens.

The increase in computational power and accessibility of seismic data in the last decades made it possible to investigate how subduction zones look like in depth. Subduction zones feature processes which happen in depths of up to several 100s of kilometres. Thus images obtained by seismological imaging on a global (e.g. Li et al., 2008) and local scale (e.g. Bostock, 2013; Kim et al., 2012; Pearce et al., 2012) are essential for understanding structures in a 3D manner.

The use of computers also refined reference frames for absolute plate motion models and a statistical investigation of parameters which could induce overriding plate strain became possible (Heuret and Lallemand, 2005; Schellart, 2008). Thereby Heuret and Lallemand (2005) proposed that overriding plate velocity determines OP strain and that around 50 % of subduction zones have an extending upper plate. The latest investigations by Schellart (2008) show, however, that ~75 % of subduction zones on Earth roll back and, excluding special subduction settings, there are only two subduction zones which show upper plate shortening, namely the Andes and some area in Japan. Those two areas have in common to be in the centre of wide subduction zones. In fact, Schellart (2008) argues that the slab edge distance is significant in determining upper plate strain and that overriding plate velocity is only significant in the centre of wide subduction zones. He attributes this to the suppression of mantle return flow in the centre of wide subduction zones and the possibility for return flow near subduction zone edges. Thus the 3D mantle flow pattern is statistically most relevant for different upper plate deformation style. The special settings, which also lead to overriding plate shortening, are related to subduction of buoyant intra-oceanic features like rifted continental crust or extinct spreading ridges.

Another field of research is directed towards the composition and metamorphic reactions in collision zones leading to upper plate deformation. The abundance of chemically bound and free (pore-) fluids in combination with dewatering reactions make subduction zones to areas of intensive metamorphism and melting (Faccenda, 2014). Hacker et al. (2015) describes subduction zones as the site of lower crustal reworking and attributes delamination of heavy crustal material and relamination or accretion of subducting, buoyant material as one of the main reasons for the evolution of the (lower) crust. DeCelles et al. (2009) propose that the cyclicity and plateau formation during Andean orogeny can be attributed to repeated delamination of heavy lower continental crust. In that way, delamination differentiates and is the trigger for deformation of

the overriding crust. Both relamination and delamination need a hot and thus thin lithospheric mantle. This was found to be a general feature in subduction zones (Currie and Hyndman, 2006), hence the processes can most likely happen.

Many of the interpretations drawn from investigations of the ideas above are of conceptual nature, and a proof of concept in a dynamic and thermo-mechanically coupled way including several processes is necessary. Do processes derived from conceptual models happen in reality? And if they do, how and what are the dominant mechanisms?

Currie et al. (2008) show with thermo-mechanical models that weakening of the continental lithospheric mantle leads to its thinning and can explain the heat flow data in back-arcs. Grool (2012) took the same model setup and showed that the amount of weakening is furthermore the main factor in determining whether and when a subduction zone rolls back and a back-arc opens. According to Grool (2012) the mantle flow pattern is not important for roll back to occur. Nevertheless, 3D numerical mechanical models of free subduction (Schellart et al., 2007; Stegman et al., 2010; Schellart et al., 2011) show that the distance to the slab edge and length of a subduction zone is very important and thus the mantle flow pattern is determining whether a subduction zone is rolling back or stationary as interpreted by Schellart (2008). The latter modelling approaches are very simplistic as they do not include thermal-mechanical coupling and an overriding plate. Recently thermo-mechanical models were also investigating as to which conditions intra-oceanic features like rifted terranes accrete at the margin or get subducted downwards (Tetreault and Buiter, 2012; Vogt and Gerya, 2014). Both find that terrane accretion is possible when the terrane is significantly weak, but do not investigate the development of the accreted margin in the long term.

These questions still remain and are going to be the topic of this thesis: 1) How does the overriding plate in a subduction system deform when including a 3D mantle flow pattern and absolute plate motions?; 2) How do phase changes associated with lower crustal delamination affect a contractional subduction system?; and 3) How does the accretion of intra-oceanic features like continental plateaus or terranes affect the crustal thickening in a contractional subduction system in the long term?

We use a 2D forward numerical modelling code called FANTOM (Thieulot, 2011) to investigate these questions and follow a similar simple setup of oceanic subduction under a continental plate as Currie et al. (2008) and Grool (2012). The thermal and mechanical evolution of the modelling domain is coupled via visco-plastic flow laws and metamorphic phase changes are accounted for. Deduced from the questions presented above, we assume that absolute plate velocities, crustal composition and thus strength, intra-oceanic plateaus, metamorphism and the mantle flow pattern are the dominating first order parameters in subduction zone dynamics. Thus these parameters are varied and/or approximated to investigate their influence. Furthermore the system is decoupled from the lower mantle transition zone, which means that influence of slab bending in this area is not accounted for.

All the models start initially with a simplified layered structure. However, the Earth is a dynamic system and inheritance of pre-existing structures most likely plays an important role.

Therefore we extended research question 2) to: How do phase changes associated with lower crustal delamination **and extensional inheritance** affect a contractional subduction system?

In the following chapter recent ideas and models which can possibly lead to different overriding plate deformation, as introduced above, are reviewed in more detail whereas the focus is going to lie on active subduction systems of the Earth. The chapter is furthermore the theoretical basis for the choice of parameters in our modelling setup. The actual setup and modelling approach is explained in chapter three. Chapters four and five are the results and discussion chapters and in the last chapter a summary and outlook about further ideas and objectives are given.

2 Subduction zones: What determines upper plate strain?

2.1 Introduction to recent subduction zones and plate velocities

To describe the interactions and nature of plate boundaries of the plates on Earth, relative plate motions are a useful tool. Nonetheless to obtain comparability between different boundaries, knowledge of the absolute plate motions (APM, i.e. knowledge about the plate velocities with respect to a presumably strong deep mantle) is necessary. To create an APM model, one needs to assume a fixed global reference frame. Several reference frames have been proposed and debated in the last decades whereof the two most prominent ones are hotspot reference frames and no-net-rotation reference frames.

Hotspot reference frames are based on the assumption that hotspot trails like the Hawaii'an emperor chain are the surface expression of stationary mantle plumes which originate in the lower mantle or the core-mantle boundary. Models which use a hot spot reference frame are divided into approaches which employ the Pacific hotspots or the Indo-Atlantic hotspots. Prominent examples are the models by Gripp and Gordon (1990, 2002) and Wessel et al. (2006) for the Pacific hotspots and the models by Müller et al. (1993) and O'Neill et al. (2005) for the Indo-Atlantic hotspots.

No-net rotation reference frames use relative plate motion models and develop them further by applying, in the simplest version, the concept that the drag of the asthenosphere on the lithosphere is zero when integrated over the whole Earth and that the torques on plate boundaries are symmetrical. Prominent models of this approach are the ones from Argus and Gordon (1991) and Kreemer et al. (2003).

Plate velocities obtained by the different reference frames can vary significantly by up to 4 cm/yr (Schellart et al., 2008). Especially velocities in the Pacific hotspot reference frame differ strongly from those in the Indo-Atlantic or no-net rotation reference frames. As plate movement is only on the scale of a few centimetres per year, these differences are crucial. Thus it is important to assess which of the reference frames has the most realistic outcome. Recently Schellart et al. (2008) made an attempt to find the most true reference frame by comparing the velocties and directions of plate motions from different reference frames with geodynamic modelling results and fluid dynamic considerations. The findings of Schellart et al. (2008) are that all investigated reference frames fit the assumptions quite well with the exception of the reference frames using the Pacific hotspots. The best fit is met by using an Indo-Atlantic hotspot reference frame from O'Neill et al. (2005), in combination with either a relative plate motion model or a no-net rotation approach.

Figure 2 shows the velocities of the plates on Earth in the Indo-Atlantic hot spot reference frame by O'Neill et al. (2005) in combination with relative plate motions by DeMets et al. (1994). Plates which are primarily oceanic (white) move generally faster than plates which are mostly composed of continental lithosphere (grey). Velocities for big oceanic plates range between 4.5-5.6 cm/yr (Philippine plate), 3.8-8.3 cm/yr (Pacific plate), 5.8-7.2 cm/yr (Nazca plate) and 5.1-6.0 cm/yr (Australian plate). An exception is the Antarctic plate, which is comparably slow. The plates which are mainly composed of continental lithosphere have velocities ranging from

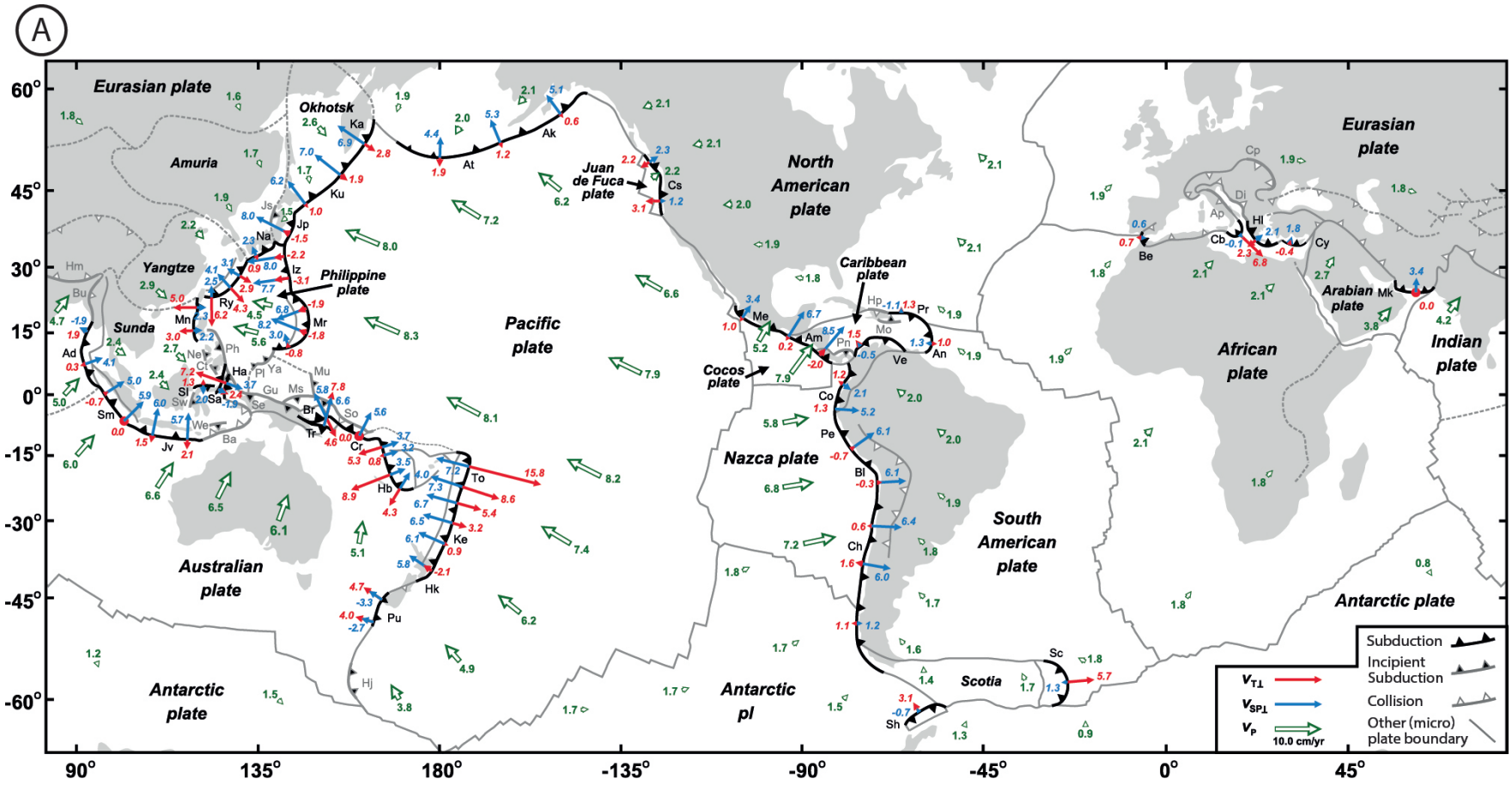

Figure 2: (Continuation of figure on next page.)

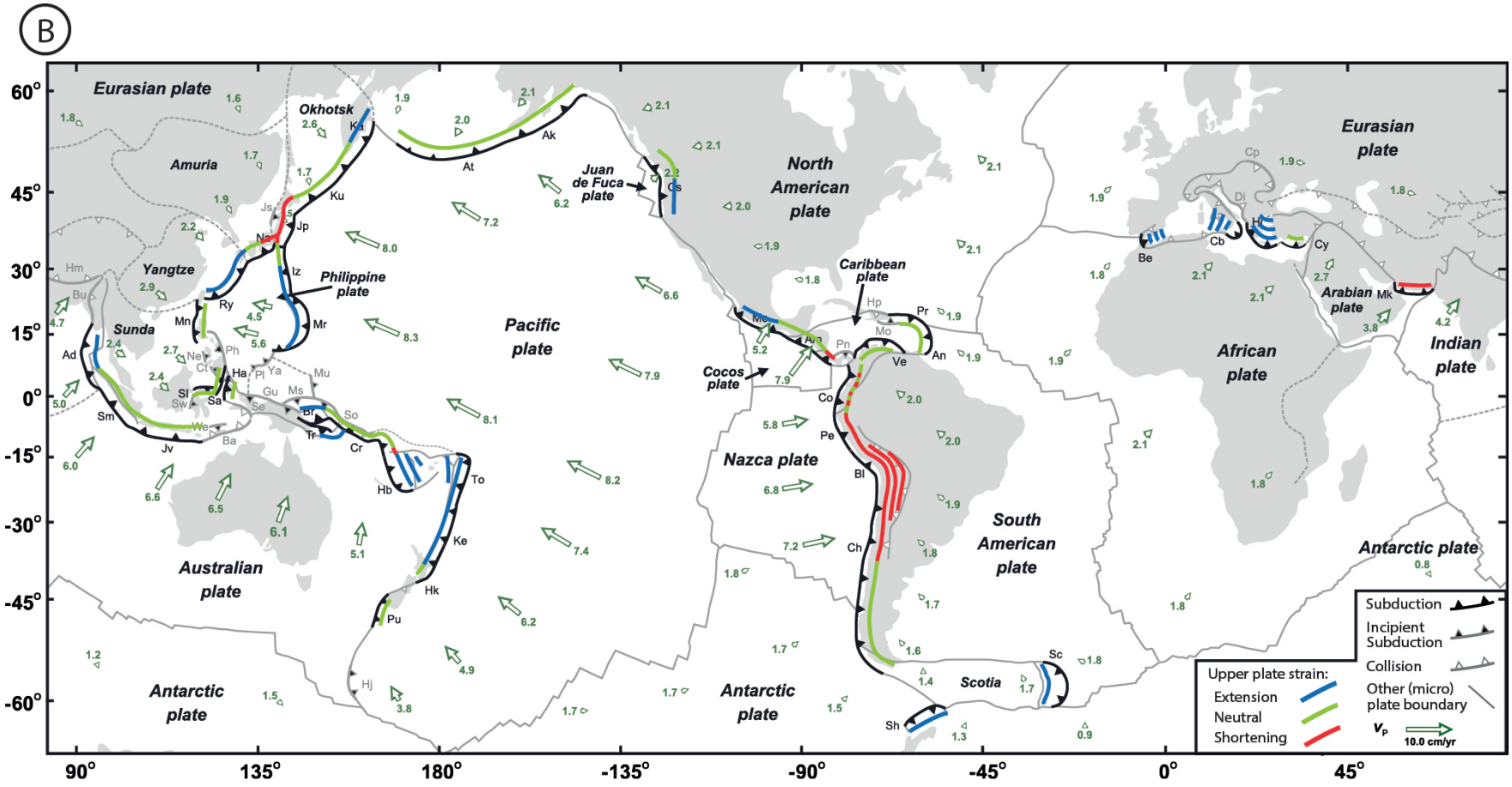

Figure 2 (Continued): Global tectonic maps showing the current plate configuration and velocities (v_P) on Earth with focus on convergent plate boundaries. A) Additionally to v_P the trench perpendicular trench migration velocity ($v_{T\perp}$) and the trench perpendicular subducting plate velocity ($v_{SP\perp}$) are plotted. Note that $v_{T\perp}$ is positive for trench retreat. The combination of v_P, $v_{T\perp}$, $v_{SP\perp}$ complemented by the upper plate accretion and deformation rate, results in an upper plate strain regime, displayed in B). Names of subduction zones: Ad-Andaman, Ak-Alaska, An-Lesser Antilles, Am-Central America, At-Aleutian, Be-BeticRif, Bl-Bolivia, Br-New Britain, Cb-Calabria, Ch-Chile, Co-Colombia, Cr-San Cristobal, Cs-Cascadia, Cy-Cyprus, Ha-Halmahera, Hb-New Hebrides, Hk-Hikurangi, Hl-Hellenic, Iz-IzuBonin, Jp-Japan, Jv-Java, Ka-Kamchatka, Ke-Kermadec, Ku-Kuril, Me-Mexico, Mk-Makran, Mn-Manila, Mr-Mariana, Na-Nankai, Pe-Peru, Pr-Puerto Rico, Pu-Puysegur, Ry-Ryukyu, Sc-Scotia, Sa-Sangihe, Sh-South Shetland, Sl-North Sulawesi, Sm-Sumatra, To-Tonga, Tr-Trobriand, Ve-Venezuela. Incipient subduction yones: Ct-Cotobato, Gu-New Guinea, Hj-Hjort, Js-Japan Sea, Mo-Muertos, Ms-Manus, Mu-Mussau, Ne-Negros, Ph-Philippine, Pl-Palau, Pn-Panama, Sw-West Sulawesi, We-Wetar, Ya-Yap. Collsion zones: Ba-Banda, Bu-Burma, Cp-Carpathian, Di-Dinaride, Hm-Himalayas, Hp-Hispaniola, Se-Seram, So-Solomon. A) and B) are modified from Schellart et al. (2011) and the upper plate strain interpretations in B) are modified from Schellart et al. (2007).

1.6-1.9 cm/yr (Eurasian plate), 1.8-2.1 cm/yr (African plate), 1.6-2.0 cm/yr (South American plate) and 1.8-2.1 cm/yr (North American plate). The Indian plate and the Arabian plate move relatively faster with velocities of respectively 2.7-3.8 cm/yr and 4.2-5.0 cm/yr. It is important to note that plates which are bound by subducting edge(s) move generally faster than those which are not. This is due to the slab pull exerted by the subducting slab, and is an argument for that slab pull is the main driving force in plate tectonics as proposed by Forsyth and Uyeda (1975). This relationship can explain the high velocities of the Australian, Indian and Arabic plates and the low velocity of the Antarctic plate.

Similar velocities can be obtained by a no-net rotation reference frame but results vary significantly in the Pacific hot spot reference frame (see Schellart et al. (2008), their Fig. 1). In the latter the velocitites for e.g. the Pacific plate are up to 11.8 cm/yr and the Nazca plate has velocities varying between 2.7-3.3 cm/yr. Thus the relationship that plates bound by subducting edge(s) move faster does not apply here.

Figure 2A also displays the trench perpendicular trench migration velocity ($v_{T\perp}$) and the trench perpendicular subducting plate velocity ($v_{SP\perp}$) (see also Fig. 3). $v_{SP\perp}$ is a useful measure to display the dip slip velocities and thus also the oblique slip portion in a subduction system. It can be observed that the majority of strikes of subduction zones are somewhat perpendicular to the plate velocity vector and the oblique fraction is commonly around 0-1 cm/yr with exceptions of up to 3-5 cm/yr as e.g. in some Western and Northern parts of the Pacific plate.

The trench perpendicular trench migration velocity ($v_{T\perp}$) in conjunction with the plate velocities of the overriding plate give a hint as to whether a subduction system is advancing or retreating. Thereby negative values indicate advancing (contractional) and positive values retreating (extensive) systems. Nevertheless $v_{T\perp}$ is also depending on the accretion rate at the margin and the overriding plate deformation rate. Thus assessing whether the dominating tectonic behaviour in the overriding plate is extensive or contractional has to be complemented by geodetic or geological evidence and can not be simply read from Fig. 2A. This was done by Schellart et al. (2007) and the resulting upper plate tectonic behaviour is plotted as colorcoding in Fig. 2B. This map and associated calculations show that trench retreat, and thus extension in the overriding plate, dominates over trench advance, with 75 % of the world's trench segments retreating. Additionally rapid trench retreat is only observed in areas close to (<1500 km) lateral slab edges and trench retreat is always comparably slow in areas further away (>2000 km) from slab edges (Schellart et al., 2007; Schellart, 2008; Schellart et al., 2008).

There are only five areas on Earth which show upper plate shortening above subduction zone: The central Andes, a wide area above the Japanese subduction zone, the Makran subduction zone, a small part above the Central American subduction and a little area above the San Cristobal/ New Hebrides subduction zone. The Makran zone is seen as a special case and its behaviour is attributed to being squeezed in between two collision systems. The upper plate shortening at the south tip of the Central American subduction zone is attributed to the subduction of a buoyant spreading ridge, and the contractional regime in the upper plate of the San Cristobal and New Hebrides subduction zone may be due to the quite complex system of plate boundaries in this

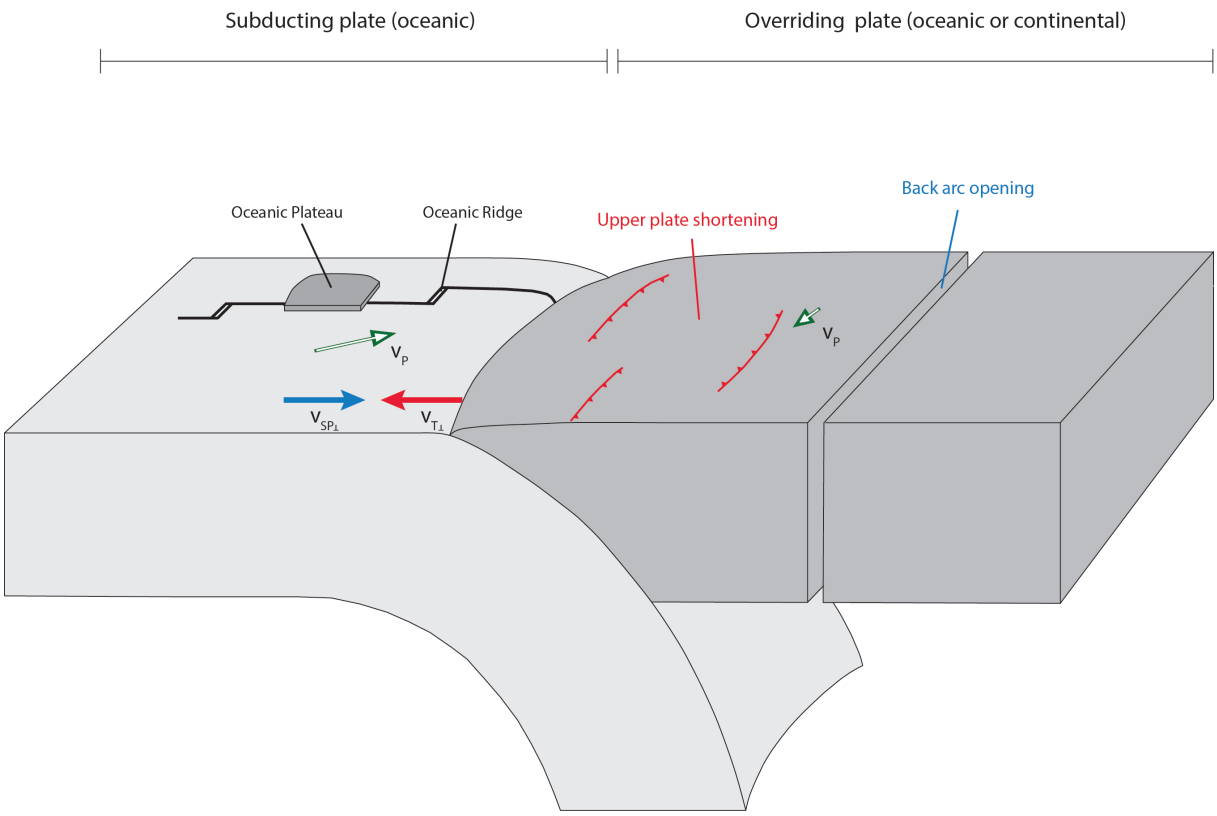

Figure 3: Simplified sketch of a subduction zone with absolute velocity vectors and buoyant structures which can be found on oceanic plates (Oceanic plateaus, Oceanic ridges). v_P is the plate velocity, $v_{SP\perp}$ is the trench perpendicular subducting plate velocity and $v_{T\perp}$ is the trench perpendicular trench migration velocity. The difference between v_P and $v_{SP\perp}$ is the oblique component of the subduction system. The combination of $v_{T\perp}$, overriding plate velocity and accretion rate at the trench determine whether the upper plate is shortened or extended. Oceanic ridges or oceanic plateaus can also induce upper plate shortening.

area, including several subduction zones with different subduction polarities and strike slip faults. The two remaining contractional subduction zones in Japan and the central Andes have the common feature to be in the center of wide subduction zones (>4000 km). They are additionally the only areas in the world which show upper plate shortening over a wide lateral extent.

Figure 3 is a simplified graphical summary of the velocities and geological features which are important and can be observed from absolute plate motion analyses. So far it has been shown that plates move faster with attached slabs, the majority of subduction zones is rolling back, subduction of buoyant structures can induce upper plate shortening and the width of a subduction zone may have an influence on its behaviour. The qualitative description of subduction zones can nevertheless not give a measure whether these observations are statistically significant and the question remains: What controls upper plate strain?

The quantitative investigation of this question, in form of statistical comparison of parameters which might determine upper plate deformation style, has been done by several groups with different datasets and different reference frames (Jarrard, 1986; Heuret and Lallemand, 2005; Schellart, 2008). Thereby not only velocities observable at the surface were considered, but

also slab structure and deeper processes as well as petrological differences were investigated. Therefore the next chapter (2.2) gives a short introduction to seismological images of subduction zones, and chapter 2.3 presents different processes connected to the rheology and composition of the lithosphere. This gives a summary of how subduction zones look like, and finally chapter 2.4 presents the statistical investigation of factors controlling upper plate strain together with recent modelling results about subduction zones.

2.2 Looking into subduction zones - seismological images of recent subduction zones

To extend Fig. 3 into depth, seismological images need to be interpreted. This chapter attempts to do this by starting with global tomographic images (Fig. 4) followed by zooming into lithospheric scale seismoglogical cross sections (Fig. 5).

Li et al. (2008) employed data of permanent and temporary seismic stations to create a global P wave speed variation model of the Earth's mantle. Results are presented as cross sections with colour coding for the speed variations so that relatively higher velocities are blue and relatively lower velocities are red (Fig. 4). Lower velocities are commonly related to hot and thus slow material and vice versa. Thus blue areas below convergent plate boundaries can be interpreted as subducting or subducted slabs. In some cross sections the seismicity is additionally plotted as white dots. Those help to delineate subducting slabs. All cross sections contain furthermore the 410 km and the 660 km discontinuity drawn as dashed lines. Both continuities can be discovered in seismic studies, but were also experimentally determined (Ringwood, 1991; Chudinovskikh and Boehler, 2001). The 410 km discontinuity is assigned to the transition of Olivine to its high pressure polymorph β-spinel (wadsleyite) and the 660 km discontinuity is, although more debated, assigned to the transformation of γ-spinel (ringwoodite) to perovskite and periclase. The latter transition is associated with a significant increase in viscosity and density. This density increase is possibly so strong that subducted oceanic crust and its polymorphs become positively buoyant at the 660 km transition (Ringwood, 1991). As the P-T conditions may vary and the downgoing slab can notably disturb the temperature field, it is likely that the discontinuities can be locally significantly shallower or deeper. Thus the upper mantle transition zone can be loosely defined to be in a wide range between 400 - 1000 km (Li et al., 2008).

Figure 4A shows the subduction zones in Central America and the Caribbean (sections 1-5), the Andes (6-9) and the Scotian subduction zone (10). The structures associated with the subduction of the Cocos plate in Middle America are quite complex with varying slab dips and slab portions which penetrate through the 660 km discontinuity (4) and some which flatten out in this area (1,2). Section 5 illustrates that slabs can also have several kinks and only partly lay down at the upper mantle discontinuity before penetrating into the lower mantle. The sections through the Andes show slabs which are mostly penetrating the transition zone. The lateral near surface dip variations are generally badly resolved but the dips of the subduction zones seem to vary locally. The Scotian subduction zone in section 10 has decreased resolution due to little data coverage in this area. Nevertheless the section shows a rather steep subduction angle.

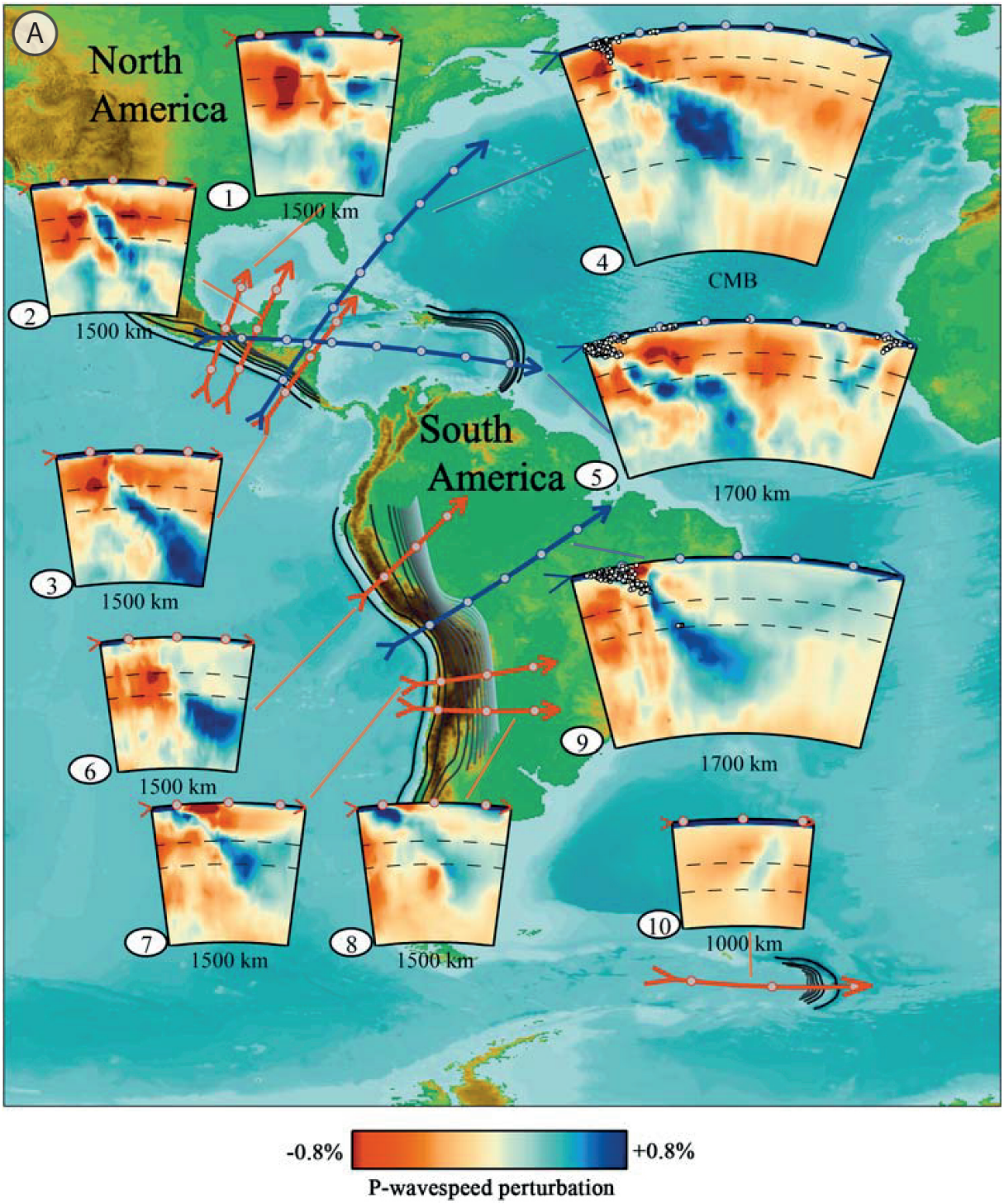

Figure 4: (Continuation of figure on next page.)

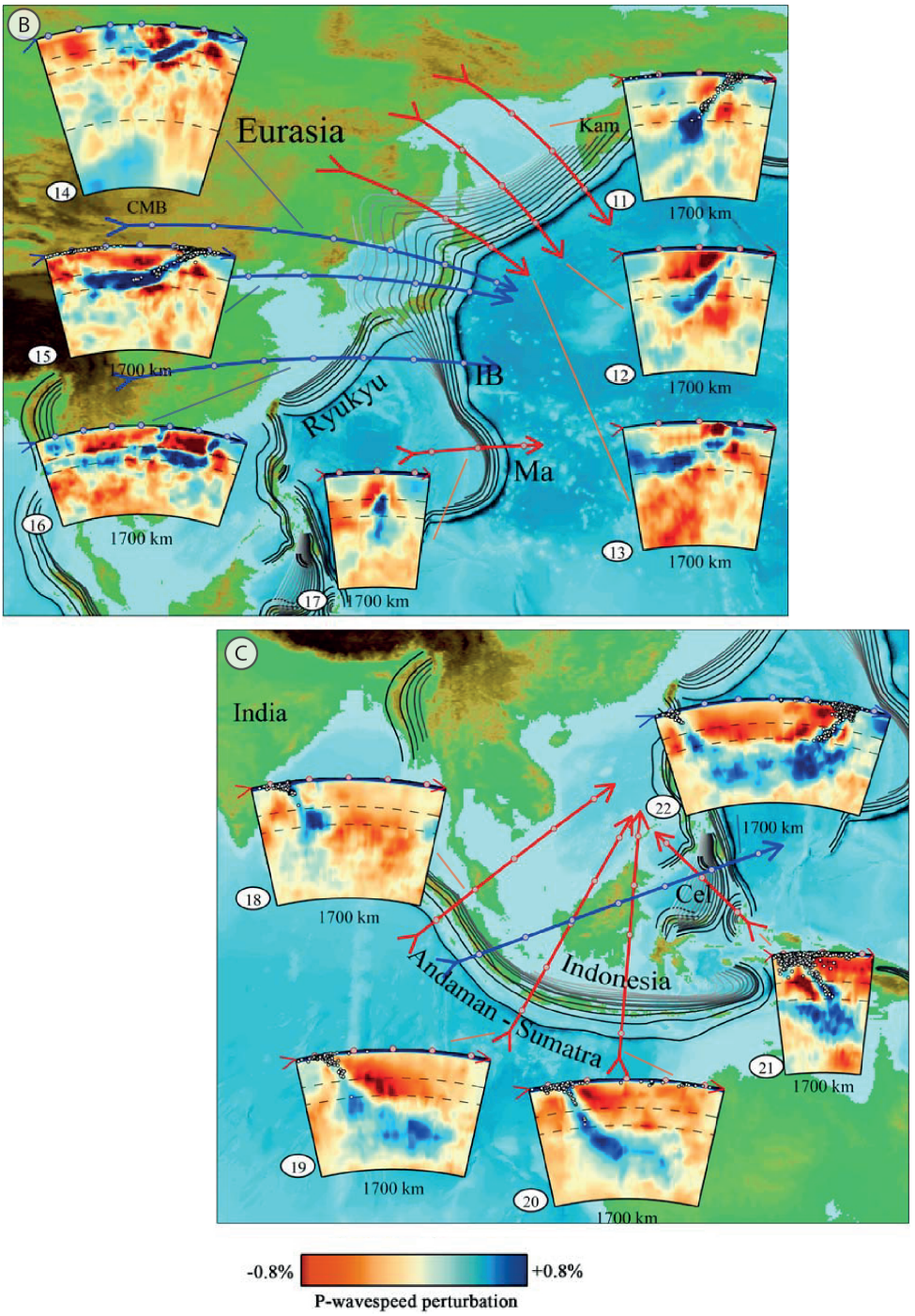

Figure 4 (Continued): Compilation of maps and cross sections obtained by a global P wave tomography survey. Red colour coding indicates low velocities and blue colours stand for relatively higher velocities. In the context of subduction zones higher velocities can be interpreted as cold, subducting slabs. In some cross sections the seismicity is added as white dots (e.g. numbers 5,9, 11, 15 and 21), delineating subducted slab. The dashed lines are the 410 km, 660 km discontinuities. The cross sections which extend down to the core-mantle boundary (CMB) have another dashed line, marking 1700 km depth. The slab dips are varying between ~30°-90° and some slabs advance through the 660 km discontinuity (e.g. below the Andes) whilst other slabs lay down on this discontinuity (e.g. Japan). Cross sections 4, 5, 9, 19, 20 and 22 have a wide fast area below the 660 km discontinuity. This can be interpreted as old subducted slab fragments. Modified from Li et al. (2008).

Figure 4B illustrates the subduction of the Pacific plate under the western Pacific island arcs from Kamchatka to Mariana. These subduction zones show strong lateral differences with steep and penetrating slabs in the north (11,12) which flatten in dip and along the lower mantle transition zone towards the south (13-15). Section 15 is probably the best example of a slab which flattens in the transition zone and does not sink into the lower mantle. Further south the slab dip steepens again, with the end member being the Mariana slab (17), which directly dives down into the lower mantle. Section 16 is also very interesting as it displays the complex situation of the Ryukyu and Izu-Bonin subduction zones.

Figure 4C shows structures associated with subduction beneath Indonesia. The slab dips along the Andaman-Sumatra subduction zone and the Celebes subduction zone are steeper than further North, and the slabs penetrate through the transition zone. Furthermore all cross sections except number 18 have a large fast area below the 660 km discontinuity in common. Li et al. (2008) interpret this as an accumulation of old slab fragments which were subducted from the East and South. Those wide fast areas can also be observed below the Andes (Fig. 4A, sections 3 and 9) which are thus possibly also related to old slab fragments.

The mantle scale cross sections from Figure 4 show that the interaction of the subducting plate with the lower mantle transition zone is important and can vary in style. Nevertheless the resolution of the figures is too coarse to properly image structures in the first ~150 km of the Earth. There are different seismological imaging techniques tailored to address this zone and a lot of data have been and are published. As a detailed review is beyond the scope of this thesis, the main source used here is a review paper by Bostock (2013), augmented where necessary.

The selection of cross sections in Figure 5 shows that a so-called low velocity zone (LVZ) can be observed in many subduction zones. Bostock (2013) reviews different ideas about the origin of this layer, but all have in common that the LVZ is related to the subduction interface. He finally promotes a model by Hansen et al. (2012) in which the LVZ is the hydrated upper part of the subducting oceanic crust. This fits with observations that the thickness of the LVZ ranges between 3 and 7 km (Bostock, 2013, and references therein). Thicker LVZ as in Alaska (Fig.5a) were attributed to the subduction of an oceanic plateau (Ferris et al., 2003; Rondenay et al., 2008).

The dip and structure of the LVZ and thus of the subducted plate can vary strongly from steep dip angles as e.g. in Central America (Fig. 5f) to flat slab subduction as e.g. in Central Mexico (Fig. 5g). Sections a-e show less extreme dips ranging from ~25° to ~55°. Indeed Cruciani et al. (2005) show that most of the Earth's subduction zones dip around 45°, when averaged over the first 250 km. Only a few subduction zones have steeper dips ranging between 45° - 67°.

Although all subduction zones have a LVZ in common, the depth extent can vary significantly. In warm subduction zones as the Cascadia or Nankai (Fig. 5d), the LVZ reaches only to depths of around 45 km whereas the LVZ in cold subduction zones reaches depths of 80 to 120 km (Alaska, northern Chile, Honshu). It is generally assumed that the LVZ disappears at the phase transition from hydrated oceanic basalt or gabbro to eclogite and the shape of the eclogite facies boundary in P-T-space can explain the different transition depths. The phase change is accompanied by a

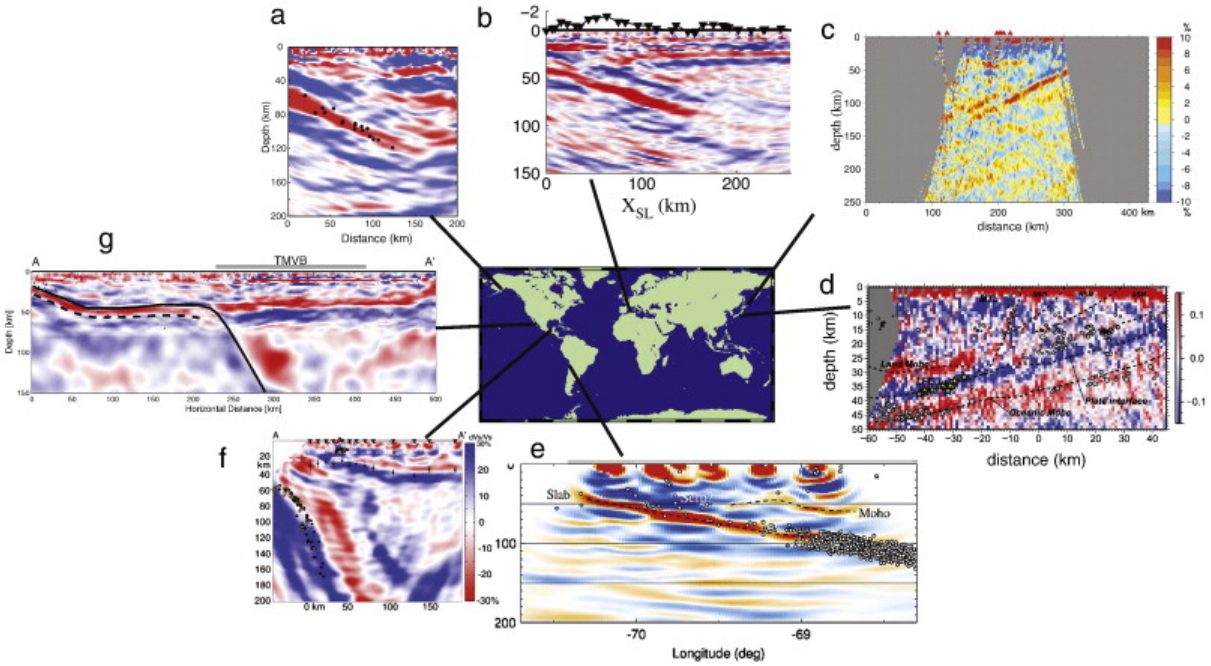

Figure 5: Some teleseismic images from different subduction zones all over the world with different thermal regimes: a) Alaska, b) Greece, c) Honshu, d) Nankai, e) Central Andes, f) Central America, and g) Central Mexico. Some subduction zones have seismicity within the slab plotted as black (a,f) or white dots (d,e). All of the sections show a low velocity layer (LVZ) near the top of the subducting slab. Images a,b,f, and g show S-velocity perturbations and the LVZ is therefore displayed as a dipping, red layer. The other sections (c-e) display the "reflectivity". Thus the top of the LVZ is a negative (blue) polarity signal and the bottom of the LVZ is the opposite, a red signal. From Bostock (2013); references for sections therein.

decrease in volume of around 10 % and dewatering of the downgoing slab. The free fluids can migrate upwards and lead to serpentinization of the mantle wedge. Free fluids and serpentine in the mantle wedge decrease the seismic velocities and erase or even invert the seismic signal of the overriding plate Moho. Thus the signal of the overriding plate Moho can be a proxy for the serpentinization of the mantle wedge. Examples for this relationship are the Hellenic and Cascadian subduction zones with strong wedge-serpentinization (see Bostock, 2013, and Figure 5 therein; Fig. 5b) and the Nankai subduction zone with less pronounced serpentinization and an intact overriding plate Moho (Fig. 5d).

2.3 Composition and thermal structure of the lithosphere and upper mantle

The missing part, before going to recent modelling results and a statistical analysis for upper plate strain style, is how the lithosphere is composed both in terms of mineralogical composition and thermal structure.

Compositional features

Traditionally continental and oceanic lithosphere are subdivided into layers of different composition (Fig. 6). Oceanic lithosphere exists on the Earth's surface commonly only for a maximum

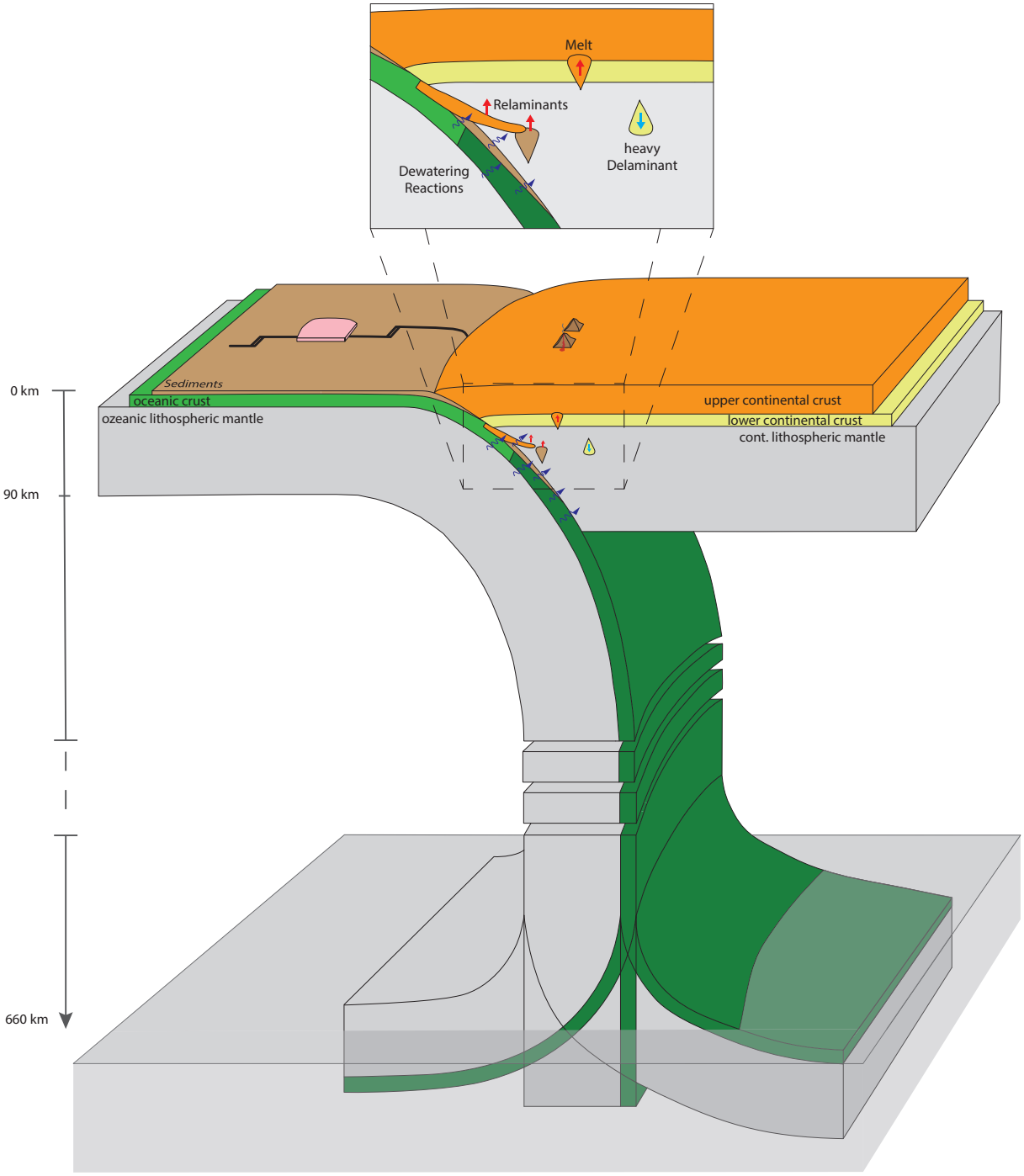

Figure 6: Simplified sketch of the compositional layering of an ocean-continent subduction zone. The subducting oceanic lithosphere consists of sediments, oceanic crust and the lithospheric mantle. Dewatering reactions of the oceanic crust during subduction lead to its eclogitization (dark green). The continental lithosphere is in this simplified sketch composed of upper and lower crust and lithospheric mantle. Other ideas about the layering of the continental crust are discussed in the text. The downgoing slab interacts with the lower mantle transition zone and can roll and bend into different directions, as described in the previous chapter. Note that the slab dip angle can actually vary significantly and the figure might display a rather uncommonly steep slab. The zoom box displays the processes delamination and relamination, which are said to be important for the formation of the lower continental crust.

time span of about ~200 Ma between creation at the mid oceanic ridges and destruction through subduction. The oldest recent oceanic lithosphere is about 280 Ma old and can be found in the South Eastern Mediterranean (Müller et al., 2008). The composition of the oceanic crust is well constrained as we can observe its creation at mid oceanic ridges. In those zones, upwelling of hot material leads to decompression melting followed by volcanic activity. Thus oceanic crust is composed of an upper layer containing volcanic rocks (MORB) and a lower layer of plutonic equivalents (gabbro), with average densities of about 2.9 g/cm^3. The thickness of the oceanic crust can vary depending on the temperature of the upwelling mantle. Seismic measurements and estimates from rare element inversions show that the thickness is 7-9 km on average and can increase to up to 9-12 km above anomalously hot mantle regions (White et al., 1992). Thermal circulation of fluids at the mid oceanic ridges can lead to hydration of the oceanic crust and also serpentinization of the lithospheric mantle below. Faccenda et al. (2009) argued that bending and fracturing of the oceanic lithosphere at a subduction zone trench can also and maybe even more effectively lead to hydration of the oceanic crust and mantle. On top of the oceanic crust marine sediments accumulate over time. The thickness can vary depending on the sediment influx from continental margins and the proximity to the margin. Thicknesses of up to a few kilometres are possible. The sediments can get scraped off in the trenches of subduction zones, building up an accretionary wedge. Nevertheless numerical models show that sediments can also be subducted far below the continental crust (Currie et al., 2007). The oceanic crust can also be pierced by hot spots and contain oceanic plateaus in the form of volcanoes or detached crustal pieces, as already mentioned in section 2.1.

The layering and composition of the continental crust is more enigmatic and variegated than the oceanic crust and one can literally find every kind of rock. The continental crust is believed to be on average andesitic to dacitic with 57-64 wt. % SiO_2 and average thickness estimates vary from ~40 km (Rudnick and Fountain, 1995) to 34.4 ± 4.1 km (Huang et al., 2013). Cenozoic collision zones like the alpine-himalaya belt are considerably thicker. Following seismic wave speed variations, the continental crust has been divided into different layers. Current models vary between a 2- to 4- layered crust (as reviewed in Hacker et al., 2015). Due to good outcrop accessability, all models have a quartz-rich upper crustal layer in common with 67 wt. % SiO_2 and thus granitoidal composition. The composition of the middle and lower crust is more difficult to constrain as data can only be sampled from a few exposed terrains and have to be complemented by xenoliths, wave speed studies and heat flow measurements. If following results from exposed terrains, the lower crust is like the upper crust andesitic to dacitic. If the lower crust was similar to xenoliths, it would be mafic. Wave speed measurements show that both compositions are possible, but that around 10-20 % of the lower crust need to be mafic (Hacker et al., 2015). Heat flow measurements can be explained by both an andesitic and mafic lower crust (Hacker et al., 2015).

To gain further insight into the nature of the lower crust, one needs to consider further geochemical and geodynamic observations connected to the formation of the lower crust. The main question still remains how an andesitic to dacitic continental crust can form, when most

mantle-derived melts are basaltic. Different processes for this so-called differentiation have been proposed whereof Hacker et al. (2015) considers the processes delamination and relamination as most noteworthy. Both are connected to buoyancy-driven flows which return mafic (lower) crustal material back into the mantle and leave more felsic material behind, thereby differentiating the crust (Fig. 6). Delamination occurs when lower crust becomes heavier than the underlying mantle and sinks into it. This requires densification reactions and high temperatures allowing for vertical viscous flow. Wolf and Wyllie (1993) and Rapp and Watson (1995) showed experimentally that the residues of amphibolite melts can transform into garnet rich, heavy (3.5-3.6 g/cm^3) pyroxenites at elevated pressures above ~10-15 kbar. Those are heavier than the underlying mantle and can thus possibly delaminate. The experimental results have been confirmed by field studies (Saleeby et al., 2003).

Relamination is the sibling of delamination, during which buoyant subducted crustal material separates from the subducting slab and rises up to the overriding plate (Fig. 6). The buoyant materials can be sediments, subducted oceanic plateaus, material derived from forearc subduction or subduction erosion, or subducted continents (Hacker et al., 2011).

Delamination might be an important factor in crustal differentiation but the chemical composition of arc lower crust is still different to delamination residues. Therefore Hacker et al. (2011) proposed that relamination is even more important for crustal differentiation than delamination. In addition to fluids, relamination and delamination can further explain the extinction of the seismic signature of the overriding plate Moho as observed in Figure 5. It becomes obvious that the zone above subducting slabs is intensively reworked and of great importance for all kinds of geological processes.

Thermal features

Delamination, relamination, melting and metamorphism are dependent on the prevailing temperatures in the lithosphere and upper mantle. The heat content and thus temperature is a function of heat production, conduction and advection. The lithosphere is dominated by a combination of heat production and conduction. Advective disturbance of the temperature field is only relevant near tectonically active areas or zones related to magmatism. Heat production is furthermore more or less restricted to the continental crust as the mantle and its melting product, the oceanic crust, have a low concentration of radioactive elements. Beginning with about 1300° the lithospheric mantle becomes fluid enough so that convection becomes the dominating heat transfer mechanism. Convection in the sub-lithospheric mantle steepens the temperature profile and the only change in temperature is through adiabatic heating or cooling. Typical adiabatic gradients in the upper mantle are in the order of 0.4-0.5 °C/km (Katsura et al., 2010). Thus the lithospheric mantle is a thermal boundary layer separating the crust and convective asthenosphere. In addition several authors (e.g. Hirth and Kohlstedt, 1996; Hirth et al., 2000; Sleep, 2005) propose that there is also a chemical difference and viscosity contrast between the lithospheric and asthenospheric mantle both within oceanic and continental lithosphere. Hirth

and Kohlstedt (1996) for instance propose that the asthenosphere is a fertile, hydrated peridotite and the oceanic lithosphere a dry, depleted peridotite. The decreased water content in the latter leads to lower viscosities. In continental cratons, xenoliths witness depleted lithosphere as well and up to depths of 200 km (Fischer et al., 2010, and references therein). Seismic studies show however that the depth extent of the lithosphere-asthenosphere boundary is not clear and varies significantly between 50-200 km all over the world (as reviewed in Fischer et al., 2010). At mid oceanic ridges (MOR) the 1300 °C isotherm is significantly elevated and oceanic lithosphere is very thin and young. The oceanic lithosphere cools and thus thickens with time and increasing distance to the MOR. Therefore the oceanic lithosphere is inherently transient and the constant thickness in Figure 6 is a strong simplification.

The continental lithosphere is, although also subject to constant reworking as explained above, much older than oceanic lithosphere and can achieve thermal steady state. Heat flow measurements show that the average surface heat flow is around 50 $\mathrm{mW\,m^{-2}}$. The upper crust is commonly said to have a heat production of 1.6-1.7 $\mathrm{\mu W\,m^{-3}}$. The middle and lower crust have lower values which depend on the layering model but range between 0.2-1.0 $\mathrm{\mu W\,m^{-3}}$ (as reviewed in Hacker et al., 2015). The mantle heat flow from the lithospheric mantle into the crust varies between 11-17 $\mathrm{mW\,m^{-2}}$. Thus heat production in the crust contributes to more than half of the surface heat flow.

2.4 Concepts of processes in subduction zones leading to upper plate deformation

By now we have seen that the subduction process involves a complex interplay between processes on different length and time scales. Thereby plate velocities, deep structures connected to slab bending in the upper mantle transition zone and chemical and thermal composition of the lithosphere have been more closely described. Still the main question is unanswered why the overriding plate deforms and how it deforms in response to different processes or parameters. A good starting point is to investigate the validity of different ideas with a statistical analysis.

Statistical analyses

Jarrard (1986) and Heuret and Lallemand (2005) made this attempt by classifying subduction zones into strain classes of upper plate strain and subsequently finding correlation coefficients. Jarrard (1986) chose to classify overriding plate deformation as: 1 - active back-arc spreading, 2 - very slow or waning back-arc spreading, 3 - mildly extensional, 4 - neutral to mild deformation in the arc (compressional) and back-arc (extensional), 5 - mildly compressional, 6 - moderately compressional with consistent folding, 7 - strongly compressional with substantial folding. Heuret and Lallemand (2005) followed the same approach but used a slightly different classification for upper plate strain: E3 - back-arc spreading, E2 - extensional, back-arc rifting, E1 - mildly extensional, 0 - neutral, C1 - mildly contractional, C2 - contractional, C3 - back-arc shortening. Both Jarrard (1986) and Heuret and Lallemand (2005) show good correlation coefficients between upper plate velocity and its strain regime, i.e. back-arc spreading when the upper plate moves

away from the trench and vice versa. Heuret and Lallemand (2005) even argue that upper plate velocity is the most important factor determining upper plate strain. They furthermore argue that 50 % of the subduction zones advance, that there is no correlation between slab age and upper plate deformation, and that mantle flows can have a significant influence on the back-arc deformation rate especially in extensional settings.

The drawback of the analyses by Jarrard (1986) and Heuret and Lallemand (2005) is the semi-quantitative approach of classifying the subduction systems on Earth into strain classes, because there will always be uncertainties of how to classify certain subduction zones. Hence the results can be biased by the author's choice. Furthermore the seven strain classes might not be distributed evenly along a strain continuum (as reviewed in Schellart, 2008). Additionally Heuret and Lallemand (2005) use a pacific hot spot reference frame from Gripp and Gordon (2002) which has shown to produce unreasonable velocities (Schellart et al., 2008). A more objective approach is used in the statistical analysis of twelve semi independent parameters and their influence on upper plate strain of 200 km long subduction segments by Schellart (2008). In his approach the upper plate strain data were compiled using geodetic measurements and complemented with geological and geophysical investigations. Thus the data set is continuous and consists of strain rates rather than strain classes and the objectivity is higher. The investigated semi-independent parameters are: 1 - overriding plate velocity, 2 - subducting plate velocity, 3 - trench migration velocity, 4 - convergence velocity, 5 - subduction velocity, 6 - accretion/erosion rate, 7 - subducting plate age, 8 - subduction polarity (e.g. E or W), 9 - shallow slab dip angle, 10 - deep slab dip angle, 11 - lateral slab edge distance, and 12 - buoyant ridge distance. A novelty in Schellart's approach (2008) is the integration of the third dimension in the investigation with parameters 11 and 12.

When relating the 12 physical parameters to the overriding plate strain (v_{OPD}), the only significant correlation is given by the trench migration velocity (v_T, 3) and the subduction velocity (v_S,5). In case of v_T this means that the trench moves towards the subducting plate when the overriding plate is extending and vice versa. This correlation seems quite straight forward as one expects that the trench moves in response to upper plate movement. Otherwise the subduction process would have nothing to do with overriding plate deformation. v_S is not so easy to explain. One would expect higher compressive stresses at higher subduction velocities, but the correlation shows a higher contractional regime at lower v_S, which suggests an anti-correlation. Additionally Schellart (2008) argues that the correlation coefficient for v_S is not significant any more, if excluding the Tonga-Kermadec-Hikurangi and New Britain-San Cristobal-New Hebrides subduction zones. Hence the correlation is based on the dominance of two subduction zone systems. To explain the variations in v_T, Schellart (2008) extends his analysis by combining several parameters and finds that a good correlation can be found by combining the lateral slab edge distance and the overriding plate velocity. In regions close to the slab edge (<1600 km), extension in the upper plate can be found independent of the overriding plate velocity and a neutral strain regime can prevail up to high overriding plate velocities ($\leq$ 7.6 cm yr^{-1}). In stark contrast to that, overriding plate extension in regions far away from slab

edges (>2000 km) is only possible when the overriding plate retreats and a neutral regime is coupled to slow overriding plate velocities (-1.2 cm yr^{-1} < v_{OP} < 1.2 cm yr^{-1}). Upper plate shortening is thus statistically related to v_{OP} > 1.2 cm yr^{-1}.

Models explaining the results from statistical analyses

Simple three dimensional geodynamic experiments give an explanation for the relationship explained in the previous chapter (Funiciello et al., 2003, 2004; Schellart et al., 2007; Stegman et al., 2010; Schellart et al., 2011). The experiments show that the sublithospheric mantle flow pattern can be subdivided into a toroidal component and a poloidal component (Fig. 7). The poloidal flow cells are independent on the distance to the slab edge and are conserving the mass on each side of the slab. The toroidal component is highly dependent on the distance to the next slab edge as this return flow transfers mass from behind the downgoing slab to the overriding plate side and vice versa. Thus areas which are proximal to a slab edge can be strongly influenced by return flow and the system can freely move in response to overriding plate velocity. Therefore the overriding plate velocity has no effect on the upper plate deformation style. Areas which are farther away from slab edges are only little affected by a toroidal flow component and consequently the subduction system is more stable and can not move so easy. Hence if the overriding plate moves towards the trench, it pushes against an immobile, rigid block of lithosphere and upper mantle and deforms contractionally. Similarly if v_{OP} is directed away from the trench, the upper plate deforms extensionally.

Nevertheless 2D thermo-mechanical models (Buiter et al., 2001; Sobolev and Babeyko, 2005; Hampel and Pfiffner, 2006) and the earlier investigations by Jarrard (1986) and Heuret and Lallemand (2005) show that upper plate velocity is important in determining upper plate strain in general. Schellart (2008) argues that the semi-quantitative approach used by Jarrard (1986) and Heuret and Lallemand (2005) is the reason for the differences. Furthermore when taking a closer look at the boundary conditions by e.g. the models of Sobolev and Babeyko (2005), one finds that the mantle flow pattern does not allow for return flow. Thus their modelling results actually support Schellart's 2008 idea that missing return flow leads to importance of upper plate velocity in determining upper plate strain.

It is, however, important to notice that the result of a statistical analysis of subduction fragments as done be Schellart (2008) and Heuret and Lallemand (2005) can be dictated by long subduction zones with very prominent features. Schellart (2008) shows that this was for instance the case for v_S. Thus every subduction zone may be determined by its own specialities. Nevertheless the results give a good hint at which parameters might possibly be important.

Which geological features stimulate upper plate deformation?

So far we have seen that a combination of mantle flow patterns and upper plate velocity is statistically relevant for upper plate strain. The 3D models by Schellart et al. (2007), Stegman et al. (2010), and Schellart et al. (2011), which support this theory, are rather simple and do not

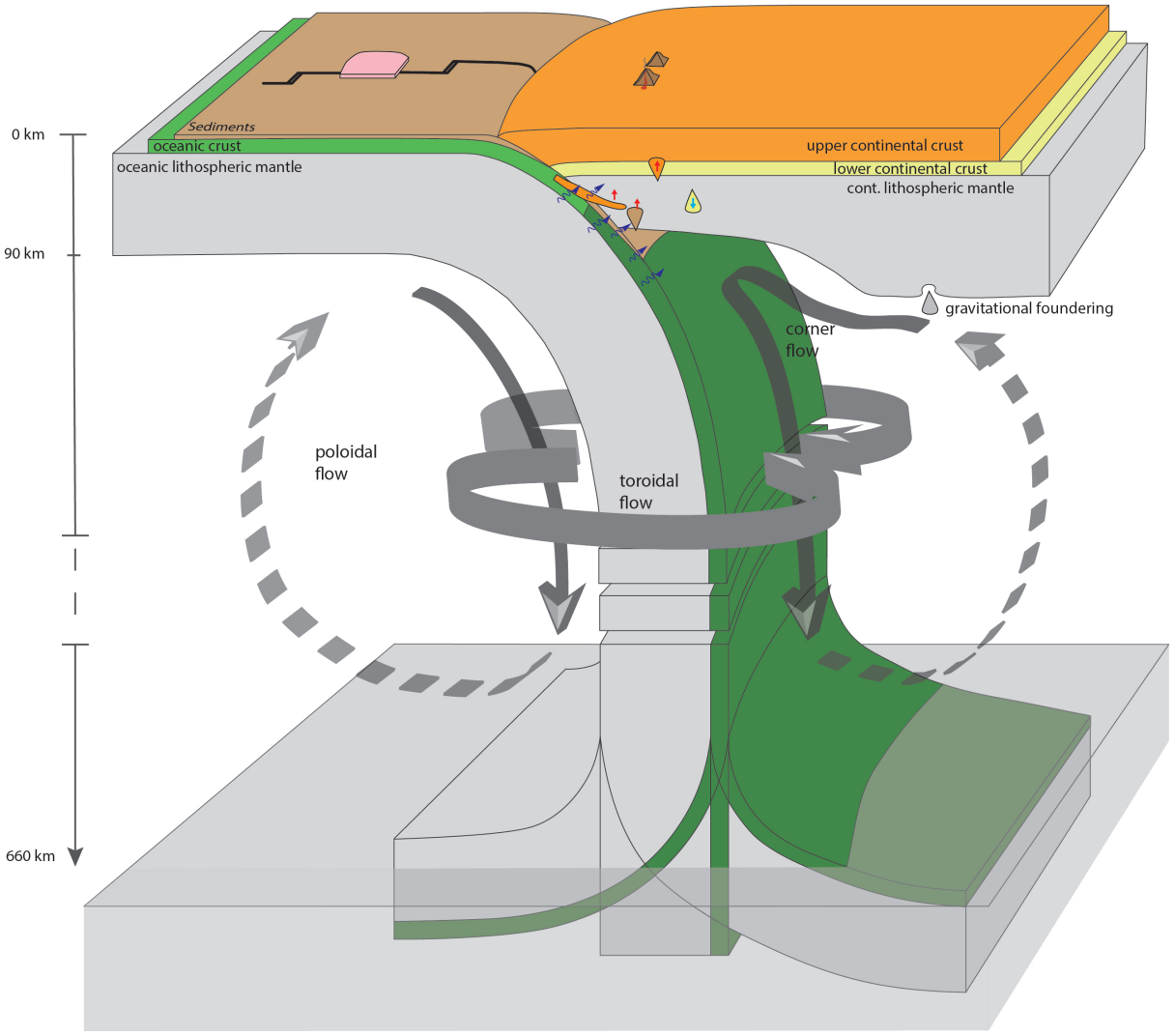

Figure 7: Simplified sketch of the compositional layering of an ocean-continent subduction zone extending Fig. 6 by mantle flow patterns. The mantle flow can by separated into a horizontal, toroidal component and a vertical, poloidal component. Whether a subduction zone can be affected by toroidal flow is dependent on its slab edge distance. This sketch of a subduction zone has a relatively narrow lateral extent and would thus be very affected by toroidal flow.

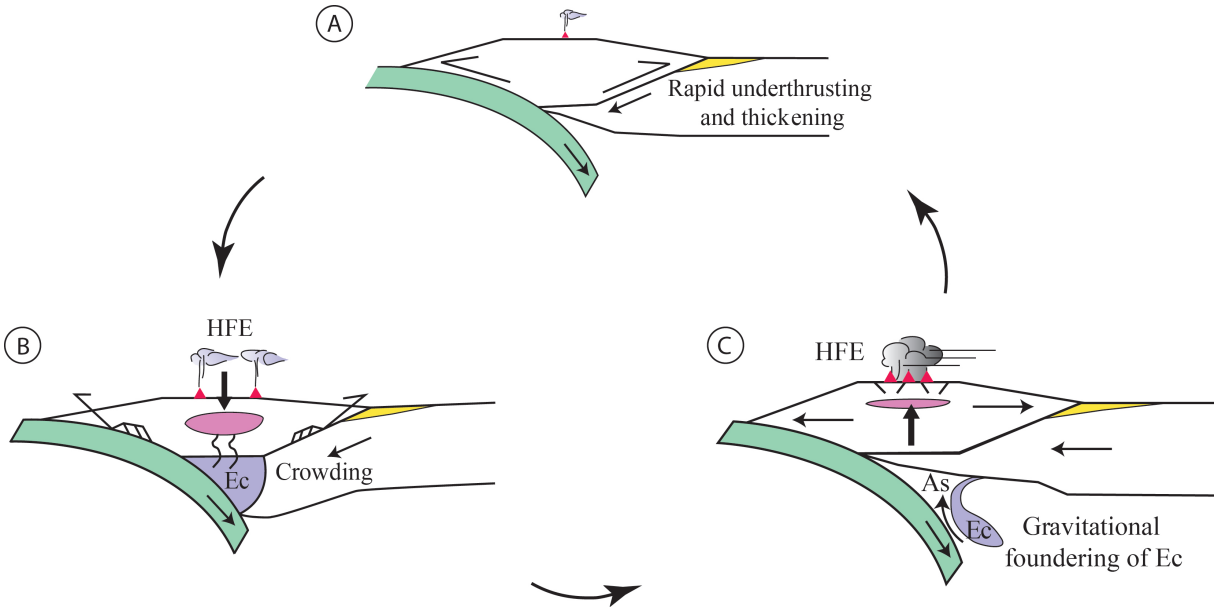

Figure 8: Simplified sketch of the cyclicity of Cordilleran mountain belts, as proposed by DeCelles et al. (2009). (A) Rapid underthrusting of the retro-continent under the thickened arc leads to foreland basin formation and arc thickening. Furthermore magmatic activity is low. (B) Melting of the underthrust crust leads to a magmatic high flux episode (HFE). The restite is eclogitised (Ec) and the mountain belt subsides. (C) Gravitational foundering of the heavy eclogite and inflow of asthenosphere (As) leads to isostatic uplift of the mountain belt. This induces gravitational collapse structures in the arc. Note that flat slab subduction could modify the cyclicity. Modified from DeCelles et al. (2009).

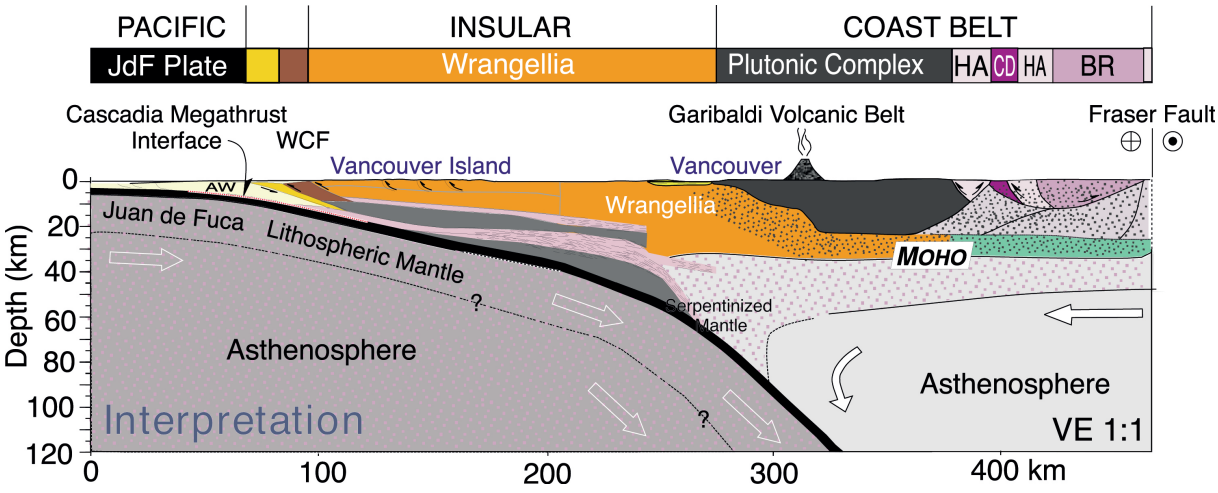

Figure 9: Interpreted cross section based on geophysical data, showing the margin of the Cascadia subduction zone at the Western Canadian coast. The margin is composed of different magmatic belts and some frontal accretion, but consist to a big amount of the possibly accreted Wrangellia terrane. Modified from Tetreault and Buiter (2012). The geophysical data are from Hammer et al. (2010).

account for thermal-mechanical coupling nor do they have an upper plate included. Figure 1 shows that deformation on Earth is focused into weak zones. Thus the upper plate has to become weaker over time and through the subduction process to allow for its deformation. Possible mechanisms for weakening are elevated temperatures, metamorphism, fluids or inherited structures. The role of fluids, metamorphism and the thermal composition has been discussed in section 2.3 and inherited structures are manifold and related to earlier deformation phases but difficult to classify. None of the factors can explain upper plate weakening by itself and a combination of several or even all parameters is probably necessary.

To allow for melting and due to lithospheric stretching one would expect high temperatures and a thinned continental lithosphere above volcanic arcs and in the vicinity of extended back-arcs. Additionally Currie and Hyndman (2006) investigated ten circum-Pacific back-arc regions which are not significantly extended and found that those have also high surface heat flow and a thin, hot lithosphere in common (~1200 °C at ~60 km depth). Furthermore those hot regions extend over a wide area several hundred kilometres (250-900 km) into the back-arc. Currie and Hyndman (2006) promote that hot and thin lithosphere is a fundamental characteristic of subduction zones and propose that the mechanism for thinning is the removal of low viscosity lithospheric mantle by small-scale convection. Furthermore they propose that the low viscosity originates from hydration by fluids from the subducting slab. The weakening can be more than a factor of 10 in comparison to cratonic lithosphere (Hyndman et al., 2005).

Coupled thermal-mechanic numerical modelling of subduction systems showed that a weakening of the sublithospheric mantle by factors between 10 and 50 leads to its thinning through gravitational instabilities and corner flow induced by the downwards drag of the subducting slab (Fig. 7). A similar behaviour of lithosphere weakening through fluids and subsequent removal through corner flow was observed by models from Arcay et al. (2005, 2006). Thus it appears that weakening of the back arc lithospheric mantle and its subsequent thinning is a major mechanism to weaken the back arc crust and make it prone for deformation. To proof this idea in the context of subduction roll-back Grool (2012) used the same model setup as Currie et al. (2008) and investigated the sensibility and necessity of different parameters for subduction zone roll-back to occur. The investigated parameters were: (i) weakening of back-arc lithospheric mantle, (ii) weakness of the weak seed (weak material to induce subduction in numerical experiment), (iii) density of the eclogite, (iv) strength of a serpentinized layer below the oceanic crust, (v) convergence velocity and (vi) the mantle flow pattern. Grool (2012) found that indeed roll back and back-arc spreading can occur only when the back arc lithospheric mantle is weak. The other parameters have only a modulating effect. So does e.g. a higher density of eclogite, which was former oceanic crust, increase the slab dip. Interestingly does Grool (2012) not report any effect when adding a return flow component (vi) and when reducing the subduction velocity from 5 cm/yr to 2.5 cm/yr.

Currie and Hyndman (2006) and Hyndman et al. (2005) do also report high heat flow values and a thin lithospheric mantle below the Andes. Thus thinned lithospheric mantle might also enhance upper plate shortening. DeCelles et al. (2009) and Pelletier et al. (2010) attribute

the formation of the Andes to the foundering of former lower crust which was partly melted and metamorphosed to a heavy pyroxenite restite. Thus they propose that delamination is the main driving mechanism for the formation of the Andes (Fig. 8). Delamination requires high temperatures and a thinned mantle lithosphere which fits with the observations from above Currie and Hyndman (2006) and Currie et al. (2008).

So far processes have been described which could induce upper plate deformation, without considering buoyant intra-oceanic features like pieces of rifted continental crust, extinct spreading ridges or other oceanic plateaus. Yet the geologic record indicates that for instance large areas along the Western North American coast have been created through the accretion of intra-oceanic terranes (Fig. 9, e.g. Jones et al., 1977; Monger et al., 1982; Hammer et al., 2010) and that recent subduction of buoyant crust modifies subduction zones as in e.g. the Ontong-Java Plateau (Mann and Taira, 2004). Recent thermo-mechanical models show that terrane accretion or subduction is dependent on the rheology of the terrane, in a way that a weak detachment zone leads to terrane accretion and a strong rheology induces terrane subduction (Tetreault and Buiter, 2012; Vogt and Gerya, 2014).

3 Methods

3.1 Introduction to geodynamic numerical modelling

Beginning with the plate tectonic revolution in the 1960s, mathematical modelling of tectonic processes started to have an important impact on geosciences. Early mathematical descriptions of Earth's processes were often solved analytically and thus subject to major simplifications. However the analytical solutions already provided very good insight into processes inside and on the Earth (e.g. McKenzie, 1969, 1978; England and Thompson, 1984). Early numerical models on the lithospheric scale were also already produced around the same time, but their approach was rather simplistic and for instance thermal and mechanical coupling was not accounted for (e.g. Minear and Toksöz, 1970).

With the development of computers, non-linear problems combining different physical laws could be numerically approximated and more sophisticated questions tackled. Thus in the following decades numerical codes were developed, which included coupling of deformation and thermal evolution of the lithosphere through a visco-(elasto-)plastic rheology. Thereby a number of numerical techniques, as for instance the *Finite Difference Method* or the *Finite Element Method*, were used and refined. Newer codes often include parallel computing and make it possible to investigate tectonic problems in 2D and 3D (e.g. Gerya and Yuen, 2007; Braun et al., 2008; Thieulot, 2011). Recently developed codes even attempt to unify mantle convection and lithospheric processes, which were previously, due to scale differences, often modelled separately (e.g. Stadler et al., 2010). For a more extensive review of the development of numerical geodynamic modelling, see Gerya (2010).

Although 3D modelling is possible now, it is still very useful to first model a problem in 2D, as it is easier to distinguish different processes in two dimensions. Most geodynamic modelling in 2D is developed around the plane strain approach. This is a major simplification of nature, because all deformation is integrated in the modelled plane and strain partitioning due to oblique collision or extension is not possible. Therefore interpreting 2D modelling results has to be done carefully. Especially comparing geological cross-sections and 2D numerical models, although done frequently, can possibly lead to wrong results. Nevertheless, because of its simplicity, 2D modelling gives a good starting point of how different processes in nature could work and for this thesis we decided to investigate our problem in two dimensions as well.

For studying subduction processes, we started out with a modified and extended version of the finite element code called SOPALE, which was initially written and developed by Phillipe Fullsack at Dahlhousie University, Halifax (Fullsack, 1995). SOPALE is a serial code and thus has strong limitations on the resolution of the models. As we wanted to model a big lithospheric domain at an acceptable resolution, we decided to use a modified version of FANTOM. FANTOM was initially developed by Cedric Thieulot and Ritske Huismans at the University of Bergen (Thieulot, 2011). To use FANTOM for our purposes, adiabatic heating, temperature-dependent conductivity and P-T-dependent phasechanges were implemented.

Geodynamic modelling relies on numerical approximations of only a few coupled equations.

Therefore it is crucial to thoroughly understand their underlying assumptions and derivations as well as their numerical implementation. Thus in the following sections of chapter 3, the governing equations and assumptions of the code (3.2) and the treatment of the equations by FANTOM (3.3) are examined in detail. The new implementations are described in more detail in chapter 3.3 as well. In the following section (3.4), the model setup and boundary conditions of our problem sets are presented. In the last section 3.6 the model sets and their modelling intention are explained.

3.2 Governing equations and assumptions

The version of the code used in this thesis numerically approximates the coupled thermal and mechanical evolution of a subduction system on the lithospheric scale in two dimensions. Vertical cross section plane strain is assumed and the thermal and mechanical properties are coupled via thermally activated power law creep of the materials in the model domain. The physics behind the modelling approach comes from the field of continuum fluid mechanics and the assumption is made that rocks can be treated as fluids with special properties.

Figure 10 shows an overview of the set of equations used for the modelling approach. In the following subsections the equations are described and derived in more detail. The meaning and units of the parameters used in the equations are displayed in table 1.

3.2.1 Mass and momentum conservation equations

We assume that the medium in our model domain is continuous, which means it has no mass-free gaps or voids on the macroscopic scale. This is reasonable, as we are dealing with rocks which can indeed have porosity and cavities, but either kind are always filled with some fluid. Material continuity can be expressed with the mass continuity equation, which can be written for a fixed point of reference (Eulerian notation) or for a moving point of reference (Lagrangian notation). The continuity equation reduces to the so-called incompressible continuity equation, when assuming that temperature, pressure and phase changes only have a minor effect on the volume of the materials in the model domain. The incompressible continuity equation has the same notation for an Eulerian or Lagrangian observer (Fig. 10, 1A (I)):

$$\nabla v = 0, \tag{1}$$

which in two dimensions and another notation is the same as $\frac{\partial v}{\partial x} + \frac{\partial v}{\partial y} = 0$. This means that the influx into each infinitesimal small material point in our model equals the flux out of each point.

To approximate the incompressibility assumption, one can use the so-called penalty formulation:

$$\nabla v + \frac{P}{\lambda} = 0, \tag{2}$$

where λ is the penalty parameter and P the dynamic pressure. λ can be interpreted as a bulk viscosity and needs to be very large in comparison to the pressures in our model domain, so

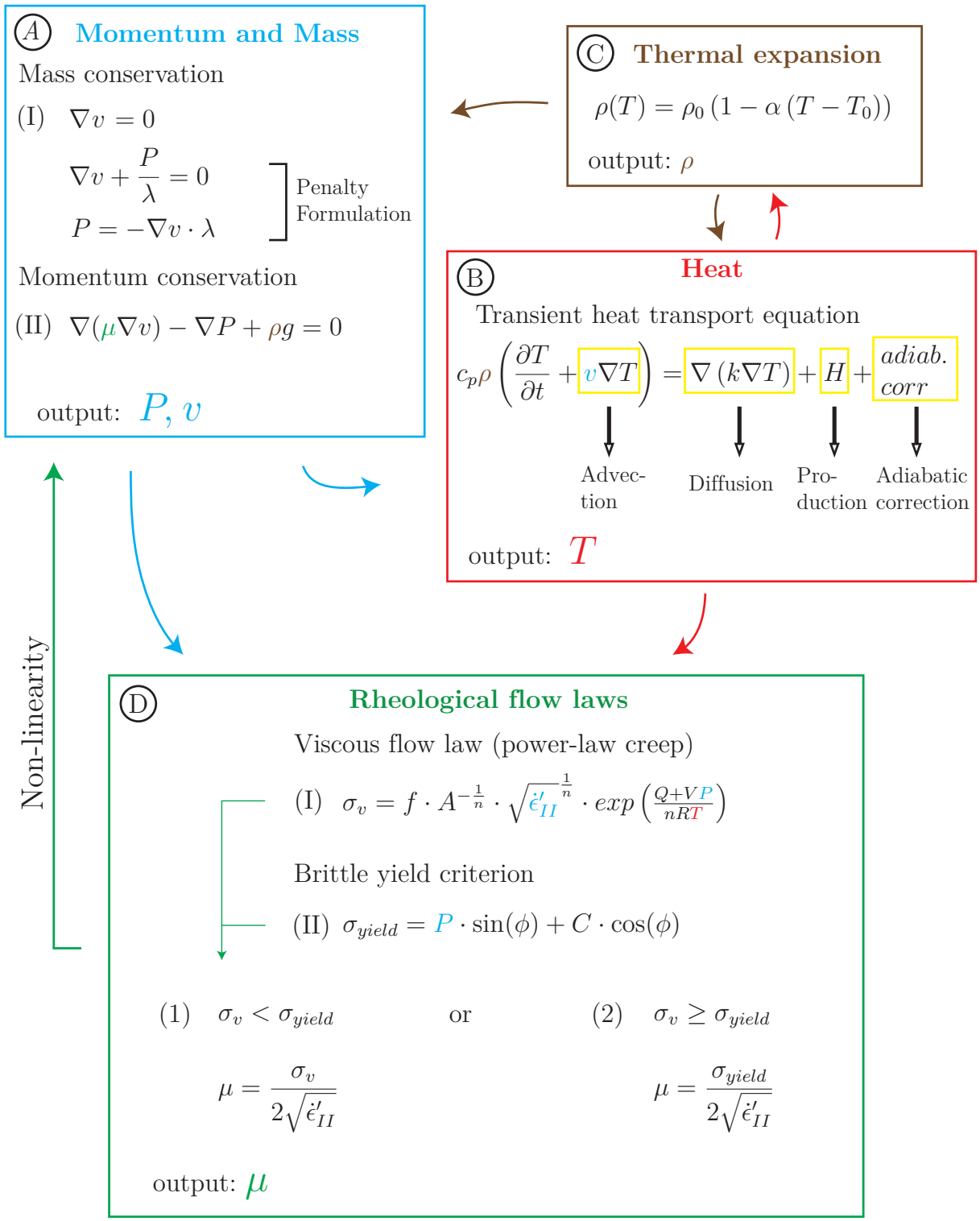

Figure 10: Flow chart showing how the different equations used in our numerical modelling approach relate to each other. (A) The momentum and mass conservation equations solve for velocities and thus strain distribution in the model domain. (B) The transient heat equation needs the velocity input from the momentum equation and solves for the distribution of heat in the model domain. (C) The temperatures are used to calculate the thermal expansion of the material in the model. (D) The rheological flow laws define the viscosities of the materials and are the coupling element between (A) and (B). The figure illustrates furthermore the non-linearity of the momentum equation, which is the reason why the equations have to be approximated numerically. Note that μ is the so-called effective viscosity.

Table 1: Nomenclature of parameters.

Symbol	Meaning	Unit
Latin letters		
A	Pre exponential power-law constant	$\mathrm{Pa}^{-1}\,\mathrm{s}^{-1}$
dt	time step	s
c_p	Heat capacity	$\mathrm{J\,kg}^{-1}\,\mathrm{K}^{-1}$
f	Scaling factor for flow laws	
g	Gravitational acceleration	$\mathrm{m\,s}^{-1}$
H	Heat production	$\mathrm{W\,m}^{-3}$
k	Thermal conductivity	$\mathrm{W\,m}^{-1}\,\mathrm{K}^{-1}$
n	Power law creep exponent	
P	Pressure (dynamic)	Pa
Q	Activation energy	$\mathrm{J\,mol}^{-1}$
R	Gas constant	$\mathrm{J\,K}^{-1}\,\mathrm{mol}^{-1}$
T	Temperature	K
$\Delta T_{Adiabatic}$	Adiabatic gradient	$\mathrm{K\,km}^{-1}$
$v = (v_x, v_y)$	Velocity	$\mathrm{m\,s}^{-1}$
V	Power-law activation volume	$\mathrm{m}^3\,\mathrm{mol}^{-1}$
Greek letters		
α	Coefficient of thermal expansion	K^{-1}
ϵ	Strain (tensor)	
$\dot{\epsilon}$	Strain rate (tensor)	s^{-1}
$\dot{\epsilon}'$	Deviatoric strain rate (tensor)	s^{-1}
$\dot{\epsilon}'_{II}$	2nd invariant of $\dot{\epsilon}'$	
λ	Penalty coefficient	$\mathrm{Pa\,s}$
μ	(effective) Viscosity	$\mathrm{Pa\,s}$
ϕ	Angle of internal friction	
ρ	Density	$\mathrm{kg\,m}^3$
σ	Stress (tensor)	Pa
σ'	Deviatoric stress (tensor)	Pa
σ_v	Viscous creep stress	
σ_{yield}	Yield criterion	

that Eq. (1) is satisfactorily approximated. The approximation is very handy as it allows for elimination of the pressure term in the continuum equation, which is explained in the next paragraphs. For further information about the validity of the penalty method, see Fullsack (1995) or Thieulot (2011) and references therein.

The deformation of a continuous medium is the result of the force balance between internal and external forces. To relate forces to deformation, an equation of motion has to be used. In continuum mechanics this equation is called the conservation of momentum equation. Again, it has an Eulerian and Lagrangian form and can in a generalized manner be written as:

$$\nabla\sigma + \rho g = flow\ accelerations\ (Eulerian/Lagrangian\ form), \tag{3}$$

where σ is the stress acting on each reference point in the medium, ρ is the corresponding

density and g is the vertical gravity acceleration. Earth materials are highly viscous and deform very slowly so that flow induced accelerations, also known as inertia, can be neglected in the conservation of momentum equation. Thus Eq. (3) simplifies to

$$\nabla\sigma + \rho g = 0. \tag{4}$$

The stress, defined as force per unit area, acting at every point in a medium can be subdivided into normal stresses (acting orthogonal to the surface) and shear stresses (acting along the surface). This partitioning results in nine stress components in the 3D-case and four stress components in the 2D-case. To display the components it is convenient to use a second order tensor, known as the Cauchy stress tensor. In 2D the stress tensor is defined as:

$$\sigma = \begin{pmatrix} \sigma_{xx} & \sigma_{xy} \\ \sigma_{yx} & \sigma_{yy} \end{pmatrix}.$$

The stress tensor can be split up into a pressure part $P = \frac{\sigma_{xx} + \sigma_{yy}}{2}$ and a deviatoric part σ', with the relationship $\sigma'_{ij} = \sigma_{ij} + P\delta_{ij}$. δ_{ij} is the Kronecker delta. Hence Eq. (4) can be written as

$$\nabla\sigma' - \nabla P + \rho g = 0. \tag{5}$$

Stress can be related to strain, when assuming that rocks behave as Newtonian fluids. The corresponding law is called the Newtonian law of viscous friction, which in the incompressibility case reduces to

$$\sigma' = 2\mu\dot{\epsilon}, \tag{6}$$

where μ is the dynamic viscosity and $\dot{\epsilon}$ the strain rate. In analogy to stress, the strain rate can also be displayed in tensoral notation, and its components $\dot{\epsilon}_{ij}$ are defined as the spatial gradients of the velocity with

$$\dot{\epsilon}_{ij} = \frac{1}{2}\left(\frac{\partial v_i}{\partial x_j} + \frac{\partial v_j}{\partial x_i}\right), \tag{7}$$

where i and j are indexes for different coordinates and x_i and x_j are spatial coordinates.

Taking Eqs. (5), (6) and (7) together and applying the incompressibilty assumption, leads to the incompressible Stokes equations (Fig. 10A, (II)):

$$\nabla(\mu\nabla v) - \nabla P + \rho g = 0. \tag{8}$$

The method introduced in Eq. (2) for the mass conservation approximation comes in handy now, as the pressure term P in Eq. (8) can be eliminated and the incompressible Stokes equations and the mass conservation equation merge together to:

$$\nabla(\mu\nabla v) + \lambda\nabla\left(\nabla \cdot v\right) + \rho g = 0. \tag{9}$$

For constant viscosity and density, which is valid for each iterative step in the numerical approach, the combined Stokes-mass conservation equations only depend on the velocity v and can be written as:

$$\begin{aligned} &\text{in x-direction: } (\mu + \lambda) \cdot \Delta v_x = 0 \\ &\text{in y-direction: } (\mu + \lambda) \cdot \Delta v_y = -\rho g, \end{aligned} \tag{10}$$

where Δ is the Laplace operator, which in 2D can be written as $\Delta = \frac{\partial^2}{\partial x^2} + \frac{\partial^2}{\partial y^2}$.

The mathematical notation of the equations used in this subsection mainly followed Thieulot (2011). For a more detailed derivation and less compact notation of the presented equations, see Gerya (2010).

3.2.2 Transient heat transport equation

Many material properties of rocks, such as density and viscosity, are not only dependent on forces or deformation, but also on temperature. Therefore it is essential to incorporate the transient heat transport equation in our modelling approach (Fig. 10B):

$$c_p \rho \left(\frac{\partial T}{\partial t} + v \nabla T \right) = \nabla \left(k \nabla T \right) + H + adiab.\ corr, \tag{11}$$

where ρ is density, c_p is heat capacity, t is time in seconds, T is the absolute temperature, v is the velocity vector, k is thermal conductivity, H is heat production.

Eq. 11 consists of the advection, diffusion, production and adiabatic correction terms, as displayed in Fig. 10B. The advection term describes the disturbance of the temperature field due to mass movement and thus needs the velocity as an input. The heat diffusion term describes heat conduction processes. The heat production term accounts for creation of heat due to radioactive decay. The adiabatic correction is a proxy for heat production or consumption due to vertical mass movement and hence due to pressurization or depressurization. It needs the vertical velocity as input and modifies the calculated temperature by a predefined adiabatic gradient. Eq. 11 does not account for shear heating.

3.2.3 Material properties

In a classical geological approach, temperature and pressure changes are responsible for mineral reactions and thus change the mineral composition of a rock. However pressure and temperature conditions are not only responsible for the composition, but also for the density in terms of thermal expansion, and viscosity of a rock. To calculate the temperature dependent density, one has to know an initial 'compositional' density ρ_0 at any temperature $T = T_0$ and the coefficient of thermal expansion α. Then the temperature-dependent density is given by

$$\rho(T) = \rho_0 \left(1 - \alpha \left(T - T_0\right)\right), \tag{12}$$

see also Fig. 10C.

The viscosity can be calculated from rheological flow laws. Those flow laws are the coupling element between the momentum and heat conservation equation, as they need input from both equations and give feedback to the momentum equation, thus inducing non-linearity (Fig. 10). The choice of reasonable flow laws plays a crucial role in geodynamic modelling, as they determine the overall behaviour of a model.

At lower temperatures rocks deform by brittle deformation and at higher temperatures rocks deform by viscous creep. Thus the materials used in the model need to have properties for viscous as well as for brittle behaviour. Furthermore for the continuum mechanical approach, these two behaviours have to be translated into viscosities using applicable flow laws.

For viscous deformation, a non-linear, thermally-activated power law creep formulation is used, which relates pressure, temperature and stress to strain rate:

$$\sigma_v = f \cdot A^{-\frac{1}{n}} \cdot \sqrt{\dot{\epsilon}'_{II}}^{\frac{1}{n}} \cdot exp\left(\frac{Q + VP}{nRT}\right), \tag{13}$$

where σ_v is the square root of the second invariant of the deviatoric stress tensor, f is a linear scaling factor, $\dot{\epsilon}'_{II}$ is the second invariant of the deviatoric strain rate tensor, Q is the creep activation energy, V is activation volume, P is pressure, R is the universal gas constant, T is absolute temperature, A is an empirical material constant and n is the power law exponent.

The brittle behaviour of rocks is modelled with a deformation law following the Mohr-Coulomb plasticity criterion

$$\sigma_{yield} = P \cdot \sin(\phi) + C \cdot \cos(\phi), \tag{14}$$

where P is pressure, ϕ is the angle of internal friction and C is cohesion. Following Byerlee's law, ϕ would be $\sim$30° for dry frictional sliding conditions. To approximate hydrostatic fluid pressures in the crust, ϕ is assumed to be lower and about 15°. The materials furthermore account for frictional plastic strain softening by linearly reducing ϕ through a predefined strain transition $\epsilon_I < \sqrt{\dot{\epsilon}'_{II}} < \epsilon_{II}$ (Huismans and Beaumont, 2003). A typical value set for strain weakening is reducing ϕ from 15° to 2° through the strain transition $0.5 < \sqrt{\dot{\epsilon}'_{II}} < 1.5$. Viscous strain has no weakening effect on the material.

Figure 10D shows the decision procedure for which flow law is used for every material point in the model. If $\sigma_v < \sigma_{yield}$, and assuming the behaviour as a Newtonian fluid (Eq. 6), the effective viscosity is given by:

$$\mu = \frac{\sigma_v}{2\sqrt{\dot{\epsilon}'_{II}}}. \tag{15}$$

For the case that $\sigma_v \geq \sigma_{yield}$, the point of consideration is outside the yield-surface and the viscosity is rescaled onto the surface using:

$$\mu = \frac{\sigma_{yield}}{2\sqrt{\dot{\epsilon}'_{II}}} \tag{16}$$

This means that a piece of rock in the modelling domain deforms by power-law creep as long as the yield criterion σ_{yield} is not reached by the prevailing stresses.

Remark on invariants of the stress and strain tensor: To compare different stressed or deformed systems, one needs to use a value which is independent from the orientation of the reference frame. This is achieved by using tensor invariants. The three different invariants T_I, T_{II}, T_{III} of a given tensor T can be computed as follows:

$$T_I = Tr[T],$$

$$T_{II} = \frac{1}{2}Tr[T^2],$$

$$T_{III} = \frac{1}{3}Tr[T^3],$$

where Tr is the sum of the elements on the main diagonal of the tensor. The second invariant of the 2-dimensional deviatoric stress tensor σ' has for instance the value:

$$\begin{aligned}\sigma'_{II} &= \frac{1}{2}\left(\sigma'^2_{xx} + \sigma'^2_{yy}\right) + \sigma'^2_{xy} \\ &= \frac{1}{4}\left(\sigma_{xx} - \sigma_{yy}\right)^2 + \sigma^2_{xy}.\end{aligned}$$

In the case of the modelling approach used in FANTOM, flow stress (σ_v) is normalized using the square roots of the second invariant of the deviatoric stress tensor, and strain rate and pressure are normalized by using the square root of the second invariant of the deviatoric strain rate tensor.

3.3 Implementation of formulas in FANTOM

3.3.1 General procedure of a model run

FANTOM is a finite element code, using an Arbitrary Lagrangian-Eulerian (ALE) formulation of the governing equations. The ALE-method involves two superposed grids, where one is used for equation solving and the other one moves through the first grid and tracks the solutions. The solution grid is an evenly distributed Eulerian grid (E-grid), with size $L_x \times L_y$ and $n_x^E \times n_y^E$ nodes. The cells are sub-rectangular and initially filled with a predefined amount of randomly distributed Lagrangian markers (L-grid/-cloud), which carry the material properties and accumulated strain. The E-grid is sub-stationary and can move in vertical direction so that the top row of the grid defines a free surface. The left and right boundaries of the E-grid have free slip (roller) conditions and the bottom boundary is vertically fixed. For each time step the numerical solutions of the governing equations are obtained on the E-grid. Hence the cell size of the E-grid defines the spatial resolution of the model. The results are subsequently transferred to the Lagrangian cloud and its particles are advected according to the obtained velocity field.The coupling of the marker and the solution grid is the main feature of the ALE-formulation. This numerical method is

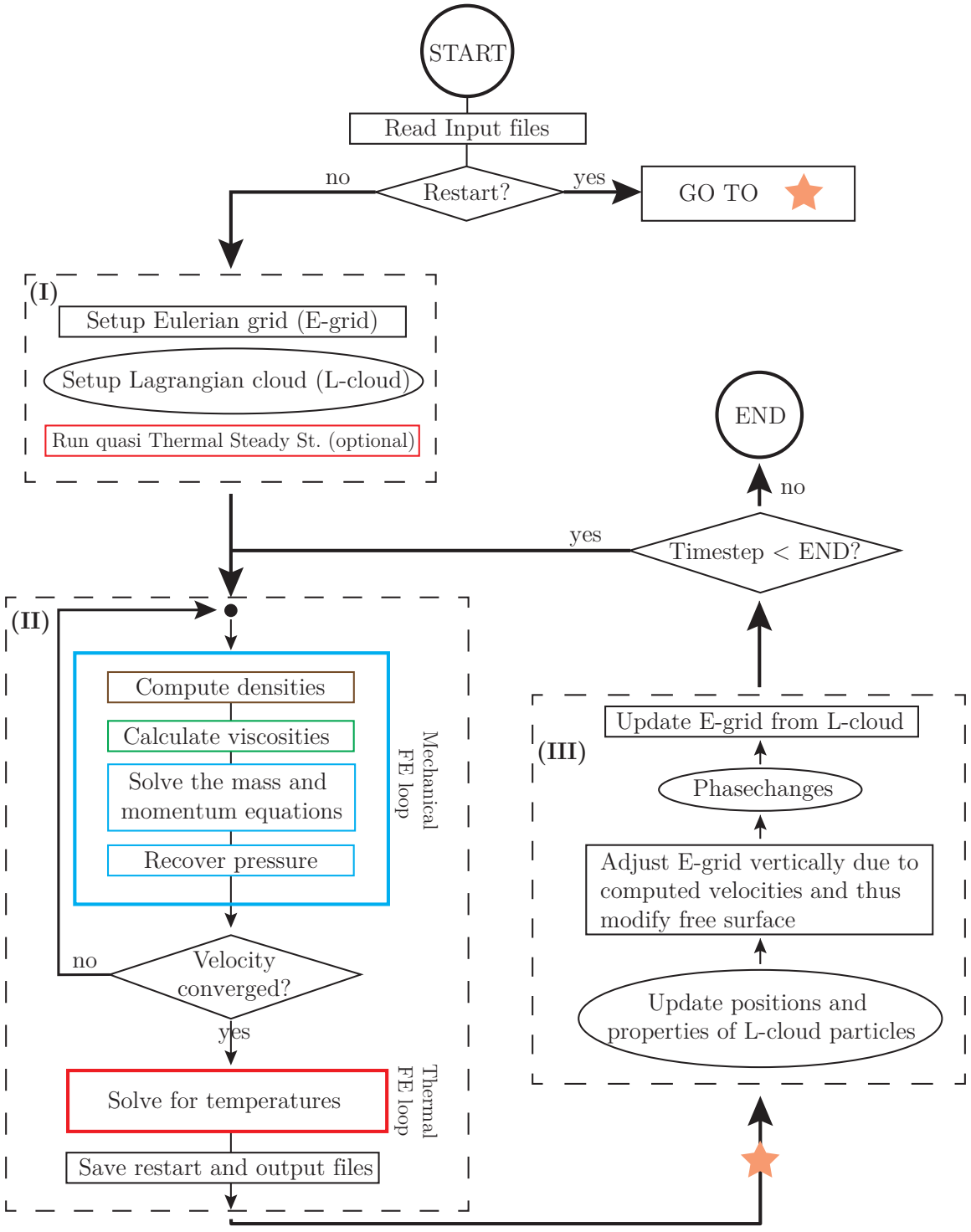

Figure 11: The figure shows the simplified procedure of a model run. Rectangles frame processes on the E-grid, oval shapes encircle processes on the L-cloud and the rhombic shapes frame boolean operator decisions. Colors correspond to Fig. 10. When executing the programme, the input files are read. In the case of a model restart, the programme directly jumps to (III). If no restart files are used, the E-grid and the L-cloud are initiated and the model can subsequently be run to quasi-thermal steady state (I). After that, the deformation and temperature evolution of the model are iteratively computed on the eulerian grid (II). The L-grid is subsequently advected accordingly and the E-grid is vertically remeshed (III). (II) and (III) are repeated for each time step until the endtime is reached.

particularly useful in geodynamic flow problems, as they often feature high and partially very localized strain.

Figure 11 shows a simplified flow chart of a model run in FANTOM: After the code is compiled and executed, input files are read. If the user chooses to restart a model, the Eulerian and Lagrangian grids are loaded from a set of restart files, otherwise the grids are initialised and the lithospheric system can optionally be run to thermal steady state. Now the time stepping loop begins until the predefined final time is reached. For each time step, a numerical approximation part (Fig. 11 (II)) and an advection/remeshing part (Fig. 11 (III)) are executed. A more detailed information about achieving thermal steady state is given in chapter (3.3.2).

During the calculation part, the combined mass and momentum equations coupled with the flow laws are iteratively approximated until a convergence criterion is reached. This involves solving equations (9, 12 - 16). The output is the spatial distribution of velocity, density, pressure and viscosity in our model domain. Subsequently the heat distribution in the model domain is numerically approximated by solving Eq. 11, and the calculated grids are saved for restarting or graphical post processing.

During the advection/remeshing part, the L-cloud is advected according to the calculated velocity field and its particle properties are updated. Furthermore the E-grid is vertically adjusted and remeshed according to the smoothed free surface. Subsequently phase changes are applied to the Lagrangian particles according to the pressure and temperature conditions at their new location in the lithospheric domain. The last step in part (III) involves updating of the E-grid properties from the advected L-grid.

For more information on the numerical implementation, see Thieulot (2011). More detailed flow charts about the implementation of the ALE-method in context of geodynamical modelling can be found on the SOPALE documentation homepage.

3.3.2 New implementations and additional features of the code

We implemented several additional features in the code, which are meant to stabilize the numerical model and make it more realistic.

The ALE formulation gets its strength from updating the properties of the nodes of an Eulerian cell from the Lagrangian markers, which are inside of it. In the current version of FANTOM the cell properties are set to be the arithmetic mean of all of its Lagrangian markers. This artificially increases the resolution of the model. Therefore I implemented a new routine, so that the cell properties are now set to be the average of the prevailing material markers in the cell.

In nature the sub-lithospheric convective mantle is assumed to become hotter with increasing depth due to adiabatic heating. We approximate this behaviour be applying a temperature correction at each time step dt according to a predefined adiabatic gradient $\Delta T_{Adiabatic}$. Thus the temperature at each node i becomes per time step:

$$T^i = T^i + (-v_y^i) \cdot dt \cdot \Delta T_{Adiabatic}. \tag{17}$$

Note that velocities are positive when directed upwards. The adiabatic correction does not only create a more natural temperature distribution in the model domain, but also prevents the asthenospheric mantle from convecting vigorously. The latter is very important when modelling subduction systems, as a lot of processes are induced by the flow pattern of the sub-lithospheric mantle.

To prevent the lithospheric system from cooling and to simulate a convective sub-lithospheric mantle, the thermal conductivity of all materials is heat dependent and between $1335°C$ and $1345°C$ the conductivity linearly increases from $k = 2.25$ to $k = 52.0$. This means that heat which is introduced at the bottom of the model will rapidly conductively advance through the sub-lithospheric mantle and attain the adiabatic gradient. Both the adiabatic correction and the heat-dependent conductivity are used in a similar way in recent numerical modelling studies using the SOPALE code (e.g. Currie et al., 2008; Butler et al., 2013).

Thermal steady state as shown in Fig. 11 (I) is not achieved by solving the steady state version of the heat equation, but by multiple solving of the transient heat equation with a big time step, so that the model domain is 1 Ga old and thus in quasi-steady state. During the quasi steady state run the velocity field is set to $v = 0$.

Pressure- and temperature-dependent metamorphic reactions play probably an important role in subduction dynamics. A holistic integration of this effect is beyond the scope of this thesis, but I implemented a simple subroutine which mimics P-T-dependent phase changes. If the P-T-conditions of a Lagrangian particle enter a predefined P-T-field, the particle changes to the material which is stable in the predefined P-T-range. Thus oceanic crust changes e.g. into eclogite according to the eclogite stability field given in Hacker (1996). The P-T-range of a phase transition has to be defined per material and several phasechanges with the same material are possible. The user can also choose whether or not to apply the retrograde transformation back to the initial material. The phase changes subroutine is executed after the advection/remeshing part of each time step (Fig. 11 (III)). The phase change procedure is not mass conserving and Hetényi et al. (2011) showed that this can significantly change the model behaviour. A mass-conserving method would be applying dilatational forces to the Eulerian elements at the time step they are affected by phase changes, as applied in the SOPALE code used by Warren et al. (2008) and subsequent work. Nevertheless as we are only interested in the first order effects of phase changes, we consider our approach as sufficient.

3.4 Model setup and boundary conditions

In this chapter the model setup and boundary conditions are explained with figure 12 and table 2 being the visual references. The choice of parameters follows mainly the values and laws introduced in the previous chapters, but an augmenting reasoning for the parameter choices is given where necessary. After the model setup description, the model sets presented in the results chapter are introduced and explained.

Oceanic subduction under continental lithosphere is modelled by using an idealised upper

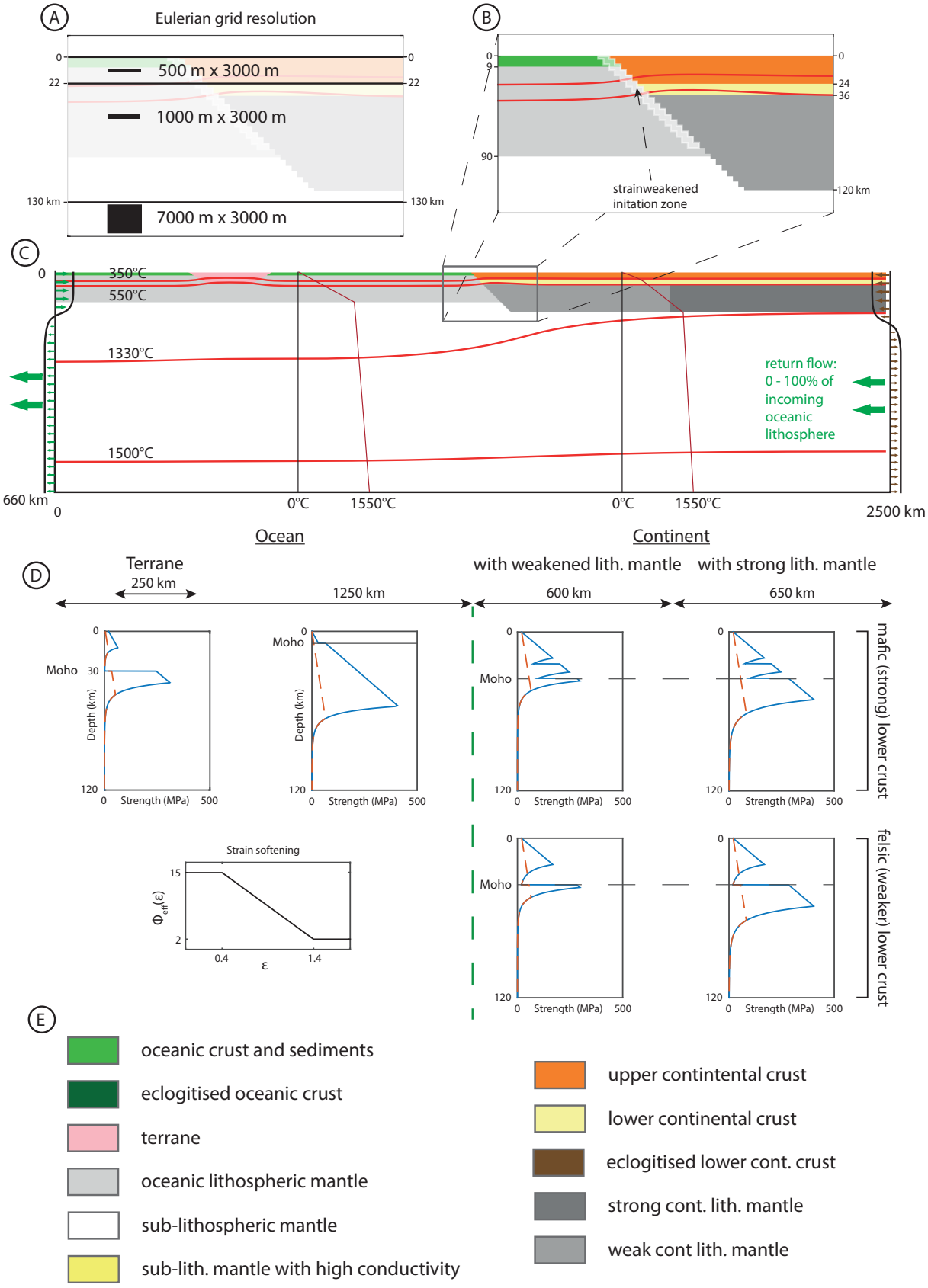

Figure 12: (Caption of figure on the next page.)

Figure 12 (Continued): Initial model setup and boundary conditions. (A) Eulerian grid resolution. (B) Zoom into the transition zone between oceanic and continental lithosphere with the thicknesses of the layers and the strain-weakened zone, which is implemented to initiate subduction. (C) Whole model domain at thermal steady state with temperature contours (red lines) and two temperature profiles for the oceanic and continental lithosphere. The same temperature contour lines are going to be used for all following modell snapshots in the results chapter. The velocity boundary conditions are sketched at the sides of the model domain. Inflow of oceanic or continental lithosphere is compensated by mantle outflow on the same boundary respectively. Poloidal return flow is modelled by inflow of mantle material on the right and equal outflow on the left side. The figure shows one terrane in the oceanic domain. Yet there can be none, one or two of those. (D)Yield-strength-envelopes (YSE) for the different materials and strain softening diagram. The flow laws for the oceanic plate and the terrane are the same for all models. The rheology of the lower crust is investigated in two model sets with the corresponding pair of (YSE). (E) Legend of the material colour-coding.

mantle scale model domain box with 2500 km horizontal and 660 km vertical extent (Fig. 12(C)). The lithospheric domain is divided in the middle by a boundary dipping 45° to the right. The left half contains oceanic lithosphere and the right half contains continental lithosphere. The oceanic lithosphere consists of 9 km of oceanic crust and sediments, and 81 km of lithosperic mantle. Due to insufficient resolution, sediments and oceanic crust are approximated by one material. The continental lithosphere consists of a 24 km thick upper crust, a 12 km thick lower crust and a lithospheric mantle reaching 120 km depth. The thicknesses of the lithospheric layers were chosen to reflect average thicknesses as described in section 2.3. The intra-oceanic terrane has a thickness of 30 km and is 250 km wide. This is slightly thicker than the average thickness of future allochthonous terranes (21 km to 26 km) as reviewed by Tetreault and Buiter (2014), but considered as a good approximation since we are mainly interested in the first order influence of terrane accretion.

The Eulerian grid consists of 833 elements in the horizontal and 227 elements in the vertical direction. The horizontal elemental distribution is regular resulting in a horizontal resolution of 3000 m. The vertical resolution is irregular, with 44 elements in the upper most 22 km, 108 elements in the following 108 km and 75 elements between 130 km and 660 km depth. Consequently, the vertical resolution is 500 m in the upper crust, 1.0 km in the adjacent lithosphere up to 130 km depth and 7.1 km in the sub-lithospheric mantle (Fig. 12(A)). The grid refinement was used to increase the resolution in the lithosphere but attain a reasonable computation time. To track deformation, an additional grid called 'visugrid' is advected after each time-step.

Fig. 12(C) shows the lithospheric domain in thermal steady state. The values for heat flow and heat production were again chosen to reflect average values (see section 2.3 and table 2). Heat conductivity is temperature dependent as explained in 3.3.2 and has the same values for all materials. Heat production is restricted to the continental crust and continental terrane(s). The lower boundary is set to be 1550 °C and the sub-lithospheric mantle has an adiabatic gradient of 0.4 °C/km. The side boundaries are isolated and the top boundary is set to 0 °C. This results in an initial thermal setup with ~1330 °C at the lithosphere-asthenosphere boundary in the continental part and ~1300 °C at the same boundary in the oceanic domain. The thickness and

thermal profile of the oceanic lithosphere correspond to an age greater than 70 Myr (Stein and Stein, 1992). The Moho temperature in the continental lithosphere is around 550 °C and the continental surface heat flow is ~53 mW m^{-2}.

Subduction of the oceanic plate under the continental plate is driven by a velocity boundary condition applied at the left side of the model domain (Fig. 12(C)). Thereby inflow of lithospheric oceanic material is compensated by outflow of sub-lithospheric mantle on the same side. This boundary condition leads to a subduction system which only has a poloidal flow component and can thus be interpreted as to represent the centre of wide subduction zones. Yet subduction zones can be influenced by toroidal return flow as well, if considering a small subduction zone or a setting near a slab edge. This flow can self-consistently only develop in 3D numerical models but an approximation can be made by imposing an additional sub-lithospheric mantle flow pattern with outflow on the left boundary compensated by inflow on the right boundary. In nature the return flow pattern is difficult to constrain as it can not be directly observed. We use a simplified approach by setting the return flow value to be a percentage of the incoming oceanic material. Hence for instance 100% return flow doubles the outflow on the sub-lithospheric left boundary. This method has the disadvantage that different subduction velocities lead to slightly different return flow velocities. However, the differences are small, and addtionally this boundary condition allows for comparability of different subduction velocities in terms of relative mass fluxes and hence accounts for the fact that return flow is a mass transfer from behind the slab to the frontal part of the slab rather than a constant velocity. The overriding plate can also move with a similar boundary condition as the oceanic plate (see Fig. 12(C)).

The materials used in this thesis have both plastic and viscous properties (table 2), as described in section 3.2.3. In the plastic domain the materials soften in a prescribed range between 40-140 % strain (Fig. 12(D)). Thereby the effective angle of internal friction (ϕ) for all materials except the oceanic crust and the intra-oceanic terrane is reduced from 15-2°. The cohesion stays unchanged at 20 MPa. To account for frictionally weak sediments on the oceanic crust and the oceanic plateau, ϕ is softened from 7-2° and the cohesion is softened from 20 MPa to 4 MPa for those two materials.

Viscous deformation is approximated using flow laws derived from laboratory experiments. Rheological flow laws are very sensitive to laboratory conditions such as strain rate and fluid fugacity. Hence their extrapolation and application to nature is subject to considerable uncertainties. Therefore a linear scaling factor f is used to scale the effective viscosities relative to their laboratory results. This approach has the advantage to test different geological setups without using additional flow laws with further uncertainties (Beaumont et al., 2006). The oceanic crust is approximated by a dry Maryland diabase rheology (Mackwell et al., 1998), scaled down by a factor of 10 to approximate wetter conditions as during the experiment. The continental upper/mid crust is approximated by a wet quartz flow law (Gleason and Tullis, 1995), which is up-scaled by $f = 5$. The composition of the lower crust is still enigmatic (see 2.3; Hacker et al., 2015). Therefore we test the sensitivity of our model to a felsic (granitoidal) lower crust and to a basaltic lower crust. The felsic lower crust is approximated by the wet quartz flow law

with $f = 5$, and the basaltic lower crust is approximated by the dry Maryland diabase flow law with $f = 0.1$. Tetreault and Buiter (2012) showed with numerical models that terrane accretion in subduction zones is only possible when the terranes are weak or have weak zones. The assumption that terranes are weak is geologically reasonable, as they include zones of (formerly) tectonic or volcanic activity. Accordingly the terranes in our model are characterised by the wet quartz flow law scaled down by $f = 0.5$. The mantle lithosphere and the sub-lithospheric mantle both consist of olivine and can thus be represented by the wet olivine flow law by Karato and Wu (1993). Yet their viscosities can vary significantly due to, amongst others, the presence of fluids or the amount of melt depletion, as described in section 2.3. Therefore, the oceanic and continental melt-depleted and volatile poor lithospheric mantle is approximated by scaling the olivine flow law by $f = 10$, and the fertile sub-lithospheric mantle is approximated by scaling the flow law with $f = 1$. To account for fluids introduced by the subducting slab into the mantle, and inherited structures, the back-arc lithospheric mantle is scaled down by a factor $f = 0.5$ over a horizontal distance of 600 km. The scaling factor is consistent with heat flow observations from modelling results by (Currie et al., 2008). The overall setup is similar to models from Currie et al. (2008).

The densities of the materials in the model domain have nominal initial temperatures close to expected temperatures in a thermally stable average lithospheric setup. During all experiments the densities of the oceanic and lower continental crust change due to metamorphic phase changes in the eclogite stability field. The densities and P-T-conditions for the phase changes are chosen from Hacker (1996). The high oceanic eclogite density (3350 $\mathrm{kg/m^3}$) represents the mafic composition of the oceanic crust and the lower continental lower crust eclogite density (3100 $\mathrm{kg/m^3}$) accounts for lithological heterogeneities. To show the effect of lower crustal eclogitisation, an additional set of models was run without eclogitisation of the lower crust. Delamination of the lower crust is commonly said to be connected to high pressure densification reactions of the lower crust inducing densities of 3500-3600 $\mathrm{kg/m^3}$ (Wolf and Wyllie, 1993; Rapp and Watson, 1995; DeCelles et al., 2009). We try to test how those high densities effect roll back or mountain building in subduction zones and run a model set with higher lower crustal eclogite densities (3500 $\mathrm{kg/m^3}$) as well. The P-T-field for this densification reaction is a bit different, but to keep things simple we use the same P-T-stability field as for the other phase changes.

As the lower boundary of the model is fixed, the subducting slab would after some time interact with it. We want to model the deformation patterns in the lithosphere independent of the slab interactions with the lower mantle transition zone. Hence, an artificial phase change is introduced at pressures relating to 500 km depth. Lithospheric material which crosses this boundary is changed into sub-lithospheric mantle with very high thermal conductivity. Through intensive testing we found out that changing the thermal conductivity from k = 52 to 312 through a temperature range of $T = 1000$ to 1050 °C gives the best trade off between weakening through fast heating and retention of a natural thermal profile in the lower part of the slab. After the new material has heated up to 1350 °C, it is converted to sub-lithospheric mantle. With this approach, we ensure that deformation processes in the lithosphere are not influenced by interactions of the

Table 2: Mechanical and thermal properties of the materials.

Parameters	Oceanic plate			Continental plate				
	Crust	Mantle lithospere	Terrane	Upper/mid crust	Lower crust (mafic,strong)	Lower crust (felsic,weak)	Mantle lithosphere [weak][e]	Sub-lithospheric mantle
Plastic rheology								
C - $C_{softened}$ (MPa)	20-4	20-20	20-4	20-20	20-20	20-20	20-20	20-20
ϕ - $\phi_{softened}$ (°)	7-2	15-2	7-2	15-2	15-2	15-2	15-2	15-2
Viscous rheology								
Flow law[a]	DMD	WOL	WQ	WQ	DMD	WQ	WOL	WOL
f	0.1	10	0.5	5	0.1	5	10 [0.5][a]	1
A ($Pa\,s^{1/n}$)[b]	5.78×10^{-27}	1.76×10^{-14}	8.57×10^{-28}	8.57×10^{-28}	5.78×10^{-27}	8.57×10^{-28}	1.76×10^{-14}	1.76×10^{-14}
n	4.7	3.0	4.0	4.0	4.7	4.0	3.0	3.0
Q (kJ mol^{-1})	485	430	223	223	485	223	430	430
V ($cm^3\,mol^{-1}$)	0	1×10^{-5}	0	0	0	0	1×10^{-5}	1×10^{-5}
Density parameters								
ρ_0 ($kg\,m^{-3}$)	2900	3250	2800	2800	2950	2950	3250	3250
ρ_0 HP ($kg\,m^{-3}$)[c]	**3350**	3250	2800	2800	**3100 or 3500**	**3100**	3250	3250
T_0 (°C)	0	1330	200	200	400	400	1330	1330
α (K^{-1})	3×10^{-5}	3×10^{-5}	3×10^{-5}	3×10^{-5}	3×10^{-5}	3×10^{-5}	3×10^{-5}	3×10^{-5}
Thermal parameters								
k ($W\,m^{-1}$)[d]	2.25	2.25	2.25	2.25	2.25	2.25	2.25	2.25
H (µW m^{-3})	0	0	1.1	1.1	0.5	0.5	0	0
c_p ($J\,kg^{-1}$ K)	750	1250	750	750	750	750	1250	1250

[a] WQ is the wet quartz flow law as described in Gleason and Tullis (1995); DMD is the dry Maryland flow law from Mackwell et al. (1998); WOL is the wet olivine flow law from Karato and Wu (1993).
[b] The laboratory derived preexponential flow law exponent has been converted to conform with the second invariants of the stress and strain rates used in the model approach.
[c] Metamorphic high pressure equivalents. The P-T-field for the metamorphic reaction coincides with the eclogite stability field from Hacker (1996). Only bold values display changes.
[d] Thermal conductivity for low temperatures. Between 1335 °C and 1345 °C the conductivity linearly increases from 2.25 to 52.0 for all materials.
[e] In square brackets are values for the weak back-arc lithospheric mantle near the subduction zone.

slab with the lower model boundary.

3.5 Numerical initiation and termination procedures

3.5.1 Subduction initiation

To ensure comparability of the models and proper subduction initiation, each model has a precursor isostatic compensation and subduction initiation phase: After the thermal steady state calculations, each model is run with varying small time steps and free slip side boundary conditions until it achieves isostatic steady state. Thereby the oceanic domain subsides by around 2.3 km. Consequently the continental plate rises by the same amount. Subsequently the models are run for 11 Myr with a constant subduction velocity of 5 cm/yr (550 km plate convergence). Subduction is initiated in the transition zone between continental and oceanic plate through a 10 km wide strain weakened zone (Fig. 12(B)). During the subduction initiation phase the return flow boundary conditions are, if included, switched on, but the continental plate is not moving. Furthermore the continental lower crust has the mafic rheological flow laws (Fig. 12(D)) during this phase. The whole continental lithospheric mantle is strong for the first 4 Myr (200 km of convergence) with $f = 10$. Afterwards the back-arc lithospheric mantle is weakened to $f = 0.5$. After 11 Myr the boundary conditions and rheologies change according to the investigated parameter set and are constant throughout the model run. The various pre-run phases were implemented so that subduction initiation deforms the continental margin as little as possible, but in the same way for all models. Thereby we assume that the processes of interest occur independent of subduction initiation.

3.5.2 Model termination

After subduction initiation, the models are run to a predefined age of commonly 125 Myr. Only the terrane accretion models and the inheritance models have different final ages of 100 Myr and 235 Myr, respectively. To minimize the computation time, the models were run using adaptive time-stepping calculated with the Courant-Friedrichs-Lewy criterion (cfl = 0.1). At some point the models can develop unnatural behaviour, which is commonly connected to forced convergence of the Stokes equation or a model crash. Usually this happens when one plate moves close to the model domain or when the continental plate is shortened for more than 600 km and the weak lithospheric mantle is consumed. If a model developed an unnatural behaviour, it was cut at the last reasonable position with the corresponding time t_{max}.

3.6 The model sets and their intention

Altogether 71 models (Table 3) were run to investigate the three questions posed in the introduction chapter:

1) How does the overriding plate (OP) in a subduction system deform when including a 3D mantle flow pattern and absolute plate motions?; 2) How do phase changes associated with lower

crustal delamination and extensional inheritance affect a compressional subduction system?; and 3) How does the accretion of intra-oceanic features like continental plateaus or terranes affect crustal thickening in a contractional subduction system in the long term?

To assess question 1), two model sets with 27 models each were run with the same varying velocity boundary conditions but a strong (SL) and a weak lower continental crust (WL), respectively. Thereby, the subduction velocity was varied between 3, 5, and 7 cm/yr, the velocity of the overriding plate was varied between 0, 1, and 2 cm/yr (directed towards the trench) and the return flow values were varied between 0 %, 50 %, and 100 %. The velocities were chosen to be in accordance with common values of absolute plate velocities (see Fig. 2). We only consider overriding plate movement which is directed towards the trench, as we assume that movement directed away from the trench leads to extension in the overriding plate. Nevertheless, three models were run where the overriding plate moves away from the trench, because they show the influence of the subduction velocity. The group of models connected to research question one were called absolute plate motions (APM) models.

To investigate the influence of metamorphism as posed in question 2), two sets with three models each were run. For each model set, the subduction velocity was constant with 5 cm/yr, but overriding plate velocity was varied between 0, 1 and 2 cm/yr . One model set was run without eclogitisation of the lower continental crust (lcc) and one with a heavy ($\rho = 3500\,\mathrm{kg/m^3}$) lower crustal eclogite.

The APM models all start from the simple layered model setup of Fig. 12. Yet the Earth is a dynamic system and inheritance of structures plays probably an important role. Hence to model a more complex subduction history, additional four models were run, where a precursor extensional setting is followed by a contractional setting. These models represent the second, extensional inheritance-related part of research question two. A subduction velocity of 3 cm/yr and no return flow or overriding plate movement is inducing the extensional OP strain regime in the overriding plate for the first 100 Myr. Subsequently, the subduction velocity increases to 7 cm/yr and the OP moves towards the trench with 2 cm/yr, thus inducing a contractional OP strain regime. The latter values were initially chosen, because they represent present-day velocities in the central Andes. However, as we will see in the next chapters, structures generated in a contractional setting are similar for different subduction and OP velocities. Thus the same results are expected for slightly varying velocities, as long as they induce a contractional overriding plate strain regime. The eclogitisation of the lower crust is varied as described above (models 1-3). Furthermore the strength of the lower continental crust is reduced (model 4).

To investigate question three, four models were run with combinations of one or two terranes and subduction velocities varying between 3 and 5 cm/yr. Thus the response between subduction velocity and the amount of terranes stacked at the margin was investigated. The same model set was run with weaker terranes with a flow law of wet quartz scaled by $f = 0.1$. The results are similar and therefore not shown here.

Table 3: Models presented in the Thesis. Positive velocities are directed towards the trench. t_max is the model run time. SL stands for a strong and WL for a weak lower continental crust. The model setup marked in blue is the reference model.

		Name	$v_{oceanic}$ (cm/yr)	$v_{cont.}$ (cm/yr)	return flow (%)	t_{max} (Ma)	Described in figure
Absolute plate motion models	The effect of $v_{oceanic}$	SL_v3_cont-1_ret0	3	-1	0	63	15
		SL_v5_cont-1_ret0	5	-1	0	75	15
		SL_v7_cont-1_ret0	7	-1	0	75	15
	Mafic (brittle/strong) lower continental crust (SL)	SL_v3_cont0_ret0	3	0	0	125	16
		SL_v3_cont0_ret05	3	0	50	125	
		SL_v3_cont0_ret1	3	0	100	100	
		SL_v3_cont1_ret0	3	1	0	121	
		SL_v3_cont1_ret05	3	1	50	125	
		SL_v3_cont1_ret1	3	1	100	125	
		SL_v3_cont2_ret0	3	2	0	60	
		SL_v3_cont2_ret05	3	2	50	65	
		SL_v3_cont2_ret1	3	2	100	66	
		SL_v5_cont0_ret0	5	0	0	125	14
		SL_v5_cont0_ret05	5	0	50	125	16
		SL_v5_cont0_ret1	5	0	100	90	16
		SL_v5_cont1_ret0	5	1	0	78	18
		SL_v5_cont1_ret05	5	1	50	125	
		SL_v5_cont1_ret1	5	1	100	125	17
		SL_v5_cont2_ret0	5	2	0	50	18
		SL_v5_cont2_ret05	5	2	50	58	
		SL_v5_cont2_ret1	5	2	100	60	18
		SL_v7_cont0_ret0	7	0	0	125	17
		SL_v7_cont0_ret05	7	0	50	125	
		SL_v7_cont0_ret1	7	0	100	50	
		SL_v7_cont1_ret0	7	1	0	60	
		SL_v7_cont1_ret05	7	1	50	115	
		SL_v7_cont1_ret1	7	1	100	60	
		SL_v7_cont2_ret0	7	2	0	38	
		SL_v7_cont2_ret05	7	2	50	35	
		SL_v7_cont2_ret1	7	2	100	46	
	Felsic (viscous/weak) lower continental crust (WL)	WL_v3_cont0_ret0	3	0	0	125	
		WL_v3_cont0_ret05	3	0	50	125	
		WL_v3_cont0_ret1	3	0	100	103	
		WL_v3_cont1_ret0	3	1	0	100	
		WL_v3_cont1_ret05	3	1	50	100	
		WL_v3_cont1_ret1	3	1	100	125	
		WL_v3_cont2_ret0	3	2	0	60	
		WL_v3_cont2_ret05	3	2	50	50	
		WL_v3_cont2_ret1	3	2	100	53	
		WL_v5_cont0_ret0	5	0	0	125	
		WL_v5_cont0_ret05	5	0	50	125	19
		WL_v5_cont0_ret1	5	0	100	80	
		WL_v5_cont1_ret0	5	1	0	60	19
		WL_v5_cont1_ret05	5	1	50	100	
		WL_v5_cont1_ret1	5	1	100	125	
		WL_v5_cont2_ret0	5	2	0	40	19
		WL_v5_cont2_ret05	5	2	50	38	
		WL_v5_cont2_ret1	5	2	100	37	
		WL_v7_cont0_ret0	7	0	0	125	
		WL_v7_cont0_ret05	7	0	50	95	
		WL_v7_cont0_ret1	7	0	100	60	
		WL_v7_cont1_ret0	7	1	0	50	
		WL_v7_cont1_ret05	7	1	50	87	
		WL_v7_cont1_ret1	7	1	100	80	
		WL_v7_cont2_ret0	7	2	0	25	
		WL_v7_cont2_ret05	7	2	50	33	
		WL_v7_cont2_ret1	7	2	100	37	

Table 3 (Continued): Models presented in the Thesis. The boundary conditions for the extension - compression models ('Andes') change after 100 Myr of model evolution to the values in brackets. no_lcc means no eclogitisation in the lower continental crust (lcc). heavy_lcc means eclogitisation of the lcc with a desnity of 3500 kg/m^3.

		Name	$v_{oceanic}$ (cm/yr)	$v_{cont.}$ (cm/yr)	return flow (%)	t_{max} (Ma)	Described in figure
The effect of lcc eclogitisation	no lcc eclogite	SL_v5_cont0_ret0_no_lcc	5	0	0	125	
		SL_v5_cont1_ret0_no_lcc	5	1	0	85	21
		SL_v5_cont2_ret0_no_lcc	5	2	0	45	
	heavy lcc eclogite	SL_v5_cont0_ret0_heavy_lcc	5	0	0	125	
		SL_v5_cont1_ret0_heavy_lcc	5	1	0	78	21
		SL_v5_cont2_ret0_heavy_lcc	5	2	0	44	
Inheritance models		SL_v3(7)_cont0(2)_ret0	3(7)	0(2)	0	235	22
		SL_v3(7)_cont0(2)_ret0_no_lcc	3(7)	0(2)	0	212	22
		SL_v3(7)_cont0(2)_ret0_heavy_lcc	3(7)	0(2)	0	235	22
		WL_v3(7)_cont0(2)_ret0	3(7)	0(2)	0	235	22
Terrane models		SL_v3_cont0_ret0_1terrane	3	0	0	100	23
		SL_v3_cont0_ret0_2terrane	3	0	0	100	23
		SL_v5_cont0_ret0_1terrane	5	0	0	100	
		SL_v5_cont0_ret0_2terrane	5	0	0	100	23

4 Results

4.1 Structure of the Results chapter

The sub-sections of the results chapter follow the order of the three research questions as presented in the previous chapter with some further subdivisions. First the structures which developed through subduction initiation during the first 11 Myr are described. Those structures are the same for all models. The chapter is followed by the description of the reference model with focus on structures which can be found in most models.

Subsequently the APM models are investigated in more detail and through six subsections. The first of those highlights the influence of the subduction velocity. The following three chapters focus on different structures which can be found in an extensional, neutral or contractional OP strain regime, and which combinations of return flow and overriding plate movement are necessary to produce those structures. As the influence of the subduction velocity ($v_{oceanic}$) is already examined in the first APM-section, mainly models with a subduction velocity of 5 cm/yr are shown. Only when the subduction velocity has a significant influence on the result, models with lower or higher subduction velocities are discussed as well. Sub-chapter five focuses on structural differences induced by a weak lower crust, and chapter six gives a statistical analysis relating the subduction velocity, OP velocity and return flow values to different overriding plate strain regimes.

The three subsequent chapters directly follow the research questions as described above, with models showing structural differences induced by different lower continental crustal eclogitisation, the inheritance models and models describing structures related to terrane accretion.

Every sub-chapter is accompanied by one reference figure in A4 or A3 depending on the chapter's extent. The figures contain two types of sub-figures: model snapshots at a certain time step and the evolution of the free-surface through time. All snapshots show the material distribution, the velocity field as arrows with relative length and the temperature field as contour lines with the 350 °C, 550 °C, 1330 °C, 1500 °C contours from top to bottom (as in Fig. 12). Some snapshots additionally show the strain rate field in grey-scale as semi-transparent overlay. This highlights deforming and darkens stable areas. Due to the big amount of models which were run, only a selection of model-snapshots is shown. For additional visualization, videos of all models listed in table 3 can be found on the supplementary CD or in this dropbox folder: https://www.dropbox.com/sh/czx0o3vokptlelh/AABTiXboioWi-PcWGXIb5qRYa?dl=0 .

4.2 The reference model

4.2.1 Subduction initiation structures

During the first 4 Myr of subduction initiation, the whole continental lithospheric mantle is strong with a scaling factor of $f = 10$. This makes the continental plate rigid so that the initial push of oceanic lithosphere is directed downwards and most of the crustal deformation is localized in the subduction channel (Fig. 13(I)). Meanwhile the margin gets uplifted to up to over 7 km height over a ~200 km wide zone. At 4 Myr the 600 km wide back-arc lithospheric mantle is weakened by reducing the scaling factor to $f = 0.5$. This results in rapid subsidence of formerly high elevated regions, partly even below sea level. Back-arc weakening furthermore facilitates slab penetration into the back-arc lithosphere. With increasing subduction depth, the subduction direction is more and more directed downwards, thereby dragging along weak lithospheric mantle material. This is enhanced by the development of two poloidal flow cells behind and in front of the slab (Fig. 13(III)). The poloidal flow cells advect the temperature field upwards in the oceanic domain and a corner flow pattern develops near the trench in the continental domain.

The slab is still relatively cold and thus stiff at depth, indicated by low strain rates, and keeps its bent structure inherited from the subduction interface. Therefore the slab turns over at depth. Eclogitisation of the lower continental crust starts around 4 Myr, and the first eclogite in the oceanic crust forms around 2.5 Myr. Note also that despite the strong continental lithosphere during the first 4 Myr, the subduction initiation phase leads to crustal thickening of the continental arc region to up to 50 km. The final subduction initiation step at 11 Myr looks similar to Fig. 13(III), but with a slightly higher plate convergence of 550 km.

4.2.2 General observations during stationary long term subduction

The model termed reference model has a subduction velocity of 5 cm/yr, no return flow and no OP movement as boundary conditions. The model is stable and shows no significant trench

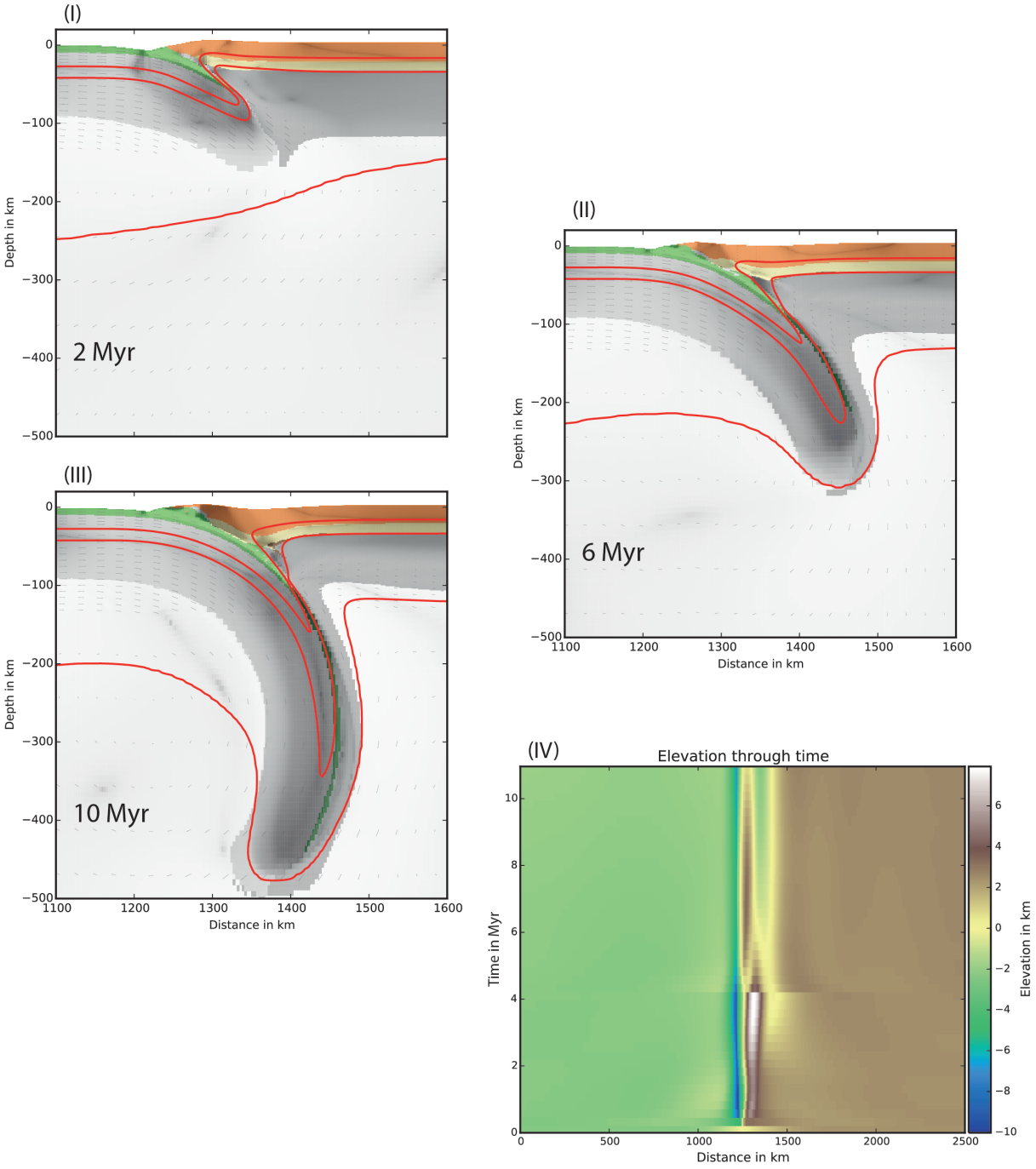

Figure 13: Four sub-figures showing the subduction initiation structures for 2 Myr, 6 Myr, 10 Myr, and the free-surface evolution of the whole initiation phase. (I) Early push phase during which the continental lithosphere is strong, and convergence is directed downwards into the sub-lithospheric mantle. (II) Weakening of the back-arc lithospheric mantle leads to slight advance of the slab. Two poloidal flow cells develop behind and in front of the slab, which advect the sub-lithospheric temperature field upwards. Additionally a corner flow pattern develops. (III) Subduction configuration shortly before the end of the subduction initiation phase. Subduction is directed downwards and drags along weak lithospheric mantle. Note the stiff, overturned slab at depth which keeps its structure inherited from the subduction interface. (IV) Elevation through time plot showing strong uplift of the arc region during the first 4 Myr followed by subsidence of the back-arc-region even below sea level after weakening of the back-arc lithosphere.

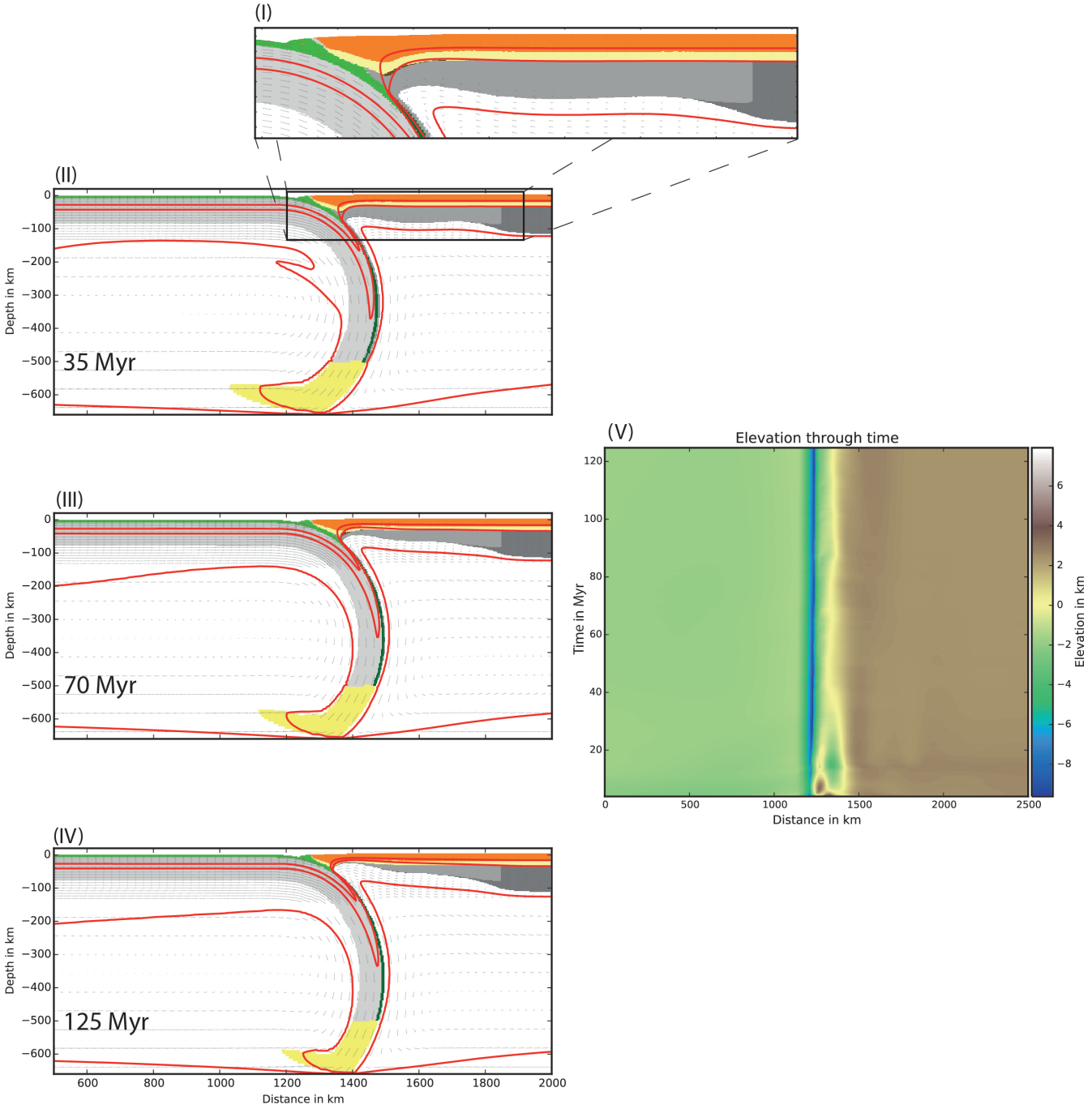

Figure 14: Figures showing different snapshots at 35 Myr, 70 Myr and 125 Myr, and the free-surface elevation evolution of the reference model. (I) Zoom into the lithospheric realm of (II). Note the undulated structure of the weak lithospheric mantle with one elevated region near the plate interface, and one elevated region near the boundary between the weakened and strong continental lithospheric mantle. (II), (III) and (IV) show steady subduction with little structural differences. The removal of weak continental lithospheric mantle through corner flow increases with time and the continental lithosphere thins to <40 km. The kink in the 1330 °C isotherm in (II) originates from two initial adjacent poloidal flow cells in the oceanic domain. (V) The steady state of the subduction zone is expressed by a straight trench line in the free-surface evolution plot.

movement and change in overriding plate elevation throughout the model run. The monotonous behaviour is convenient, as it illustrates general processes and structures applicable to all other models.

The poloidal flow cell in front of the slab progressively moves weakened lithospheric material towards the trench, where it is dragged downwards with the subducting slab. Thereby the lithosphere-asthenosphere boundary (LAB) develops an undulated pattern with two elevated regions (Fig. 14(I)). One of thoses regions is situated near the trench, and the other elevated LAB region is in the vicinity of the boundary between the weak and strong continental lithospheric mantle. The latter is shifted a bit to the right from the actual boundary, as poloidal flow drags the strong lithospheric mantle a few kilometres towards the trench, draping and protecting the overlying weak lithosphere from removal (Fig. 14(I)).

With proceeding subduction, the lithospheric mantle gets further thinned through corner flow. After around 70-80 Myr it is almost completely transferred downwards so that corner flow starts to erode continental crust, thereby removing the little portion of lower continental crust eclogite which had formed (Fig. 14(III,IV)). Note that the continental margin gets slightly eroded by subduction erosion, compensated by extension in the OP.

Fig. 14(II) shows a loop in the 1330 °C temperature contour line, which is absent in the following model development. The loop is related to the initial mantle flow pattern in the oceanic domain which consists of two adjacent poloidal flow cells inducing a downward advection of the temperature field at their junction. With proceeding subduction, the two poloidal flow cells merge together as one cell. Hence the temperature contour loop only develops once and is gone when subducted downwards at around 40 Myr.

4.3 Absolute plate motion models

4.3.1 Influence of the subduction velocity

We ran three models with an OP velocity of -1 cm/yr and varying subduction velocities of 3, 5 and 7 cm/yr. Thereby first insight into extensional structures can be gained. Additionally and more importantly, when moving away and extending the overriding plate, the system is more sensible to back- and forwards directed movement induced by the subducting slab. This nicely shows the influence of the subduction velocity.

All three models have in common that the movement of the overriding plate induces back-arc opening after a certain time of subduction (Fig. 15). Furthermore back-arc opening uses and is focused in the weak zone induced by the elevated LAB at the boundary between weak and strong continental mantle lithosphere. During back-arc opening, a more than 500 km long continental piece remains attached to the trench, while the continental hinterland moves out of the model domain with 1 cm/yr. When the subduction velocity is slow (3 cm/yr), back-arc opening happens at around 20 Myr (Fig. 15(A)). Back-arc opening is followed by trench retreat with approximately 0.25 cm/yr, and slight slab flattening. A moderate subduction velocity of 5 cm/yr delays back-arc opening to ~25 Myr and the trench position does not change during

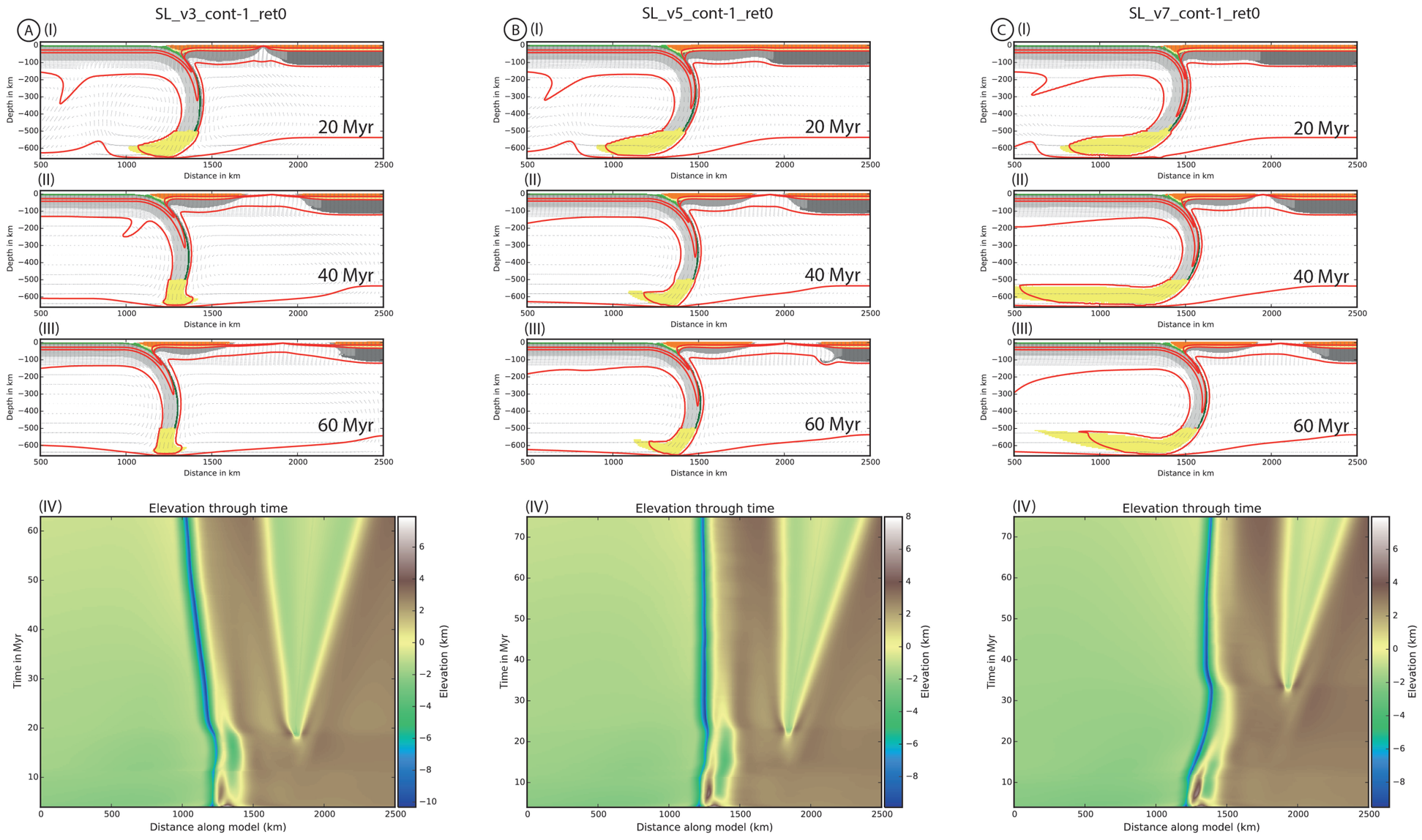

Figure 15: Figure consisting of three sub-figures (A-C), each representing a model setup with different subduction velocity and an OP velocity of -1 cm/yr. The sub-figures consist of three cross sections from the respective model run for 20 Myr, 40 Myr and 60 Myr, and the corresponding free-surface evolution plot. (A) Figures showing the influence of a slow subduction velocity of 3 cm/yr. Continental break up happens at 20 Myr (I) and in the following period, the subduction zone slowly retreats. (B) Figures showing the influence of a medium subduction velocity of 5 cm/yr. Continental break-up is delayed and happens at around 25 Myr. During proceeding subduction, the trench position is stable. (C) Figures showing the influence of a high subduction velocity of 7 cm/yr. Back-arc opening happens significantly later than in (A) and (B), at around 30-35 Myr. The trench is generally moving landwards with higher velocities before back-arc opening.

proceeding subduction (Fig. 15(B)). When the subduction velocity is high (7 cm/yr), back-arc opening is even further delayed to ~35 Myr. During the first 35 Myr of subduction, the oceanic slab follows the retreat of the continental lithosphere and becomes further overturned (Fig. 15(C)(I)). When the back-arc opens, the overturned slab leads to slight trench retreat until a stable subduction angle is achieved. Subsequently the trench advances slightly with of $<$ ~0.2 cm/yr.

The different subduction velocities have also direct influence on the mantle flow velocity and thus on the corner flow speed. Hence the removal of weak lithospheric mantle is sped up by higher subduction velocities (compare Fig.15(A-C)(III)).

The three models show that higher velocities favour subduction zone advance, and lower velocities favour subduction zone retreat. Furthermore a higher subduction velocity increases corner flow induced removal of the continental lithospheric mantle.

4.3.2 Extension in the overriding plate - the influence of return flow

The previous chapter showed that extension in the overriding plate can be invoked by a retreating OP. This chapter focuses on how different extensional structural styles in the overriding plate develop in relation to an interplay between the subduction velocity and amount of return flow.

In chapter 4.3.1 we showed that a slow subduction velocity favors trench retreat. This does also affect a subduction setting where the OP is not moving and is presented by model SL_v3_cont0_ret0 (Fig. 16(A)). The weak lithospheric mantle is continuously convectively removed (Fig. 16(A)(I)), until the continental lithosphere is sufficiently thinned and a ~150 km wide arc is rifted off the continental plate (Fig. 16(A)(II)). The space for trench retreat is accommodated by slight slab flattening, especially in the sub-lithospheric mantle with high conductivity (as shown in Fig. 15(A)). Additionally subduction erosion of the arc creates space for trench retreat. As these mechanisms are not very effective, the back-arc spreading is slow with an average trench retreat velocity of 0.3 cm/yr and it takes 90 Myr of steady subduction until the continental lithosphere is thinned enough for trench retreat to occur. Furthermore the continental crust does not break during back-arc spreading, but thins extremely.

A similar structural style can be created when including a return flow of 50 % to the reference model (SL_v5_cont0_ret05, Fig. 16(B)). In this setup the subduction zone would be stable without return flow, as shown in chapter 4.3.1, but the return flow leads to subduction zone retreat. Again back-arc spreading is related to thinning of the continental lithosphere through corner flow, but continental break up happens earlier at around 75 Myr. Furthermore the crust breaks up completely and the retreat velocity is around 0.7 cm/yr. Note that subduction erosion diminishes the arc size here as well.

When increasing the return flow value to 100 %, back-arc opening occurs faster (33 Myr, Fig. 16(C,I)) and opening exploits the weakness induced by the elevated LAB at the boundary between the two lithospheric mantle materials. The trench retreat velocity is ~0.8 cm/yr. This

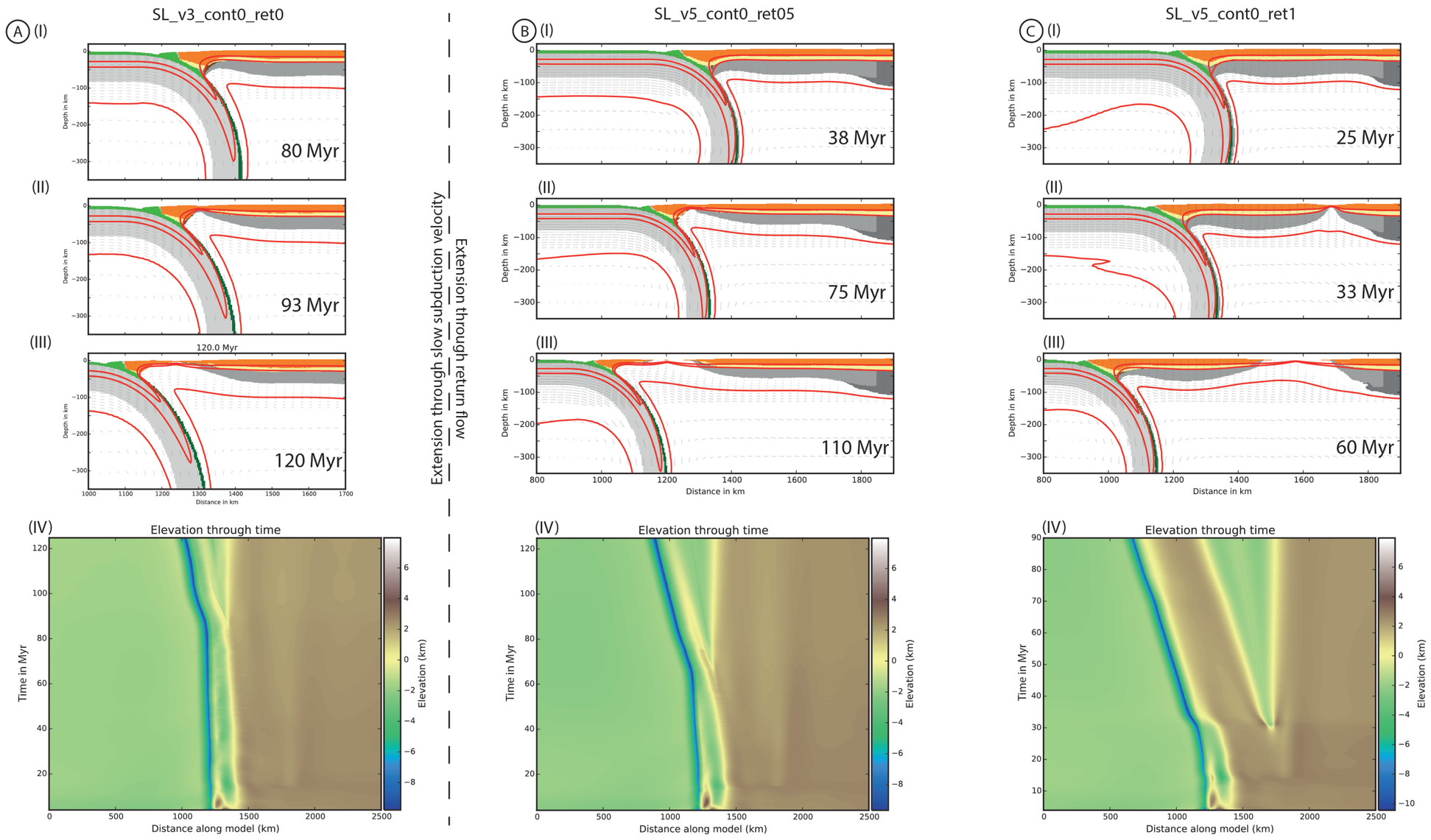

Figure 16: Three sub-figures (A-C) showing snapshots and the free-surface evolution of three models, which show different styles of extension. (A) Snapshots and free-surface evolution of a model with a subduction velocity of 3 cm/yr. After the continental lithosphere is extensively thinned through corner flow, it rips apart at around 90 Myr (II). Extension is accommodated by slight slab flattening and subduction erosion at the margin (III). (B) Snapshots and free-surface evolution of a model with subduction velocity of 5 cm/yr and 50 % return flow. The extensional structures are similar to those in (A), but trench retreat occurs earlier at 75 Myr (II) and the overriding plate breaks up completely (III). (C) Snapshots and free-surface evolution of a model with subduction velocity of 5 cm/yr and 100 % return flow. Extension happens relatively early, at 33 Myr, (II) and continental break up is focused in a zone farther back in the hinterland.

structural style characterized by a wide rifted arc develops with all subduction velocities at high return flow values. Additionally the same structural style develops when subduction velocity is slow (3 cm/yr) and the return flow is only 50 %.

Hence we can conclude that effective trench retreat and back-arc opening can only develop when a toroidal return flow is active. Yet steady, slow long term subduction can also induce extension in the overriding plate, although only after a long time and not very effectively. In our models the actual position where the plate breaks is determined by a trade-off between thinning of the initially thickened arc region through corner flow and the amount of return flow imposed on the subduction system. Thereby high velocities and lower return flow rates enhance corner flow, thus favouring rifting of a small block, while slow velocities and high return flow rates favour back-arc opening further inland and rifting of a wide lithospheric block.

4.3.3 Neutral strain regime in the overriding plate

The reference model already showed that a neutral strain regime in the overriding plate is possible when the continental plate is stationary, return flow is not allowed and the subduction velocity is 5 cm/yr. Fig. 17(A) shows that a neutral OP strain regime is also prevailing when the subduction velocity is higher (7 cm/yr). However, the higher subduction velocity also leads to slight trench advance after the continental lithosphere is considerably thinned through corner flow. The advance is compensated by subduction erosion, and the arc is only slightly thickened (Fig. 17 (A)(II)).

A neutral strain regime can also be created, when the overriding plate velocity balances the plate retreat initiated by return flow (Fig. 17 (B)). Note that in the latter model, overriding plate movement is slightly higher than trench retreat and the arc crust thickens a bit (Fig. 17 (B)(II)). However this thickening is attenuated by subduction erosion and the overall strain regime is neutral.

4.3.4 Shortening in the overriding plate - the influence of overriding plate movement

The previous chapters showed that the overriding plate strain regime is a result of the balance between return flow and overriding plate movement, modulated by the subduction velocities. This chapter describes structures created in a contractional strain regime of the overriding plate and the corresponding parameters.

A contractional strain regime is created by overriding plate movement towards the trench (Fig. 18 (A,B)), if this movement rules out trench retreat induced by return flow (Fig. 18 (C)). Different combinations of overriding plate veolocity and return flow values can induce upper plate shortening. Yet contractional structures are similar in all models and the timing of deformation is the only main difference (Fig. 18). This applies also to models with higher and lower subduction velocities.

Initially the push of the overriding plate is translated into trench retreat, compensated by slab

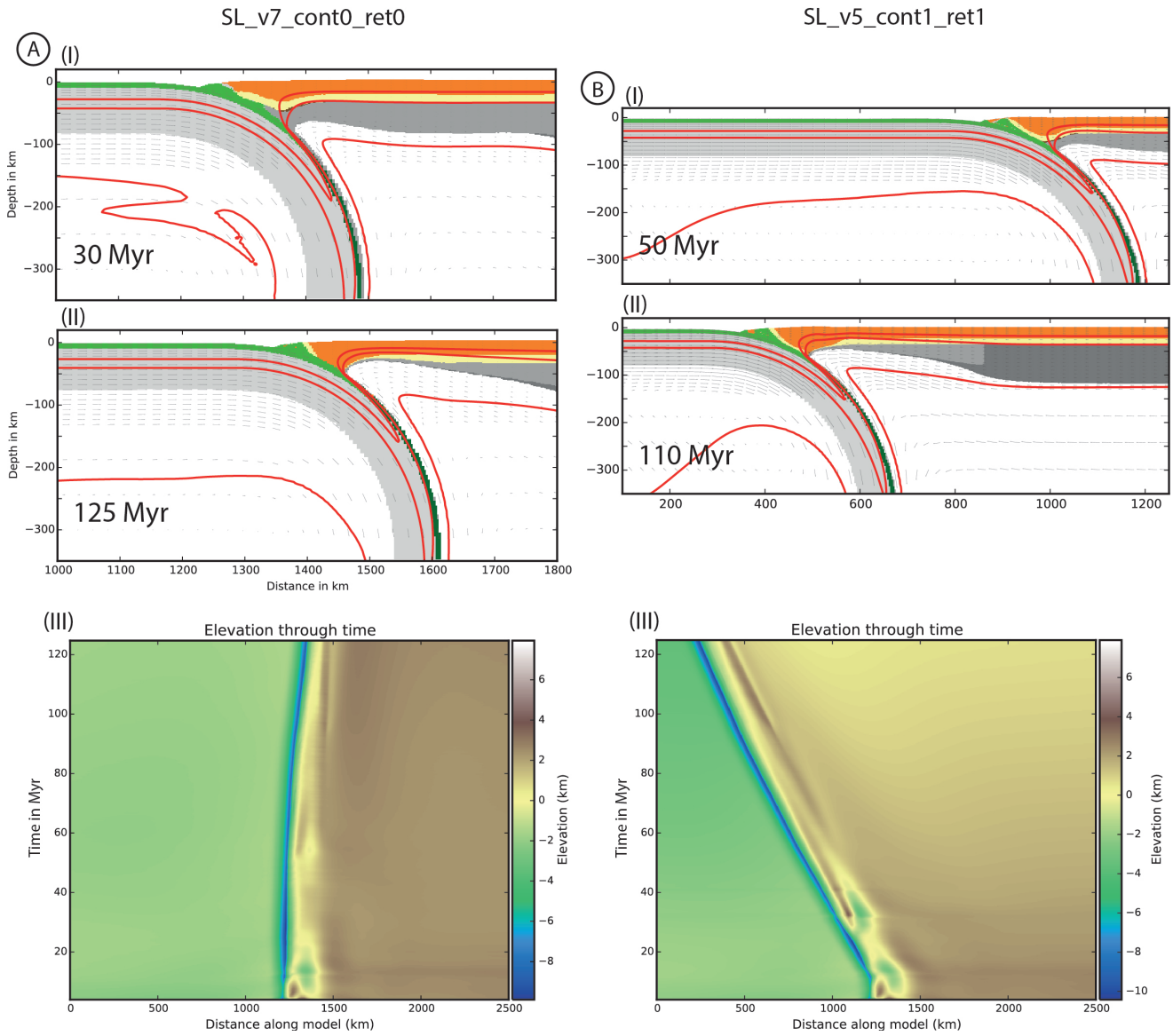

Figure 17: Figure showing two models which have a neutral overriding plate strain regime throughout the whole model run. (A) Snapshots and free-surface evolution of a model similar to the reference model, but with higher subduction velocity (7 cm/yr). The slightly increased subduction velocity leads to trench retreat after the weak lithospheric mantle has been significantly thinned. Trench retreat is compensated by subduction erosion (II). (B) Snapshots and free-surface evolution of a model where return flow induced trench retreat and overriding plate movement are balanced. Only slight thickening occurs at the margin (II).

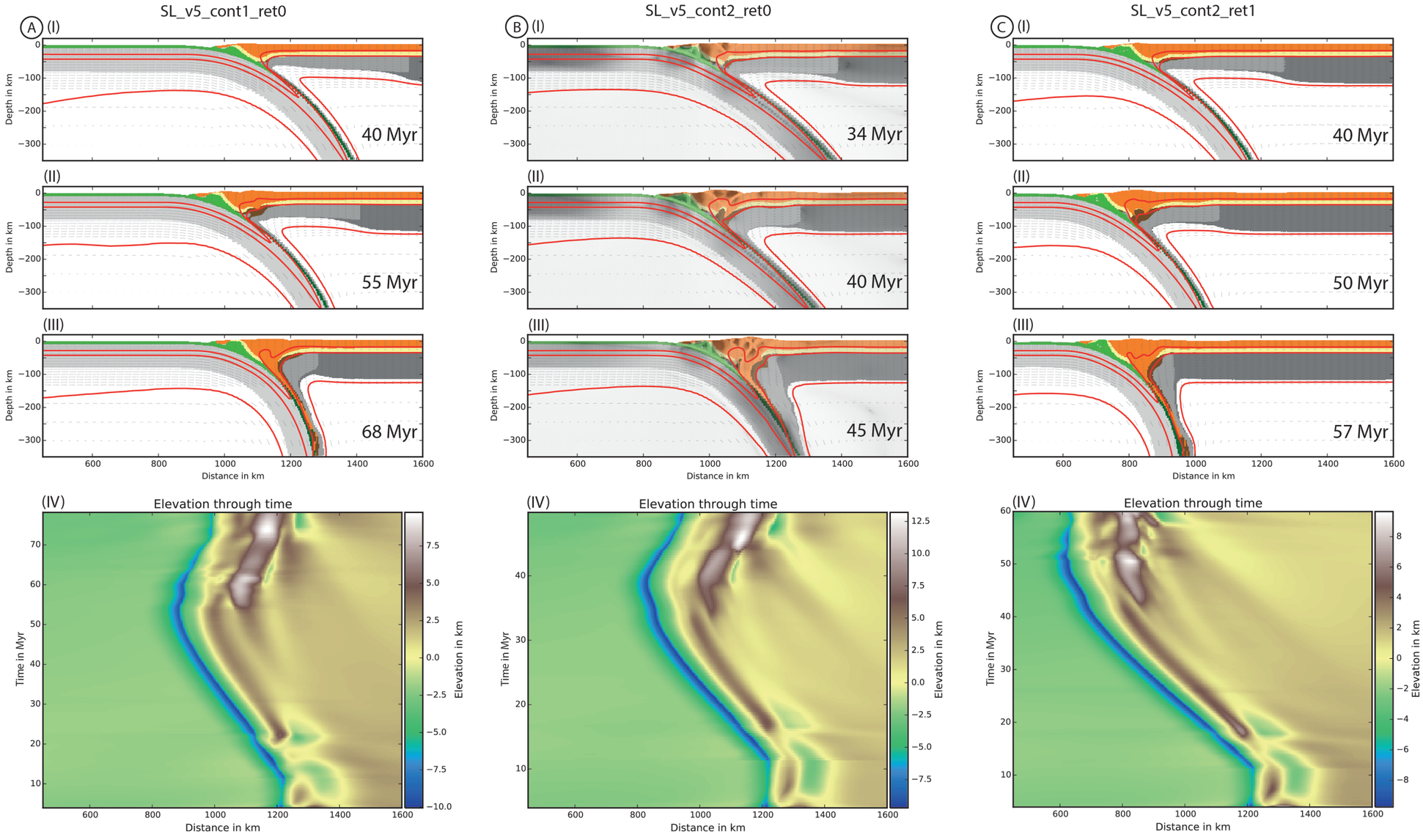

Figure 18: Figure showing three models where the overriding plate is shortened. The snapshots of the different models represent similar stages during subduction initiation, showing that the deformation pattern is similar for all contractional models, and only the timing is different. (A) Model snapshots and free-surface evolution plots showing shortening structures when the upper plate is moving towards the trench with 1 cm/yr. (B) Model snapshots and free-surface evolution plots showing shortening structures when the upper plate is moving towards the trench with 2 cm/yr. (C) Model snapshots and free-surface evolution plots showing shortening structures when the upper plate is moving towards the trench with 2 cm/yr and return flow of 100 % is included. The strain rate overlays as grey-scale in the sub-figures of (B) delineate the structures related to contraction in the overriding plate. The structure description is applicable to all contractional models. (I) Initially overriding plate movement leads to slab flattening. After the weak lithospheric mantle is sufficiently thinned through corner flow, the continental crust shortens and a fault zone dipping to the right is formed around 100 km inland from the trench. (II) Further shortening creates a pop-up structure above a flake of lower crustal eclogite. Additionally the slab starts to steepen and the subduction zone advances. (III) Continued shortening is accommodated by entrainment of the continental crust along the subduction zone interface. (IV) The free-surface evolution plot shows that the overriding plate velocity initially leads to trench retreat and little OP shortening. During OP shortening, a < 200 km wide mountain range forms and the trench advances. (A,C)(IV) show, that return flow or lower OP velocities modulate the structures slightly.

flattening and minor thickening in the OP (Fig. 18 (A-C)(I)). The amount of slab flattening, and thus trench retreat, is dependent on the velocity of the overriding plate, and a higher velocity leads to a flatter slab (Fig. 18 (A,B)(I)). Furthermore return flow reduces slab flattening (Fig. 18 (C)(I)). At some point corner flow has thinned the continental lithosphere enough so that the push of the overriding plate is translated into crustal shortening (Fig. 18 (A-C)(II)). Thereby the slab steepens again and the trench advances. Onset of the shortening phase is accompanied by the creation of a lower crustal eclogite flake (Fig. 18 (A,C)(II)). Whether this initiates contractional structures is shown in chapter 4.4, but eclogitisation appears to have an influence.

The shortening phase can be subdivided into two phases. In phase one, contraction is accommodated by the creation of a pop-up structure in the centre of the arc (Fig. 18 (B)(II)). The pop-up structure is bordered by two fault/shear zones whereof the left is developing and active before the right one (Fig. 18 (B)(I)). During phase one, the continental crust also thickens through pure shear to the right of the pop-up structure and the lcc becomes partially eclogitised. In phase two, further shortening is accommodated by entrainment of the hinterland continental crust in the subduction channel down to depths >250 km. Thereby underthrusting of the entrained crust happens along the right fault zone of the pop-up structure from phase one (Fig. 18 (B)(III)). The movement is also documented through the loop in the temperature profile in the vicinity of the shear zone. Additionally several other antithetic fault zones form in the continental crust during phase two.

The two contractional phases can also be seen in the free-surface elevation plots of Fig. 18. During activity of the left pop-up fault zone, a <50 km wide elevated region starts to develop. When the right fault zone becomes active, the elevated region grows to ~100 km width. Additionally a little basin below sea level develops to the right of the shear zone. During phase two, the eclogite flake gets entrained and separated and a very high (>12 km) and narrow mountain range forms without a bordering basin. The second retro-arc basin forming towards the end of the model runs is related to indentation of the strong mantle lithosphere. The surface evolution plots also show, that return flow reduces trench advance during the shortening phase.

Note that all the models show some accretion of oceanic material at the margin. The subducted oceanic crust is bypassing the first continental block at the trench, but some material is not subducted further than the first couple of kilometres and rises buoyantly. Thereby a pocket of oceanic material accumulates 100 km inland from the trench. With time this pocket can breach the overlying crust and separate a block of continental material from the continent, as examplified in Fig. 18 (C)(III).

4.3.5 The influence of a weak continental lower crust

A neutral OP strain regime is characterised by the lack of deformation in the OP. A weak lower crust does not change this, and the parameters inducing a neutral strain regime in the models

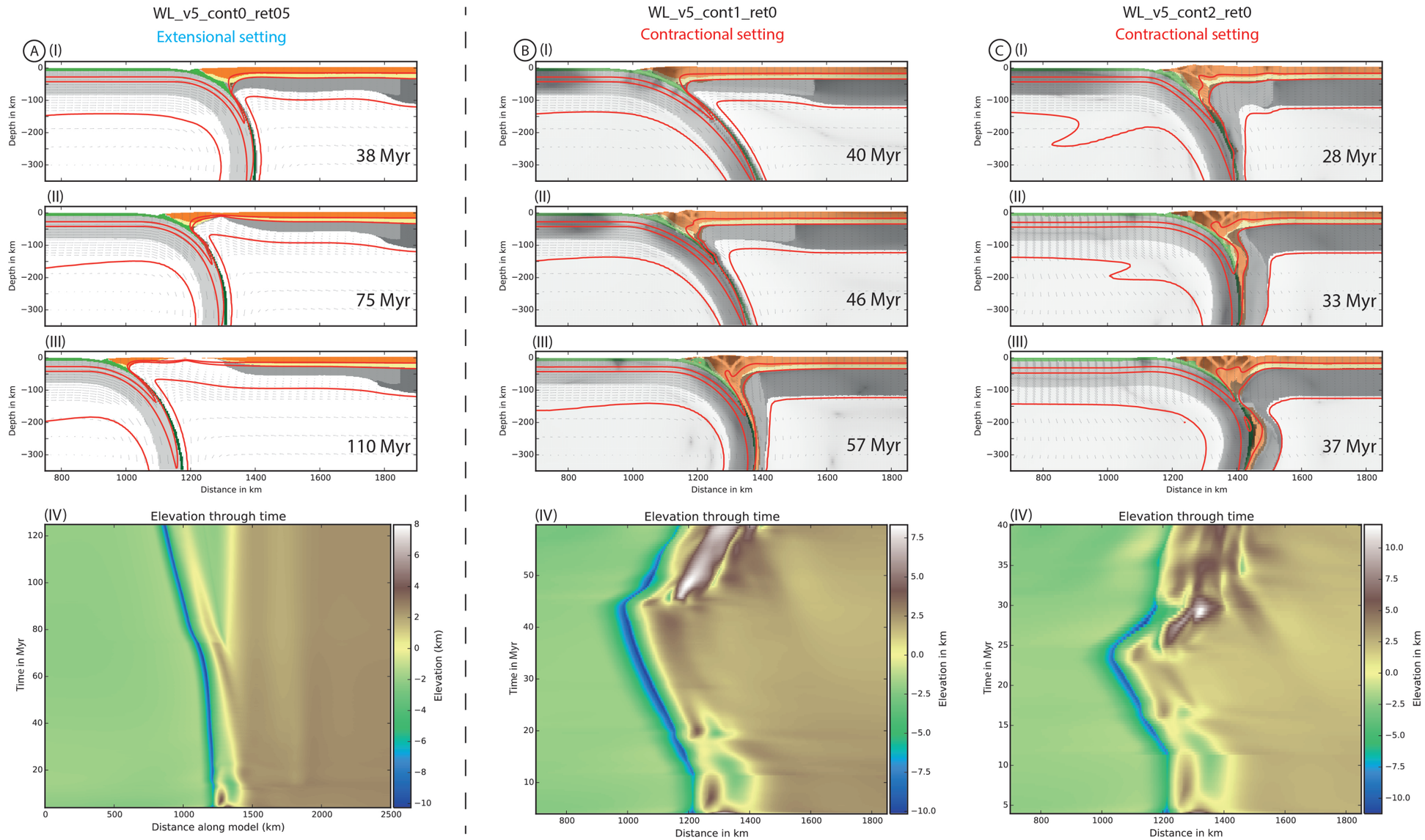

Figure 19: Figure consisting of three sub-figures, which show the structures induced by a weak lower continental crust in an extensional (A) and contractional setting (B,C). (A) The structures developing when the OP is extending are similar to the extension structures of models with a strong lower crust. Corner flow thins the weak lithospheric mantle (I,II), leading to back-arc opening, strong thinning and even rupture of the upper crust. (B) Upper plate movement leads to slab flattening and corner flow induced thinning of the lithosphere (I). The subsequent shortening in the overriding plate is first accommodated by underthrusting of a $< 50\,\mathrm{km}$ thick piece of continental crust (II), before a pop-up structure develops as the arc and the retro continental crust is entrained with the subducting slab (III). (C) Similar structures develop with a fast OP ($2\,\mathrm{cm/yr}$). Yet the underthrusted continental piece is subducted further down (II) and the pop-up structure is composed of more than two thick-skinned thrust slices.

with a strong lower crust also induce a neutral strain regime in models with a weak lower crust. The same accounts for structures that develop when the overriding plate deforms extensionally (compare Fig. 16 (B) and Fig. 19(A)). This holds both for the rifting of short, and wide arcs.

The structural differences are bigger for structures related to a contractional OP strain regime (Fig. 19 (B,C)). Generally the weak lcc leads to an earlier deformation of the continental plate and the formation of a lower crustal eclogite flake is less prominent. The models with a weak lower crust also have an initial trench retreat phase accompanied by slab flattening. Yet the transition between trench retreat and trench advance together with slab steeping is almost instantaneous (Fig. 19(B,C)(IV)) and without a transition phase as seen in the SL-models. The abrupt change in trench movement direction is accompanied by underthrusting of a < 50 km thick piece of continental crust along a fault zone ~100 km inland of the trench (Fig. 19 (B)(II), (C)(I)). The fault zone corresponds to the left boundary fault of the pop-up structure as described in the previous chapter. So far the behaviours of all the contractional models with a weak lower continental crust are similar and independent of the overriding plate velocity. In the following deformation phases overriding plate velocity plays an important role. In the model with an OP velocity of 1 cm/yr, the underthrusting of the continental piece stops after ~5 Myr and further shortening is accommodated by underthrusting and entrainment of the hinterland continental crust. Thereby a pop-up structure as observed in Fig. 18 is created. However no basin below sea level develops on the retro-side of the mountain belt. In the model with overriding plate velocity of 2 cm/yr, the higher velocity leads to subduction of the initially underthrust piece of continental crust (Fig. 19(C)(II,III)). Further shortening forms several anti-thetic faults (Fig. 19(C)(II)) and the final indentation of the strong continental lithospheric mantle creates stacking of two thick-skinned crust-slices in the retro side. Finally a ~300 km wide orogen forms. Note however that the numerical solution after 30 Myr is not converging properly in this model, leading to an unnatural velocity pattern in the oceanic plate. Hence the results of this model have to be handled with care.

Models with higher subduction velocities, but otherwise the same parameters as in Fig. 19 (B,C), show overall the same structures. Example WL_v7_cont2_ret0 (not shown as figure, see animations), however, shows no initial underthrusting of continental material, but contraction is only accommodated by entrainment of the retro-continent. Thus contractional models with a weak lower continental crust are more diverse than the contractional SL models, but show overall similar structures.

4.3.6 Which parameter does what - evaluation of the APM models

So far we saw, that the subduction velocity can induce a neutral or slightly extensional OP strain regime, return flow induces always an extensional OP strain regime, and movement towards the trench is the only possibility to induce overriding plate shortening. Furthermore all the structures related to the different strain regimes were described. To visualize the single value

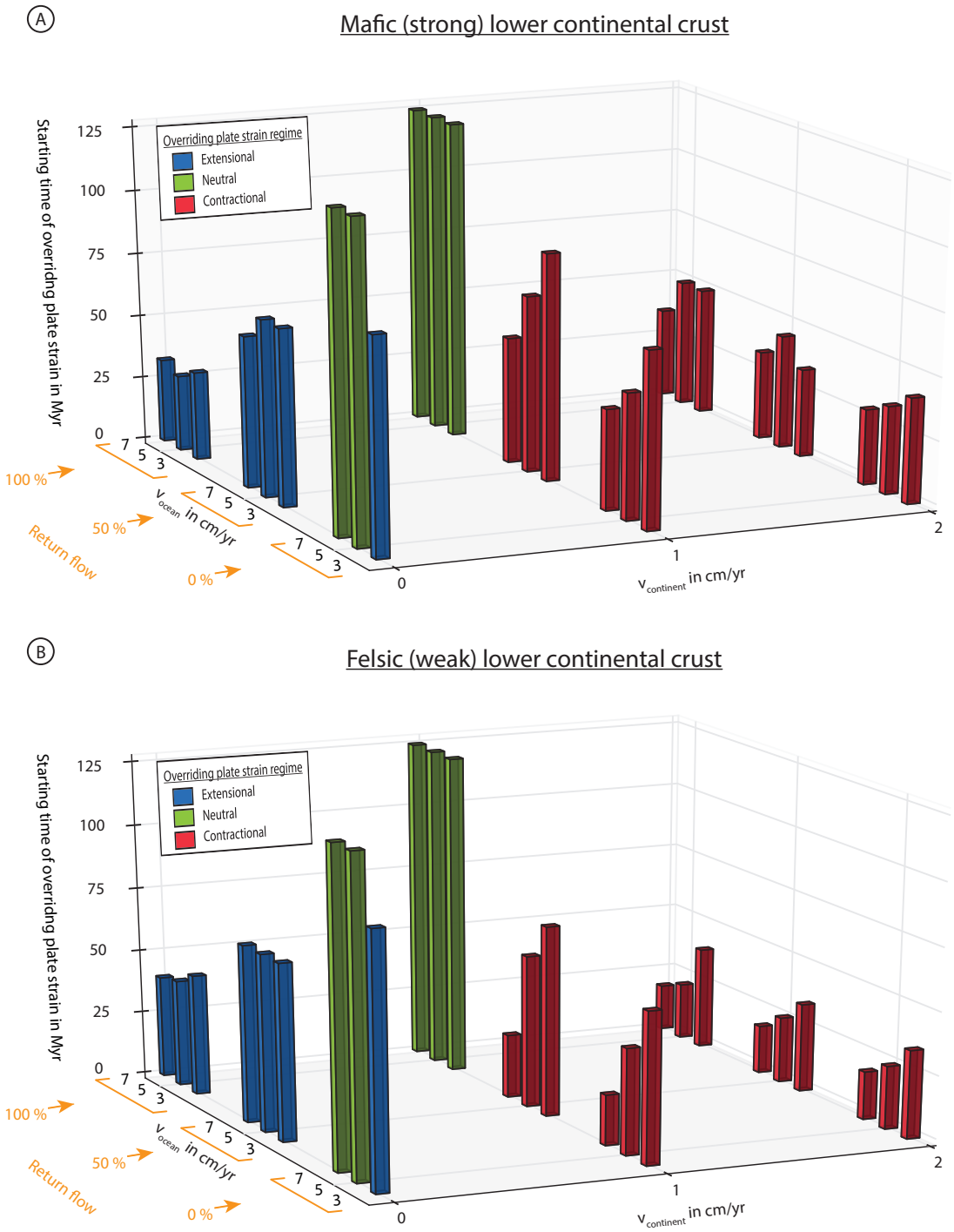

Figure 20: Bar charts for the 27 APM models with a strong (A) and weak (B) lcc, relating the subduction velocity, overriding plate velocity and return flow values with the onset (height of bars) of the corresponding overriding plate strain regime (colours). Almost all triplets have the same colour and typically the height within each triplet is inversely proportional to the subduction velocity. The latter relationship is especially pronounced in a contractional setting and when the lcc is weak. The only exception where a triplet has different colours is the setup without return flow and a static OP. The influence of the return flow and the overriding plate velocity are antithetic, with the return flow favouring and speeding up extensional deformation and vice versa. The differences between A and B are only in the nature of timing of onset of deformation. A weak lower continental crust delays extensional deformation and quickens the onset of contractional deformation.

influence, as well as the combinations of the three parameters, all 27 SL- and WL-models were classified according to their OP strain behaviour and the onset of deformation in the OP (Fig. 20). The onset of deformation is defined as the timing, i.e. when the OP crust either forms a thrust fault (contractional regime) or is significantly rifting apart (extensional regime).

Generally, and as already observed in chapter 4.3.1, the subduction velocity has no significant influence on the OP strain regime and thus every triplet in the bar charts plot has the same color. The only triplet, where the subduction velocity has influence on the overriding plate strain regime is at zero return flow and a static continent (Fig. 20, triplet in the foremost corner). In this setup, the low subduction velocity of 3 cm/yr induces an extensional strain regime, as shown in Fig. 16 (A). Yet Fig. 16 (A) also shows that extension is slow and continental break up does not occur during the model run.

Although the subduction velocity does not determine the strain regime, it has an influence on the timing of deformation, and models with a higher subduction velocity generally deform earlier. This trend is more pronounced in the models with contractional deformation in the OP and in the models with a weak lcc (Fig. 20).

An increase in return flow increases the likelihood and earliness of an extensional strain regime and delays the timing of contractional deformation in the overriding plate. In contrast to that does an increase in v_{OP} increase the likelihood for OP shortening, and also quickens the onset of shortening in the overriding plate. Hence the effect of the return flow and the effect of the overriding plate movement are antithetic. The triplet for 100 % return flow and 1 cm/yr v_{OP} shows that both velocities can cancel each other out, creating a neutral strain regime (compare Fig. 17 (B)).

Chapter 4.3.5 showed that a weak lower continental crust affects and increases the variety of structures in contractional settings. However, the type of OP strain regime is independent of the rheology of the lower crust and differences are only seen in the timing of deformation. Thereby a weak lcc delays extensional deformation, but quickens the onset of shortening.

4.4 The influence of lower crustal eclogitisation in contractional settings

Figure 18 A(II) shows that contractional deformation is accompanied by the formation of a flake of lower crustal eclogite. How this influences deformation and whether an even heavier lower crustal eclogite induces different structures is subject of this chapter. The influence is exemplified through three models (Fig. 21 (A-C)) which all have the same velocity boundary conditions but with no lcc eclogitisation, standard lcc eclogitisation ($\rho = 3100$ kg/m^3), and a heavy lcc eclogite ($\rho = 3500$ kg/m^3) respectively. The model with standard eclogitisation was already shown in 18 (A).

The initial phase of trench retreat, slab flattening and lithospheric thinning is the same for all three models (Fig. 21 (A-C),(I,IV)). In the following deformation phase, the models without eclogitisation and with standard eclogitisation behave very similar as well. Shortening is accommodated by the formation of a pop-up structure followed by entrainment of the retro crust,

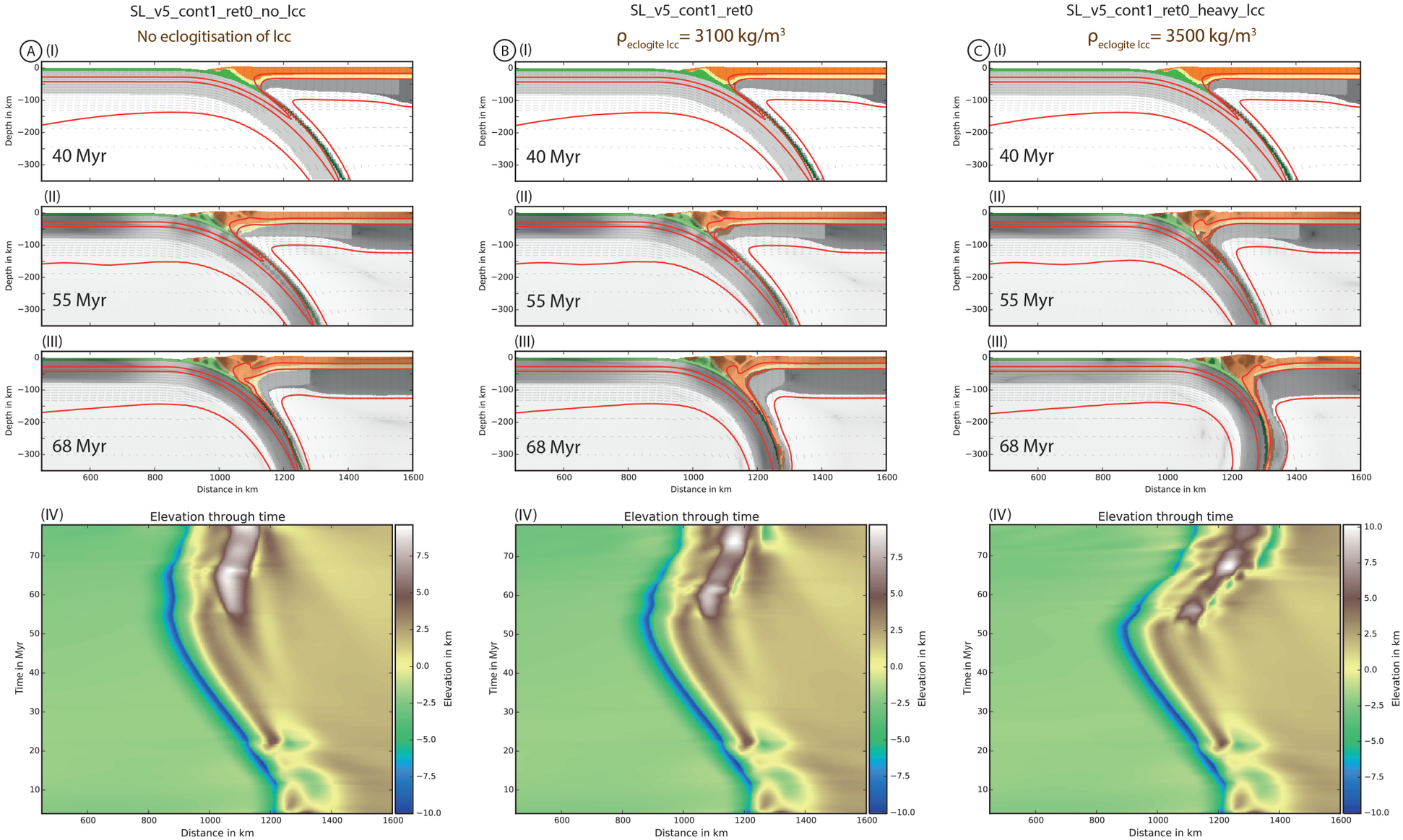

Figure 21: Three sub-figures (A-C), composed of model snapshots and the free-surface evolution, showing the influence of lcc eclogitisation on the formation of shortening-structures in the OP. All model snapshots (I-III) are taken at the same time. To delineate deformation structures, sub-figures II and III have a strain rate overlay in grey-scale. (A) Model without eclogitisation. The shortening structures in the OP are very similar to the standard model (B), and the major difference is the delayed formation of structures and a wider orogen. This can also be seen in (IV). (B) Model with standard eclogitisation as used for all the APM models ($\rho = 3100\,\mathrm{kg/m^3}$). The structures have been described in Fig. 18 already. (C) Model with a heavy lower crustal eclogite ($\rho = 3500\,\mathrm{kg/m^3}$). The heavy eclogite induces earlier deformation, and favours shortening accommodation through retro crust entrainment (II,III). The formed orogen is furthermore smaller.

as described in chapter 4.3.4. The main difference between the two models is that trench advance is slower and the mountain range is ~50 km wider without a lcc eclogite (Fig.21 (A,B)(IV)). Furthermore no basin below sea level forms on the retro side of the orogen in the model without a lcc eclogite.

The model with a heavy lcc eclogite follows the same general trend and shows faster trench advance and a narrower mountain range than the model with a standard lcc eclogite. However the structures are a bit different. Thinning of the lithospheric mantle leads also to formation of an eclogite flake below the thickened continental crust, as displayed in Fig. 21 (B)(II). The heavy lcc eclogite suppresses longterm activity of the left pop-up boundary fault, and shortening is almost exclusively accommodated by underthrusting and entrainment of the retro continent (Fig. 21 (C)(II)). Hence, only a relatively small, ~100 km wide pop-up structure forms accompanied by two short (< 3 Myr) periods of retro basin formation.

Summarizing we can say that eclogitisation speeds up shortening and trench advance, and makes the resulting orogen smaller. Although heavy lower crustal eclogite alters the structures and activity of faults, the overall structural style is not changed through different eclogite densities.

Note that the basins, which form on the orogen retro-side at the end of the model runs, are related to indentation of the strong continental mantle lithosphere.

4.5 Extension and then convergence - Inheritance models

The previous models show that any kind of deformation of the OP needs a thinned continental lithospheric mantle. To test the effect of an already thinned and even extended continental margin on the formation of contractional structures, four models were run with a 100 Myr long precursor extensional phase followed by a contractional velocity setup with $v_{oceanic} = 7$ cm/yr and $v_{OP} = 7$ cm/yr. The velocity boundary conditions are the same for all models, but changed are the eclogitisation of the lower crust (Fig. 22 (A-C)), and the strength of the lcc (Fig. 22 (D)). The model with the weak lcc (Fig. 22 (D)) includes standard eclogitisation.

After 100 Myr of slow subduction, the continental crust is thinned and extended for all the models (Fig. 22 (A-D) (I)). The structures are very similar and only the model with a standard eclogite shows unexpectedly less extension (Fig. 22 (B)(I)). Furthermore the margin with a weak lower crust shows a bit more accretion of oceanic material than the other models.

The first phase of contractional deformation is characterised by docking of the rifted arc onto the continent followed by underthrusting and entrainment of the retro-continent into the subduction channel. This structure develops almost identically in the three models with different eclogitisation and a strong lower crust (Fig. 22 (A-C)(II)). The model with a weak lower crust also shows a similar structure, but with a less coherent former arc block (Fig. 22 (D)(II)).

The second deformation phase is characterised by the formation of a second thick-skinned thrust sheet, which thrusts under the existing thickened margin (Fig. 22 (A-D)(III)) and is subsequently

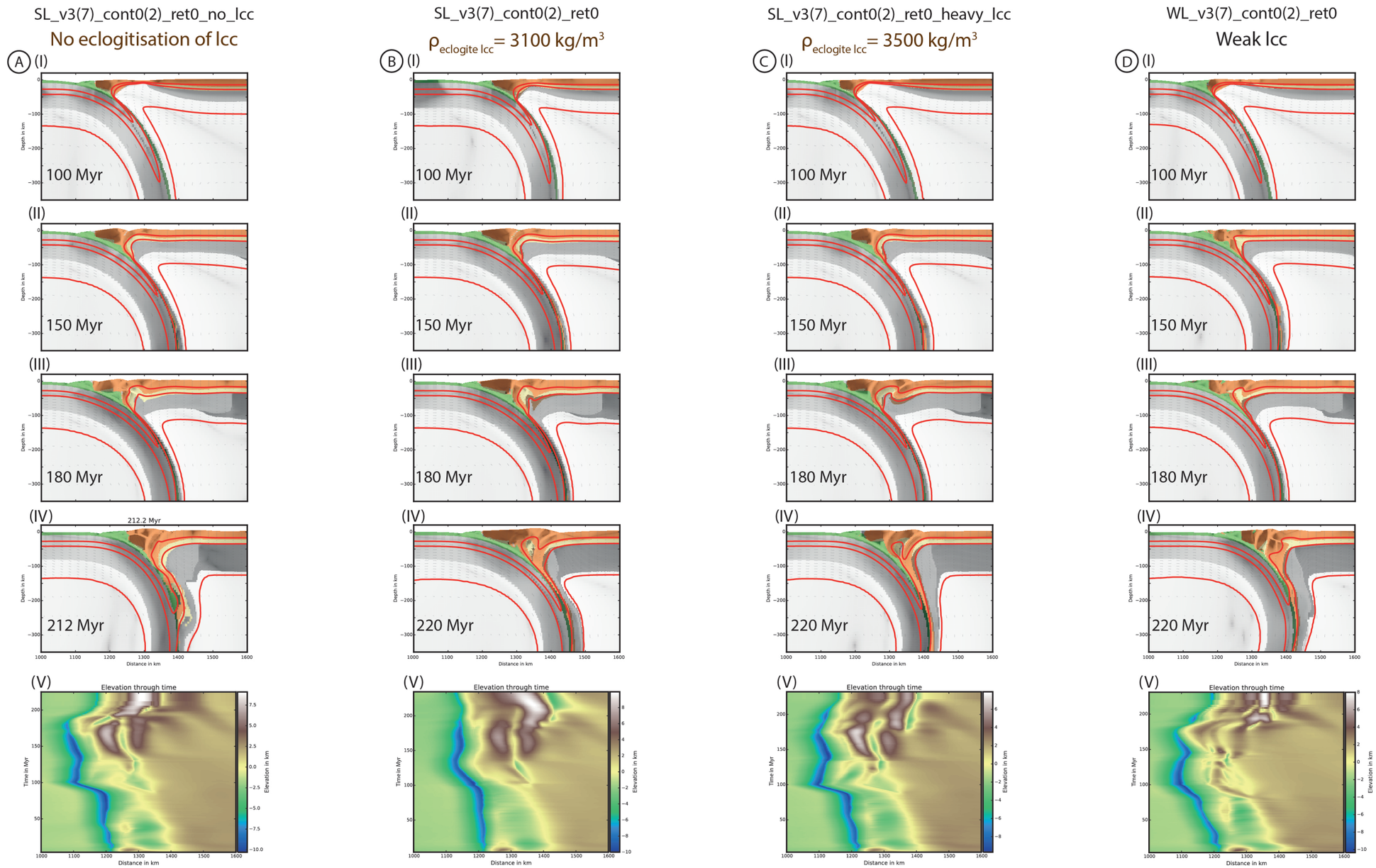

Figure 22: Figure consisting of four sub-figures (A-D), each displaying snapshots and the free-surface evolution of one Inheritance model. The boundary conditions are the same for all four models, as displayed in the headers. Changed are the eclogitisation of the lcc with no eclogitisation in (A), standard eclogitisation in (B) and a heavy lcc eclogite in (C). The fourth model (D) has a weak lcc with standard eclogitisation. The first snapshots (I) are very similar and show the extensional structures before velocity change. The second snapshots (II) are also quite similar and show the rifted arc, which has been docked onto the continent again, followed by underthrusting of the continental crust. The hinterland is furthermore slightly thickened through pure shear. Snapshots III and IV display the second phase of shortening. This phase is characterised by formation of a second thrust sheet further inland, which thrusts under the thickened margin. The two separated thrust sheets are most prominent in the models with a strong crust including eclogitisation (B,C), evidenced through the loop in the 350 °C contour in snapshots (B,C)(III,IV) and the free-surface evolution plots (V). The second deformation phase is in models A and D characterized by merging of the first and second thrust sheet. Note also the rotated tip of the first thrust sheet in snapshot (D)(III).

entrained downwards into the subduction channel (Fig. 22 (A-D)(IV)). This shortening phase happens in principle in all models, but is significantly influenced by the model differences.

The models with a strong lcc and eclogitisation (B,C) show that formation of the second thrust sheet is preceded by the formation of an eclogite flake at the tip of the thrust sheet (Fig. 22 (B,C)(III)). This eclogite flake guides the thrusting, and a stack of two distinct thrust sheets forms (Fig. 22 (B,C)(IV)). The thrust stack can also be observed in the free-surface evolution plots (Fig. 22 (B,C)(V)) and in the loop of the 350 °C contour line in snapshots of Fig. 22 (B,C)(IV). The heavier eclogite however induces earlier deformation and has a stronger influence on the guidance and formation of the second thrust sheet. Additionally the depressions separating the two thrust sheets are deeper in the heavy lcc eclogite case.

The lack of lcc eclogitisation (model A) leads initially also to formation of a second thrust sheet (Fig. 22 (A)(III)). However no clearly separated thrust sheets form in the following contractional period. Shortening is furthermore complicated as a part of the thickened margin is sheared off and subducted downwards during the formation of the second thrust sheet (visible as subducted block at ~300 km depth in Fig. 22 (B)(IV)).

In the model with a weak lcc (D), the second deformation phase is also connected to the creation of a second thrust sheet further inland (Fig. 22 (D)(III)). Simultaneously the tip of the first thrust sheet rotates by around 45° in an anti-clockwise direction. Further thrusting of the second thrust sheet under the thickened margin merges the rotated block and the second thrust sheet, and one wide thrust sheet with different strain compartments forms (Fig. 22 (D)(IV)). The quite complex deformation history is also reflected by the variegated structures of the free-surface.

Crustal thickening is in all the models restricted to a ~200 km wide area.

4.6 Terrane accretion

Four models were run to investigate whether terrane accretion is a viable mechanism for the creation of a thickened continental crust, and how accreted terranes develop over time. $v_{oceanic}$ was varied between 3 and 5 cm/yr and the oceanic plate carried 1 or 2 continental terranes.

In all four models, the terranes were initially sheared off the oceanic crust and stacked at the margin (Fig. 23 (A)(I), (B)). However the following development was more variegated and a function of the subduction velocity. Thereby the development followed the same procedure for one and for two accreted terranes. An exception was the model with one terrane and with a subduction velocity of 3 cm/yr (Fig. 23(A)).

In the latter, the slab breaks off shortly after terrane accretion and the subduction zone is re-initiated (Fig. 23(A)(I)). The forced subduction re-initiation leads to downwards drag of the accreted terrane and injection into the weak continental lithospheric mantle (Fig. 23(A)(II)). This leads to the formation of gravitational instabilities of weak and cold mantle lithosphere (Fig. 23(A)(III)). Furthermore plumes of terrane material rise from ~300 km depth and get entrained again through corner flow, thus creating a lively and dynamic system. Finally almost

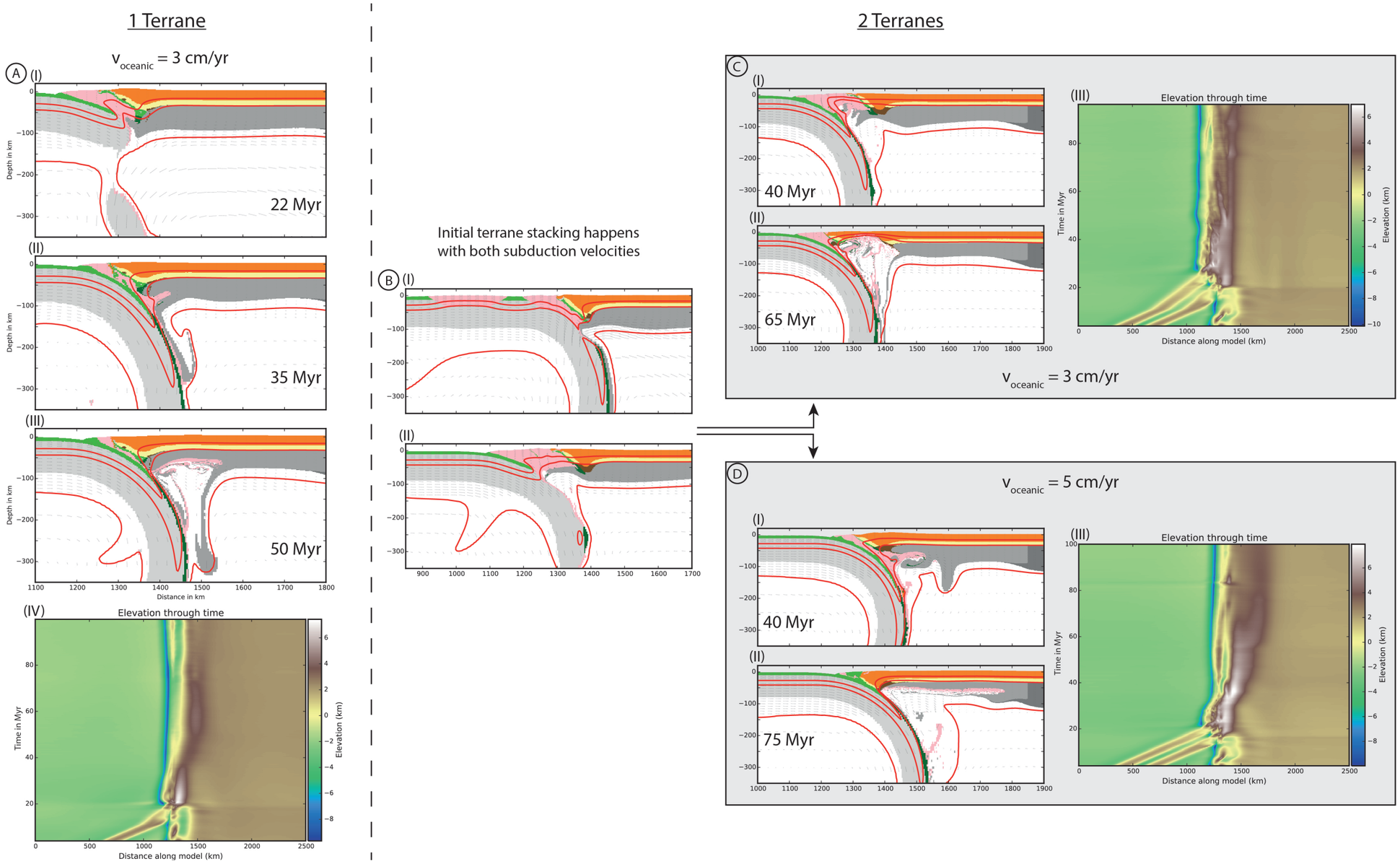

Figure 23: Figure showing the different dynamics of a margin subject to terrane accretion. The developments are generally the same whether one or two terranes are accreted at the margin, and all models show initial terrane accretion. Sub-figure (B) shows how terrane accretion looks like for the two terrane case. The past-accretion development is dependent on the subduction velocity (C,D) or whether the slab breaks off and the subduction zone is re-initiated (A). (A) The only model which shows slab break off has one terrane and a subduction velocity of 3 cm/yr (I). During subduction re-initiation the accreted terrane gets dragged down and buoyantly injects into the weak lithospheric mantle (II). This leads to gravitational instabilities and a lively small scale convection driven by the corner flow and buoyant rise of material until finally almost no material is left at the margin (III). (C) The development is very similar when the subduction velocity is 5 cm/yr, with underplating and gravitational instabilities (I and II). The free-surface evolution plate (III) shows that underplating leads to margin uplift. (D) The development after terrane stacking is different when the subduction velocity is 3 cm/yr. The tendency of the slow subduction velocity for trench retreat keeps the trench at the new position further oceanwards (I). Some terrane material gets dragged down and buoyantly rises, thereby inducing OP extension and finally continental breakup (II).

no accreted material remains at the margin and the slow subduction velocity leads to trench retreat after approximately 75 Myr. Note that material which is dragged down below 500 km depth is converted to the highly conductive lithospheric mantle, and thus terrane material successively vanishes artificially out of the system.

A very similar behaviour develops with time after terrane stacking for the models with 5 cm/yr subduction velocity (Fig. 23(D)). However, the accreted material is in this case not dragged down due to forced subduction re-initiation but through a higher subduction velocity. The bent curve of the trench in Fig. 23 (D)(III) delineates the stacking and subsequent trench advance until the terranes have been removed from the margin.

A different behaviour develops in the model with 2 terranes and $v_{oceanic} = 3$ cm/yr. In this model, the slab does not break off after terrane accretion and no forced subuction re-initiation forces down the accreted material. Furthermore the slab stays after terrane accretion at the new position offset oceanward from the initial trench position. However subduction does as well drag down terrane material, which rises from depths of around 300 km (Fig. 23(C)(I)). The buoyant rise leads to extreme thinning of the OP and finally even to continental break up and rifting of an arc block towards the trench (Fig. 23(C)(II)). The repeated rise and corner flow induced entrainment leads here as well to a lively dynamic behaviour. Finally only a small portion of accreted material remains at the margin.

Note that the underplating and buoyant rise both lead to uplift of the continental margin (Fig. 23(C,D) (III)).

5 Discussion

The results chapter showed that the models develop a wide variety of structures based on some basic principles. I propose that only the first order differences between the models can be discussed, as there are many more parameters which have to be explored before a detailed structural analysis is possible. Through comparison of the model results I identified three factors which *control* the strain regime of the overriding plate. The three factors are 1) the subduction velocity, 2) the return flow, and 3) the overriding plate velocity . Yet shortening of the overriding plate is more complex than to be solely determined by a combination of the three parameters and I additionally identified two factors, which *modify* the structures or timing of shortening in the overriding plate. The two factors are a) the eclogitisation of the continental lower crust and b) extensional inheritance.

The discussion chapter follows the above introduced systematics, and first the factors controlling OP strain and subsequently the factors modifying OP shortening are presented. The influence of a weaker lower crust has shown not to be strong. However some systematics could be identified here as well, and the influence of the weak lower crust is shortly discussed in a subsequent chapter. Afterwards the fate of accreted terranes is discussed in light of the previous chapters. Finally a simple comparison with natural examples is given, and factors which need to by explored further are discussed.

5.1 Factors controlling overriding plate deformation

The analysis of the absolute plate motion models (Fig. 20) shows, that the subduction velocity, positive overriding plate velocity, and the return flow intensity are the three factors controlling overriding plate deformation (Fig. 24). The subduction velocity can either induce an extensional or neutral strain regime, and has influence on the timing of deformation. Return flow induces extension in the OP and is more effective than a low subduction velocity and thus the main factor controlling back-arc opening. Positive overriding plate velocity has shown to be the only factor that can induce shortening of the overriding plate. The combination of the three parameters controls the onset and type of OP deformation. Note, however, that movement of the OP away from the trench is also a possibility to induce back-arc spreading.

The bar-charts of the model-analysis (Fig. 20) show that a specific strain regime in the continental crust starts only after a certain amount of time after model initiation. The timing of onset of deformation is variable and different for all the models, but all kinds of deformation have in common to be related to lithospheric weakening through corner flow induced gravitational removal of the continental lithospheric mantle. Therefore the weakening of the continental lithosphere is the connecting link between the three different controlling parameters (see Fig. 24). Additionally the onset of deformation divides the influence of each controlling parameter into influence on the pre-deformation phase and on the deformation phase.

The following three chapters discuss the influence of the three controlling parameters in more detail, thereby refining and zooming into different puzzle-pieces of Fig. 24.

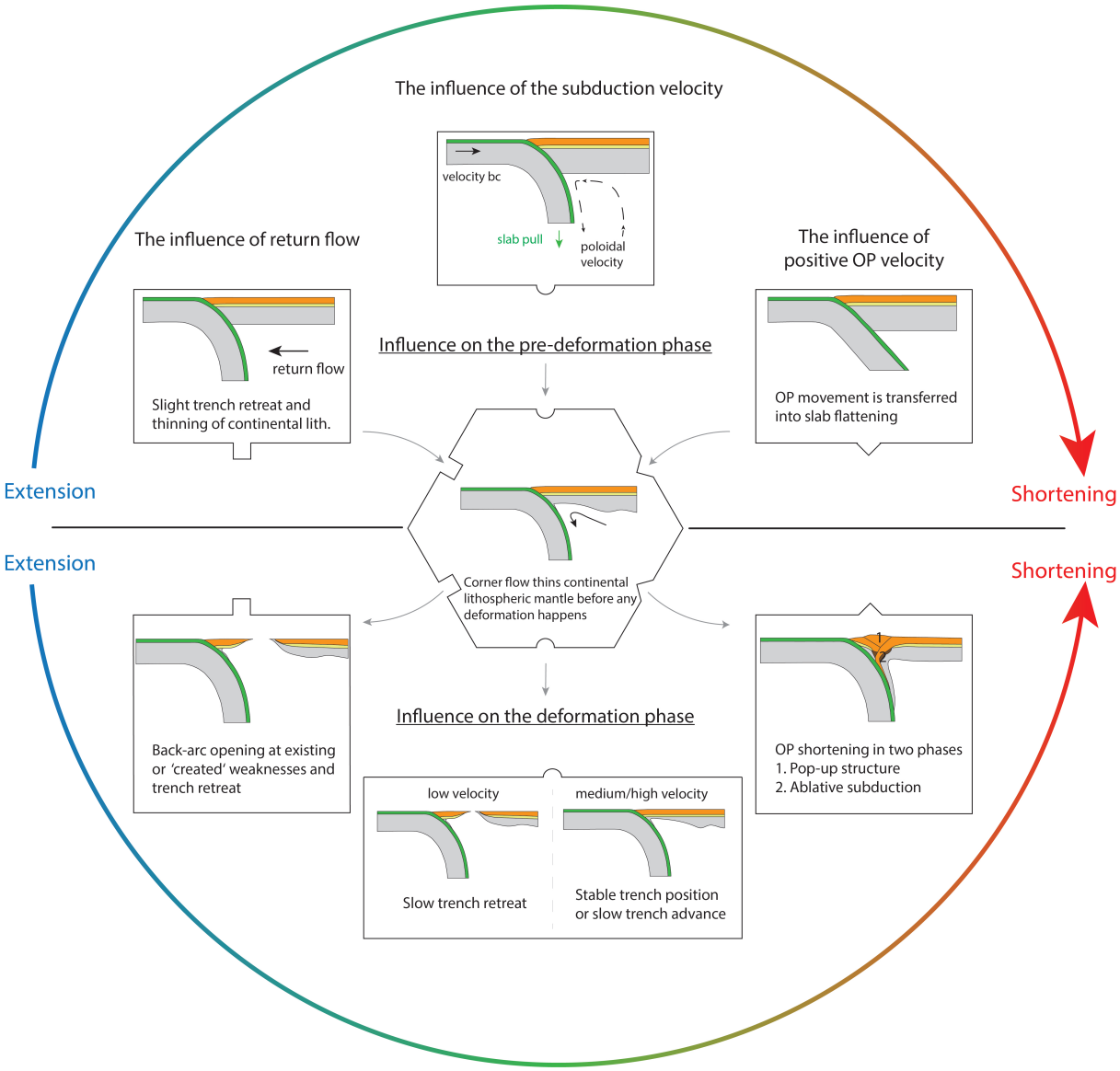

Figure 24: Diagram showing the influence of return flow, subduction velocity and positive OP velocity on the OP strain regime. Thinning and thus weakening of the continental lithospheric mantle is needed for any deformation to occur and thus the link between the three parameters but also between the influence of each single parameter on the pre-deformation phase (upper half of the circle) and the deformation phase (lower half of the circle). A more detailed description of the influence of each parameter is given in the next three figures.

5.1.1 The subduction velocity

The influence of the subduction velocity on the OP strain is twofold and related to the poloidal flow velocity, and the balance between negative buoyancy of the slab, and the velocity boundary conditions (Fig. 25).

The poloidal flow is invoked through downwards drag of the lithospheric mantle along the frontal interface of the subducting slab. Thus a higher subduction velocity leads to faster poloidal flow. Consequently, as corner flow is part of the poloidal flow cell, corner flow is sped up by higher subduction velocities and vice versa. Corner flow induces removal of the weak lithospheric mantle which in turn weakens the continental lithosphere and allows for overriding plate deformation according to the prevailing stress regime. Hence a higher subduction velocity leads to faster poloidal and thus corner flow. This leads to faster removal of the continental lithospheric mantle and finally to faster onset of deformation of the overriding continental lithosphere. This is nicely depicted by triplets connected to a contractional OP strain regime in Fig. 20 (B), as the bar height is inversely proportional to the subduction velocity. Yet the poloidal flow velocity is apparently not the only factor determining the onset of deformation, as not all triplets in Fig. 20 show the inverse proportionality.

Generally the downgoing slab is a few 100 °C colder than the surrounding mantle and thus negatively buoyant. The negative buoyancy induces slab pull, and the slab sinks into the sub-lithospheric mantle with a 'natural sinking rate'. The sinking moves the slab downwards and drives the oceanic plate towards the trench. The sinking rate competes with the velocity boundary condition, as only a pre-defined amount of material flows into the model domain, independent of how fast the slab sinks into the sub-lithospheric mantle. This means that if the velocity boundary condition is smaller than the natural sinking rate of the slab, the subduction zone has a tendency to retreat, and if the velocity boundary condition is higher than the natural sinking rate, the subduction zone has a tendency to advance.

My models show that a low velocity of 3 cm/yr induces trench retreat and back-arc opening. Hence the natural sinking rate for the slab subducting with 3 cm/yr is higher than the velocity boundary condition of 3 cm/yr, and the subduction zone has a tendency to retreat, thereby inducing late (after 90 Ma) back-arc opening. It appears that the natural sinking rate of a slab subducting with 5 cm/yr is approximately 5 cm/yr. Therefore the slab has a stable position during the reference model run and does not move although the OP is strongly thinned through corner flow (Fig. 14). Furthermore, the natural sinking rate of a slab subducting with 7 cm/yr is smaller than the velocity boundary condition and the slab tends to advance. This advance is in my models mostly compensated by subduction erosion (Fig. 17 (A)). Summarizing we can say that the subduction velocity dependent retreat- or advance-tendencies of the models are a result of the differential velocities created by the natural sinking rate and the velocity boundary condition. Note furthermore that the downwards advection of the temperature field through increased subduction velocity is apparently not sufficiently creating a higher natural sinking rate to account for the increased subduction velocity. The fact that the slab below 500 km depth

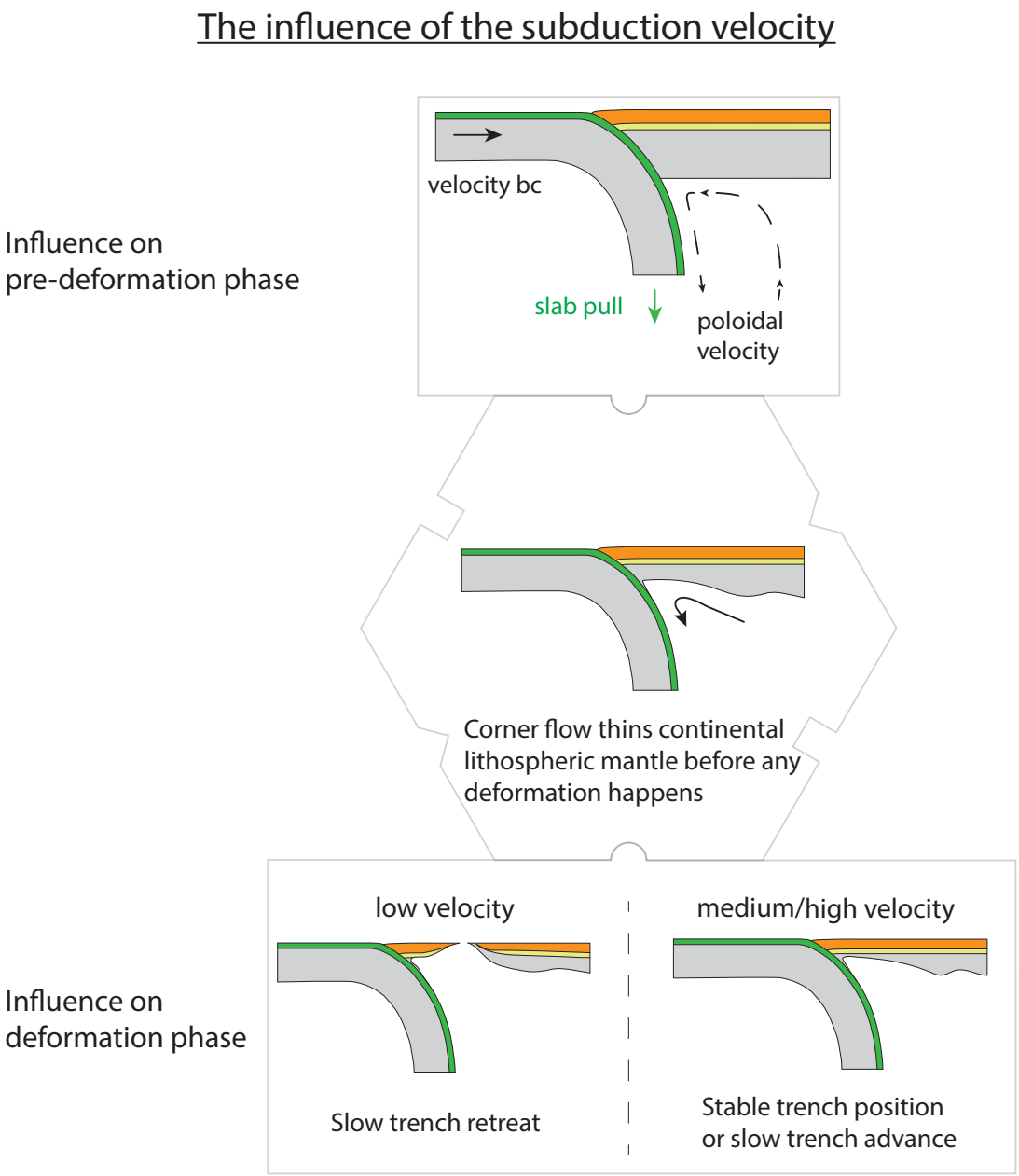

Figure 25: Figure showing the twofold influence of the subduction velocity. A higher subduction velocity leads to a higher poloidal velocity and thus to faster removal of the weak continental lithospheric mantle through corner flow. Hence a higher subduction velocity leads to earlier deformation of the OP. The velocity boundary condition (bc), and thus the subduction velocity is competing with the material buoyantly transferred downwards through the natural sinking rate of the slab. The natural sinking rate in my models is higher than a subduction velocity of 3 cm/yr, and this setup leads to trench retreat after lithospheric thinning. A medium velocity of 5 cm/yr is in balance with the natural sinking rate and leads to a stable trench position, while a high velocity of 7 cm/yr leads to trench advance, compensated by subduction erosion.

is transferred into a highly conductive material weakens the effect of slab pull and decreases the natural sinking rate. Thus the velocities can not be directly transferred to nature and the natural sinking rate is generally underestimated.

The development of the influence of the slab pull force on the subduction system is nicely documented in the subduction initiation phase (Fig. 13). At start of subduction initiation, the oceanic plate is pushed into the continental plate and induces thickening of the continental margin. Subsequently the negative buoyancy of the slab kicks in and subduction is directed downwards. Subduction initiation on Earth is a debated topic and possible mechanisms are induced and spontaneous subduction (Stern, 2004). Induced subduction resembles the subduction initiation mechanism used in my models, and is likely to produce thickened continental crust at the margin. Spontaneous subduction is induced by the strong negative buoyancy of the future slab and will not necessarily produce a thickened margin.

Forsyth and Uyeda (1975) propose that slab pull is the main driving force for plate tectonics. This theory is supported by higher absolute plate motions of plates attached to an actively subducting slab (cf. Fig. 2). However, also plates without an attached slab move (cf. South American plate, Fig. 2), showing that far field forces have also a significant impact on plate velocities. Schellart (2008) finds that 75 % of subduction zones on Earth retreat, independent of the subduction velocity. This indicates that on Earth slab pull is in general stronger than far field forces. Transferred to my models this means that, to represent the characteristics of subduction zones on Earth, the natural sinking rate needs to be bigger than the velocity boundary conditions. This is best illustrated by the models with an oceanic plate velocity of 3 cm/yr. However, our models nicely illustrate the relationship between far field forces and slab pull, and show which range of behaviours are possible.

The retreat- or advance- tendencies are only significant for models without return flow and a static OP. Whenever return flow or overriding plate movement are included, the tendencies are ruled out. As some kind of overriding plate movement or return flow are most likely always happening in nature, the retreat- and advance-tendencies induced by different subduction velocities can only be interpreted together with the mantle flow pattern and the OP movement.

Nevertheless, the influence of the subduction velocity on the timing of OP deformation is important to note and independent of the driving forces.

5.1.2 The return flow

Generally return flow results in a mantle flow pattern opposite to the subduction direction (Fig. 26), and its influence can again be split up into influence on the pre-deformation phase and influence on the deformation phase.

During the pre-deformation phase, the continental lithosphere is thick and coherent, so that the forces transferred from return flow onto the subducting slab and from there as tension forces onto the continental plate are not high enough to rupture the overriding plate. However a slight amount of trench retreat is accommodated by OP thinning through pure shear. At the point

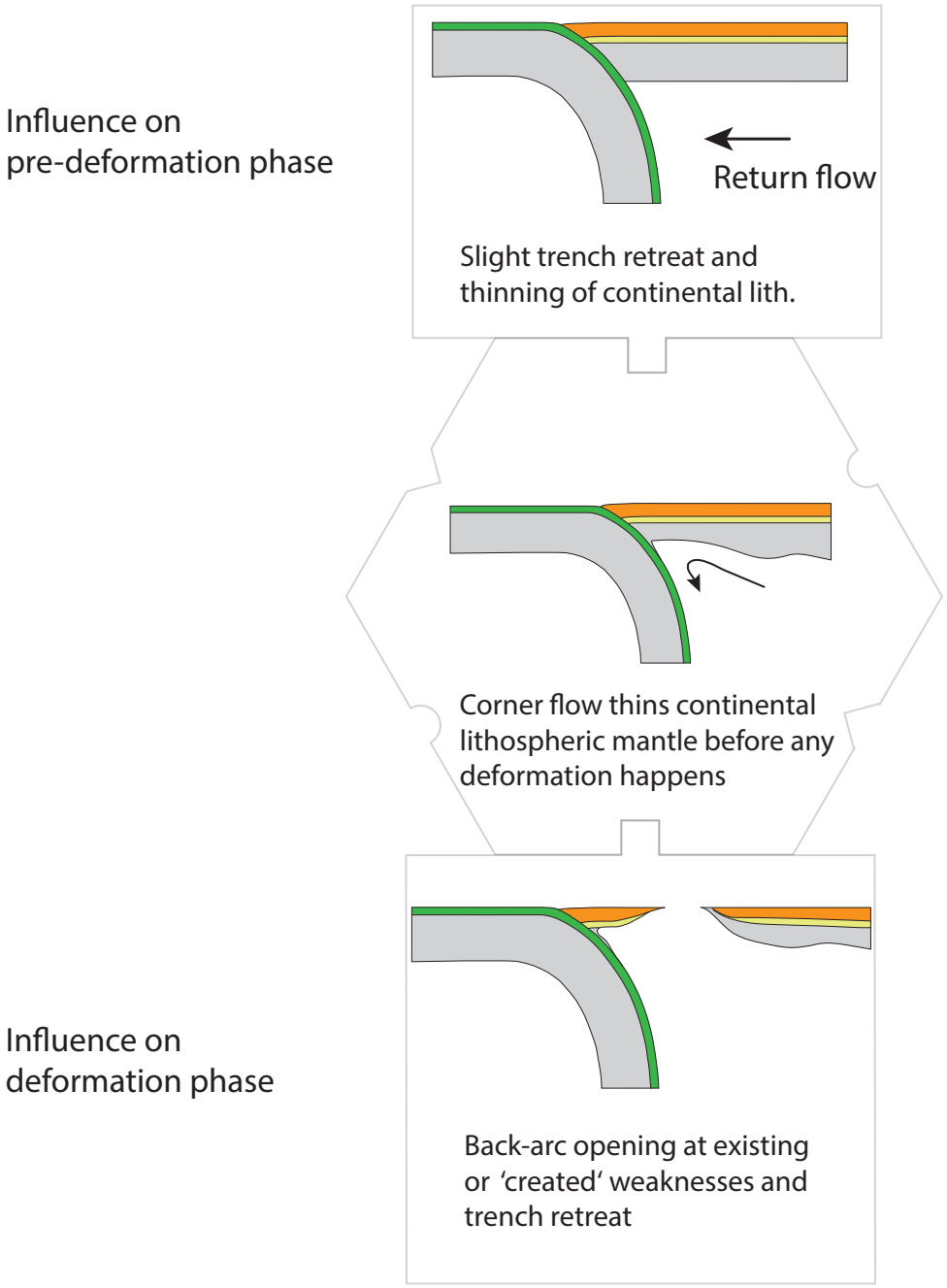

Figure 26: Figure showing the influence of return flow on a subduction zone. Initially the tensional force exerted by return flow on the OP is not strong enough to rupture the continental plate. Yet slight trench retreat is accomodated by pure shear thinning of the OP. When the continental lithosphere is weakened enough through corner flow, the return flow force overcomes the coherence of the continental lithosphere and the plate ruptures followed by back-arc opening and trench retreat. Note that the initial margin thickening and the shape of the weakened lithospheric LAB are also important in determining where the continental plate actually ruptures. Inherited weaknesses can additionally be used to initiate back-arc opening.

when the overriding plate is weakened enough, both through pure shear thinning and through corner flow induced thinning, the return flow forces overcome the continental plate coherence and the plate ruptures. This leads to back-arc opening and constant trench retreat.

Fig. 16 shows that a low return flow rate favours rifting of a small continental block, while a high return flow rate favours rifting of a wider block. This is related to an interplay between the structure of the continental LAB, the subduction velocity and the thickened continental margin. The LAB of the weakened continental lithosphere has an undulated structure with two structural highs, related to the corner flow induced removal of the weakened mantle lithosphere. During the first few million years after subduction initiation, the right structural high causes a greater weakening of the continental lithosphere than the left structural high. This is possibly related to the initially thickened continental margin. With time and further corner flow induced removal, the left structural high gets bigger than the right structural high and weakens the continental lithosphere more than the right structural high. High return flow rates, exerting a high tension force onto the continental plate, tend to rupture the OP faster and thus exploit the right undulated structure. In contrast to that, lower return flow rates exert a smaller force, and thus corner flow has more time to thin the continental plate near the margin and only a small continental block gets rifted off the margin. Higher subduction velocities increase corner flow and thus favour rifting of a smaller block. However, this behaviour is probably entirely related to the initial thickening of the continental margin through forced subduction and not necessarily a feature of nature.

In our model setup, the 600 km wide weakened back arc lithosphere is attributed to fluid induced weakening and inherited weaknesses. Long term geodynamic numerical subduction models including fluid flow show that fluid induced weakening of the overriding plate does not reach further than ~300 km behind the trench (Arcay et al., 2005, 2006; Faccenda et al., 2012). Hence back-arc opening far away from the trench is probably due to reactivation of inherited weaknesses, while back-arc opening within the first 300 km of the trench can also be related to fluid induced weakening. In our modelling approach, we did not differentiate between the type of weakening, and this is something to be explored in more detail. Nevertheless, the models show, that all kinds of weakening need corner flow guided removal of the lithospheric mantle.

Toroidal flow is inherently a three dimensional feature and probably more variable in time and space than can be approximated using 2D models. The slab edge of the Tonga-Kermadec subduction zone (cf. Fig. 2) retreats e.g. really fast and with up to ~16 cm/yr, while in my models the retreat velocities are much slower and in the order of some mm/year. Furthermore return flow is in my approach modelled as an imposed velocity, while in reality return flow develops dynamically as a result of slab retreat. Hence my models can not dynamically investigate the variable influence of return flow. However, the models show that return flow is an effective mechanism and probably even necessary for trench retreat and back-arc opening to occur.

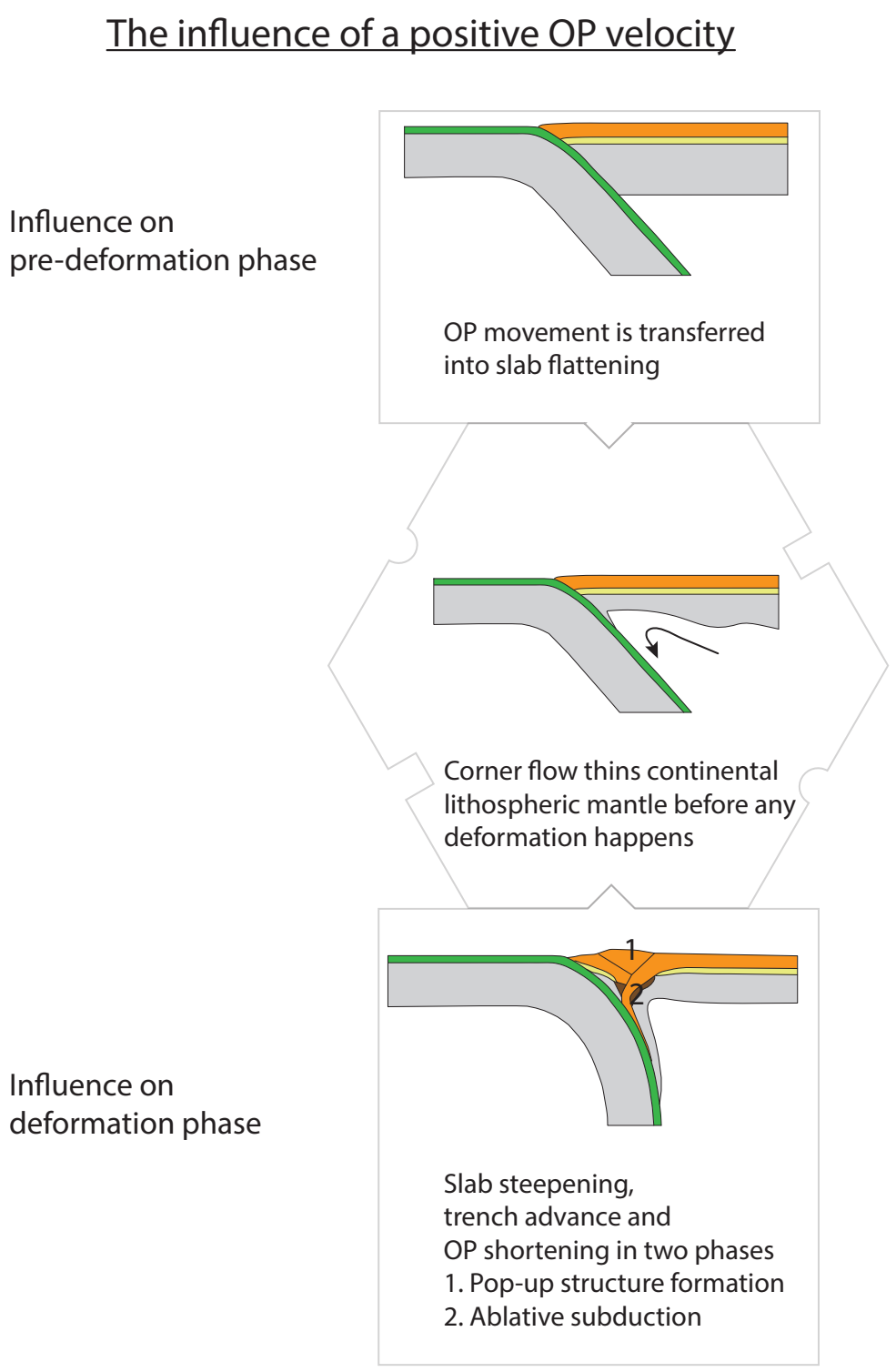

Figure 27: Figure showing the influence of a positive OP velocity. The OP movement is transferred into slab flattening until the continental plate is sufficiently weakened through corner flow so that the resistivity force of the subducting slab overcomes the strength of the continental plate. Subsequent shortening is accommodated through two deformation phases. In phase one a set of antithetic faults, bordering a pop-up structure, is active. The second phase is dominated by entrainment of the hinterland crust into the subduction channel, called ablative subduction. Ablative subduction limits the width of the orogen to $<$250 km. During the shortening phase, the slab swings back into a steep position again and the trench advances.

5.1.3 The overriding plate velocity

Figure 15 shows that OP movement directed away from the trench induces back-arc opening similar to the behaviour in response to high return flow rates. This is reasonable as the imposed velocity boundary condition induces a tensional stress regime in the overriding plate, which leads to rupture and back-arc opening after lithospheric weakening. Hence return flow and negative OP movement induce the same stress field and are in a way related.

A contrasting behaviour can be observed when the OP moves towards the trench. Initially the continental plate is strong and coherent, so that the movement is transferred into slab flattening and trench retreat (Fig. 27). Through ongoing subduction, corner flow thins the continental plate until the resistance of the slab against the OP push is bigger than the strength of the continent, and the OP shortens. As a response to shortening, the slab swings back into a steep position. This speeds up shortening and the trench advances slightly.

Initially shortening is accommodated by thrusting of the first 50 km of the continental margin under the continent. Almost simultaneously an antithetic fault forms further inland, where the hinterland is thrusted under the arc region, and a pop-up structure forms (Fig. 27). Further shortening is accommodated by entrainment of the hinterland crust into the subduction channel. Thereby a back-arc foreland basin forms, which is below sea-level (Fig. 18 (B)(IV)). Entrainment of overriding plate material into the subduction channel was named ablative subduction by Tao and O'Connell (1992). The ablative subduction phase goes on until the weak lithospheric mantle material is consumed and the strong hinterland lithospheric mantle indents. Due to ablative subduction, the width of the orogen is limited and does not exceed 250 km. Hence ablative behaviour can be seen as the main factor determining the structures and behaviour of my contractional models.

Ablative subduction is a function of the density of the ablated material and the viscous drag exerted by the subducting plate. Once the hinterland continental crust is thrust into the vicinity of the subduction channel, it gets dragged downwards. This shows that the rheology of the subduction channel is strong enough to overcome the buoyancy forces of the under-thrusting continental hinterland. The viscous drag is even strong enough to create a sub-marine back-arc foreland basin. It also overcomes the buoyancy forces at depth, so that the ablated continent subducts down to depths >500 km and vanishes due to the artificial phase change in this depth range.

The temperature field in the models show that the rheology in the subduction channel up to ~150 km depth is dominated by brittle deformation. Hence in the uppermost 150 km, viscosity in the subduction channel is essentially determined by an angle of internal friction of 2°, and this viscosity is strong enough to induce ablative subduction. Sobolev and Babeyko (2005) conducted models where the frictional parameters of the subduction channel were significantly reduced. Their results show that ablative subduction is inhibited by a weak subduction channel, and a wide, Andean style orogen can be created. A frictionally very weak subduction channel is also geologically reasonable, as dewatering reactions in the downgoing slab could lead to a strong

increase in pore fluid pressure near the plate interface, which counteracts friction and possibly even leads to frictionless conditions (Sibson, 1990).

5.2 Factors modulating overriding plate shortening

The previous chapter showed that shortening of the overriding crust is dominated by a long lasting phase (10's of Ma) of ablative subduction, which is preceded by a shorter phase (<10 Ma) of crustal thickening and pop-up formation. The following two sections examine the influence of the lower crustal eclogitisation and extensional inheritance on the shortening behaviour.

5.2.1 The eclogitisation of the lower crust

Ablative subduction is initiated through forced underthrusting of the retro-continent under the arc, opposed by the buoyancy of the continental material. When the continental crust enters the subduction channel, the push from the continent is augmented by the drag of the subducting slab and the influence of the buoyant crust becomes less important. The force balance and influence of these three forces determine speed and onset of deformation.

During the formation of the pop-up structure, hence at the start of ablative subduction, a flake of continental lower crustal eclogite forms at the root of the pop-up structure. In the models without ($\rho = 2900\,\mathrm{kg/m^3}$) and with standard eclogitisation ($\rho = 3100\,\mathrm{kg/m^3}$), the (eclogitised) lower continental crust is lighter than the surrounding mantle and buoyantly counteracts the thrusting of the retro-crust under the arc. Nevertheless small differences can also be observed here, as deformation is slower and ablative subduction onsets later in the model without eclogitisation (Fig. 28). The lower crustal eclogite with high density ($\rho = 3500\,\mathrm{kg/m^3}$) is heavier than the surrounding mantle. Hence its formation leads to a negatively buoyant lower crust. This results in faster deformation, earlier onset of ablative subduction and entrainment of more crustal material. Furthermore the eclogite induces shortening, and is no counteracting factor. Fig. 22 (C)(III) shows how the eclogite induces deformation and guides the under-thrusting of a second ablative thrust sheet.

The different eclogite densities also have an influence on the morphology of the mountain-belt. The depth of the retro-arc foreland basins (Fig. 21 (IV)) is proportional to the density of the lower crustal eclogite. Additionally, faster and earlier onset of shortening by a heavy eclogite leads to a smaller orogen. Hence there is an inverse proportional relationship between the width of orogen and the density of the lower crustal eclogite.

Heavy lower crustal pyroxenite is in my models approximated by the same phase change stability field as eclogite as proposed by Hacker (1996). However, Rapp and Watson (1995) showed that a heavy lower crustal pyroxenite only forms at significantly higher temperatures than eclogite and additionally only the restites of a melt-extracted lower crust are metamorphosed (cf. Hacker (1996), his Fig. 1 and Rapp and Watson (1995), their Fig. 11). I tried using the stability field by Rapp and Watson (1995), but the thermal setup of my models never led to temperatures high enough to create lower crustal pyroxenite. However, the models do also

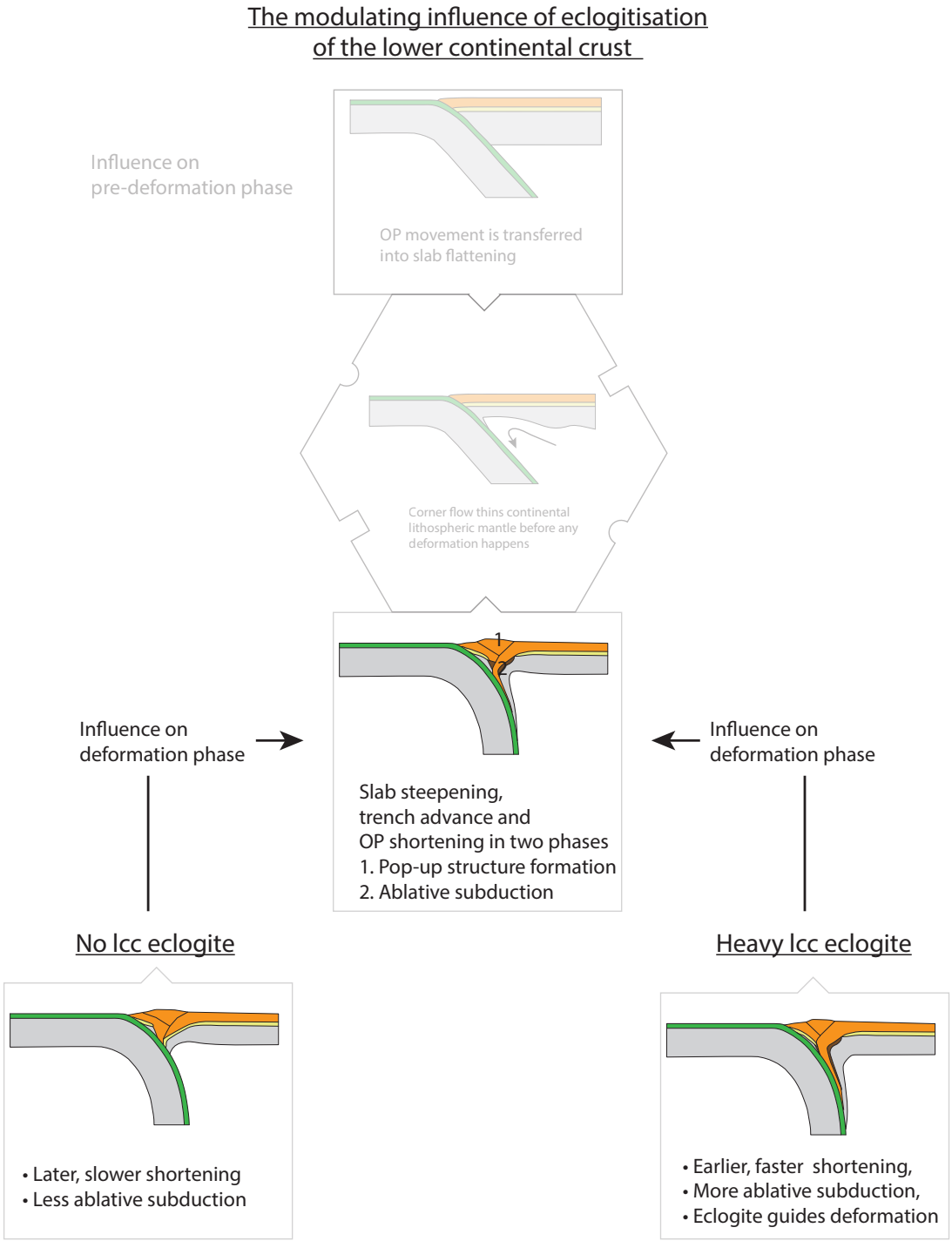

Figure 28: Figure showing the influence of lower crustal eclogitisation on the shortening phase of the models. Ablative subduction is the result of the force balance between push of the continent under the thickened arc, drag of the entrained hinterland crust in the subduction channel and positive buoyancy of the ablated material. The latter is enhanced (no eclogitisation) or reduced (heavy eclogite) by different types of lower crustal eclogitisation of the continent. Accordingly, no eclogitisation leads to delayed shortening with less ablative subduction, and high eclogite densities lead to earlier and faster ablative subduction. Furthermore the heavy eclogite is less dense than the surrounding mantle and induces and guides ablative subduction, while the other setups counteract ablative subduction.

not account for melting and melt migration, which probably has a significant influence on the upwards advection of the temperature field and could lead to temperatures allowing for pyroxenite formation in the continental lower crust. Therefore I chose to use the simplest setup possible and all phase transitions of the lower continental crust followed the P-T-space from Hacker (1996). Hence pyroxenite forms in the models at temperatures which are lower than we would expect in nature. The lower temperatures lead to higher viscosities, and possibly prohibit detachment of a negatively buoyant eclogite flake. Instead, the thrust slice attached to the eclogite flake is dragged downwards and crust is removed through ablative subduction. The relatively strong continental rheology additionally supports this behaviour.

The phase change temperatures and oversimplified temperature development of the subduction zone without melting, might thus possibly be the reason that delamination of heavy eclogite flakes can not be observed in the models. Nevertheless we can attest with our models, that eclogitisation and different lower crustal densities have an influence in the timing of shortening, and can induce deformation.

5.2.2 Extensional inheritance

The inheritance models show similar behaviour as the normal shortening models, and the main difference is of structural nature (Fig. 29). Shortening in the extended OP first leads to docking of the rifted block. Subsequently a first thick skinned thrust sheet starts to develop and thrusts under the docked block. However this first thrust sheet is not further used for ablative subduction, but a second thrust sheet forms further in the hinterland. Apparently the back-arc lithosphere is strongly weakened through corner flow, so that the push of the OP is transferred into the creation of a new thrust sheet, rather than ablation of the first one. The new thrust sheet is subsequently used as the main feeder of continental material into the subduction channel during ablative subduction. Hence the main difference between normal shortening models and shortening models with a pre-extension phase is the margin structure. Instead of a pop-up structure, a thrust stack forms after the docking of the rifted block.

5.3 The Influence of a weak lower continental crust

A weaker lower continental crust leads to earlier onset of shortening in models with contractional setting, and later rifting in models with extensional setting. Additionally a weaker lower crust leads to a bit more various structures in contractional models, with several anti-thetic faults in the pop-up structure.

All deformation in the overriding plate occurs only after the plate has been thinned and thus weakened through corner flow, as extensively described in the previous discussion chapters. Consequently the relationship that a weaker lower continental crust leads to earlier deformation in a contractional regime is straight forward. However, a weak lower crust leads also to delayed back-arc opening in an extensional regime. This, at first unexpected behaviour, is probably due to a prolonged phase of pure-shear dominated thinning of the continental crust before brittle

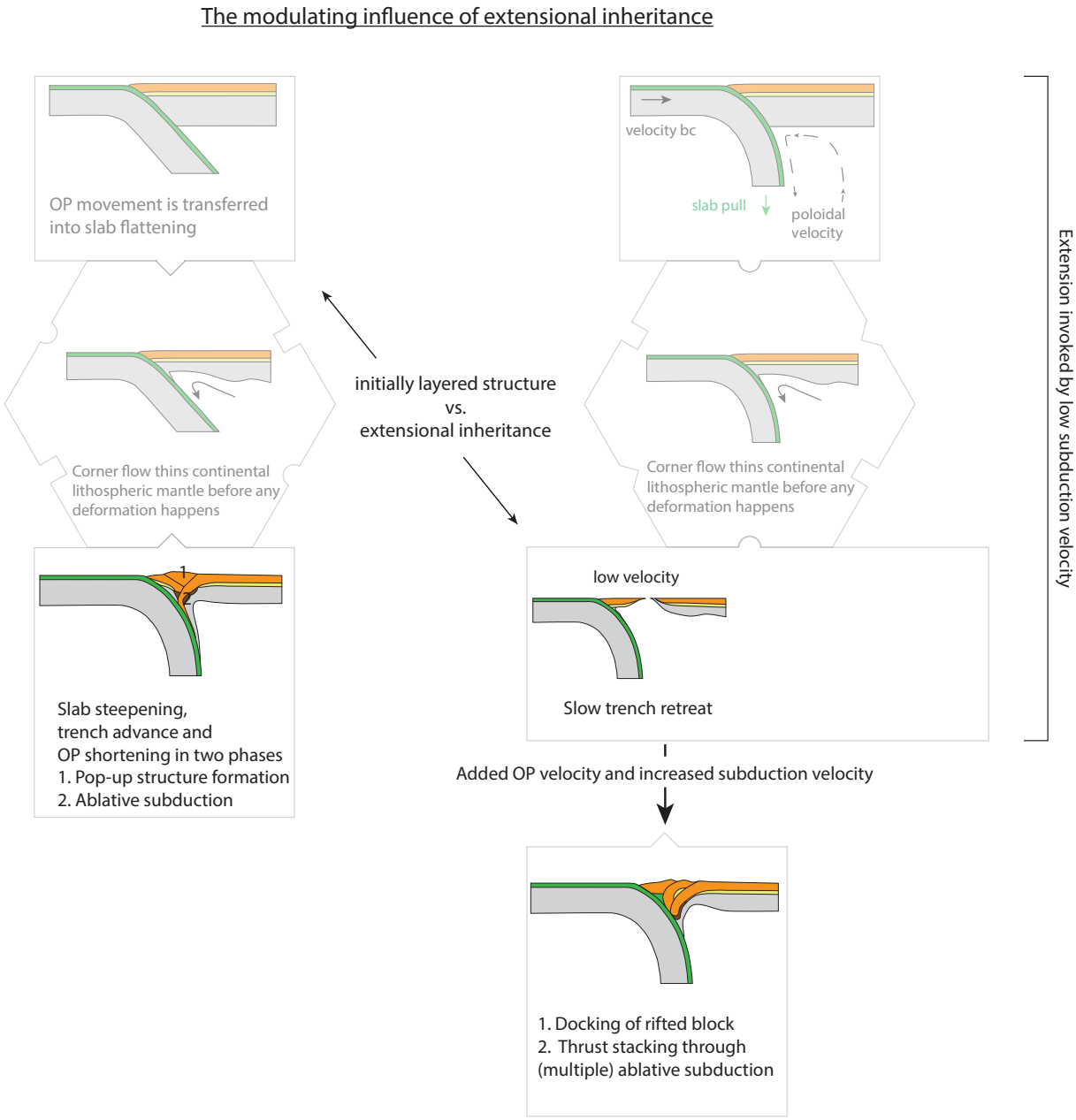

Figure 29: Figure showing the influence of extensional inheritance in a contractional setting. The left side is the same as Figure 27 and shows the structures that develop after shortening of an initially layered structure. The right side shows the development of the extensional inheritance and the structures after shortening of an extended margin. The main differences between both contractional model setups are of structural nature.

rupturing.

In all the models, the upper crust was modelled with a wet quartz flow law (Gleason and Tullis, 1995) scaled by the factor $f = 5$. To be consistent, the influence of a felsic (weak) lower crust was approximated with the same flow law. Other thermo-mechanical modelling results show, contrary to my results, that a weak (lower) continental crust can have a strong influence on the structural style of the models (e.g. Huismans and Beaumont, 2011, 2014). However, the weak (lower) crust is in their approach approximated by the same wet quartz flow law, but with a scaling factor of $f = 0.02$. Hence their weak crust is much weaker than my weak crust. It would be interesting and will be the next step, to investigate the deformation behaviour of my models with a very weak crust. The relationships concerning timing of deformation will probably be amplified, and more variational structures foundering in the weak lower crust will form.

5.4 Terrane accretion

The models including one or two intra-oceanic terranes show initially frontal terrane accretion at the margin, because the terrane is frictionally and viscously weak. This is in accordance with models by Tetreault and Buiter (2012) and Vogt and Gerya (2014), which also show, that weak terranes can accrete at the continental margin. Tetreault and Buiter (2012) furthermore demonstrate with a multi-layered terrane setup, that the detachment of terranes is focused into weak zones and terranes can also only be partially accreted.

Both publications focus on the parameters which lead to terrane accretion or subduction and do not show how the models develop further after accretion. My models show that the post-accretion behaviour is variable and determined by the subduction velocity, the overriding plate strain regime, the rheology of the subduction channel and possible subduction re-initiation (Fig. 30).

If the subduction velocity is low, the overriding plate strain regime is slightly extensional and the slab has a tendency to retreat. Nevertheless, the accreted material has the same rheological parameters as the subduction channel. Therefore a lot of accreted material is dragged down and a lively small scale convection develops under the arc. This enhances extension in the OP. Finally only a little piece of accreted terrane material remains at the margin.

If the subduction velocity is medium to high, the overriding plate strain regime is neutral and the subducting slab has a tendency to retain its position or even advance slightly. The combination of the slab's tendency to retain its position and the weak material, leads to downwards drag of the accreted material until nothing is left at the margin. At depth, the buoyant material injects plume-like into the continental lithospheric mantle, leading to gravitational instabilities of the continental lithospheric mantle. This is a very effective mechanism for thinning of the lithosphere. Furthermore this mechanism is probably a sufficient way to differentiate the (lower) crust through relamination as proposed by Hacker et al. (2015). Currie et al. (2007) show that a similar behaviour can be modelled by subduction of buoyant sediments.

The model with one terrane and a low subduction velocity shows that a low subduction velocity

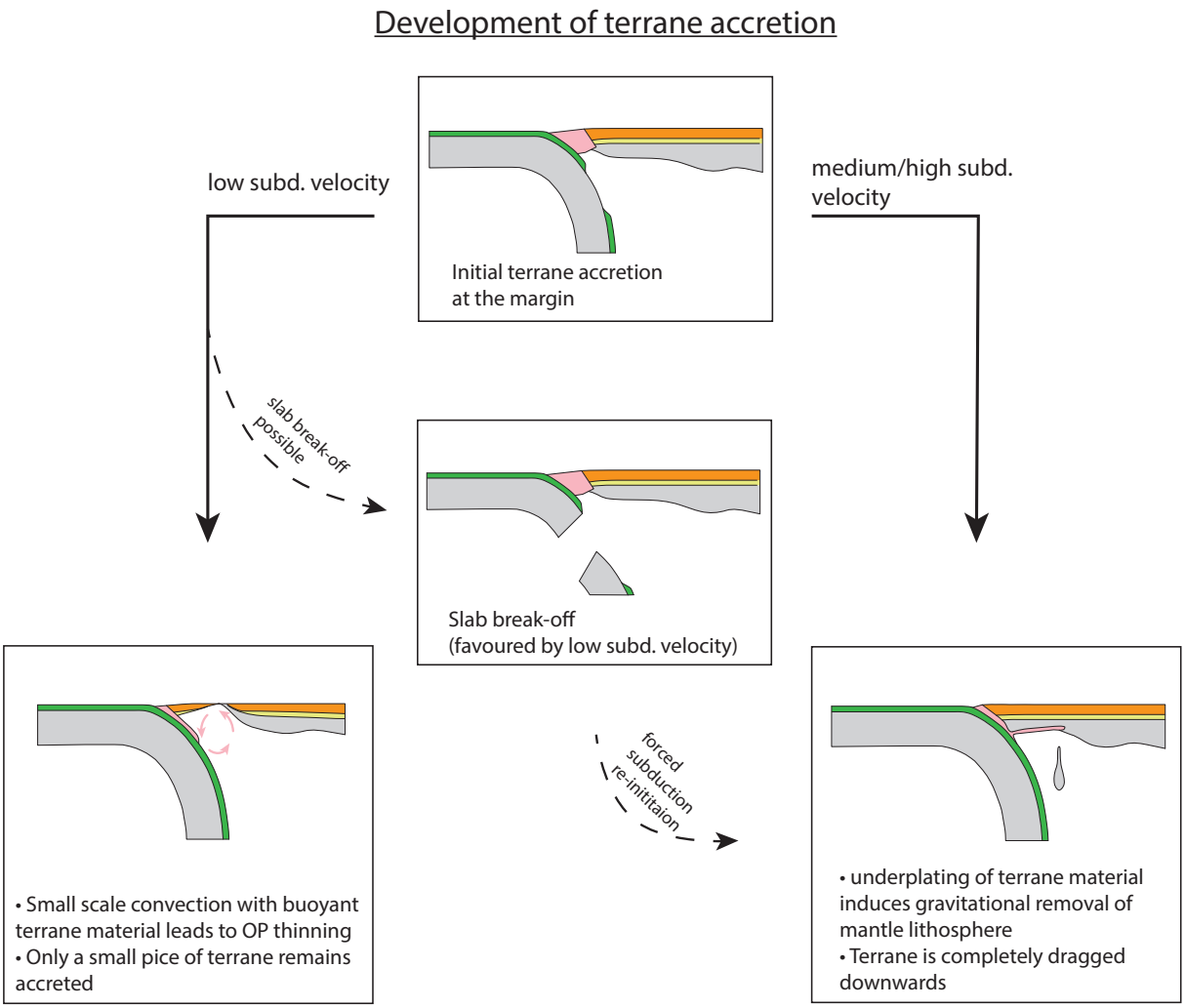

Figure 30: Figure showing the long term evolution of accreted terranes. Generally the terranes are frictionally and viscously weak enough to be accreted at the margin. However, this weakness leads in the post-accretion phase to its removal from the margin through subduction erosion. If the subduction velocity is low (3 cm/yr), the overriding plate has an extensional strain regime. The dragged down material builds up a small scale convection cell under the arc, which in turn enhances OP plate extension. Finally only a little piece of accreted material remains at the margin. A medium or high subduction velocity (5-7 cm/yr) leads to a neutral OP strain regime. This leads to plume-like injection and under-plating of the dragged down accreted material into the weak continental lithospheric mantle, until no accreted material is left at the margin. The under-plating induces gravitational instabilities of the weak mantle and is an efficient way to thin and differentiate the continental lithosphere. A similar behaviour can be created through forced subduction initiation after slab break-off.

can also lead to slab break-off after terrane accretion. Subsequent forced subduction re-initiation pushes the accreted material under the continental plate, and the model develops the same post-accretion behaviour as the models with higher subduction velocity. This is a nice example of how forced subduction initiation pushes into the continental margin, and shows additionally how weak the accreted material is in comparison to the continental crust. Vogt and Gerya (2014) also show a model, which includes slab break-off after terrane accretion. However their subduction model is driven by spontaneously moving plates without a velocity boundary condition and thus the subduction zone does not re-initiate after break-off.

Apparently, the interplay between the overriding plate strain regime and the rheology contrast between the subduction channel and the accreted material determines the post-accretion behaviour. In my models the accreted material has the same frictional rheology as the subduction channel, and always gets viscously dragged down. If the OP is in a tensional stress state, buoyant rise of the terrane material enhances continental break-up. If the OP is in a neutral or compressional stress state, the material is underplating and speeds up removal of the mantle lithosphere. The subduction velocity modifies the behaviour slightly, as the viscous drag is enhanced with higher subduction velocity. Note that the extensional OP strain regime is in the two presented models coupled to the subduction velocity. Hence the single influence of each of the parameters is not clear, and further modelling combining a higher subduction velocity with extension in the OP (e.g. through return flow) would be interesting.

5.5 Applicability and comparison of model results to nature

One of the main results of this thesis is that overriding plate strain is determined by the return flow efficiency and the overriding plate velocity. The subduction velocity modifies the system but is generally ruled out by the other two parameters. Note, however, that the interplay of far field forces and natural slab sinking rate is responsible in inducing slab retreat and thus return flow. The return flow intensity is in nature limited by the distance to the slab. Thus the return flow intensity can be translated into slab edge distance with the relationship that a long distance means little or no return flow. We find that return flow is necessary for efficient back-arc opening to occur. Hence only areas in subduction zones which are near slab edges can retreat efficiently.

Positive overriding plate velocity is the only factor inducing shortening of the overriding plate in our models. However, the model results with 100 % return flow and 1 cm/yr OP movement show that return flow can compensate the OP velocity, and induce a neutral OP strain regime. Hence slab edge distance and thus the possibility for return flow in combination with the OP velocity are the main factors inducing deformation of the overriding plate.

Statistical analyses of the subduction zones on earth by Schellart (2008) show that the biggest statistical significance for OP strain is the slab-edge distance in combination with the OP velocity (as reviewed in Chapter 2.4). This is nicely displayed by the Andes and the Japanese subduction zones, which show OP shortening in the centre of their wide subduction zones. Schellart (2008) also shows that subduction velocity has no significant influence on the overriding plate strain

regime.

Hence with our absolute plate motion models, we could reproduce first order factors on earth which are responsible for the deformation of the OP in subduction settings. However, as we are using 2D models of forced subduction, the precise quantification of the different velocities is subject to limitations, as discussed in the last sections.

Accordingly a detailed comparison of structures created in the models and found on Earth is not possible without further exploration of the parameter space. A proposal of parameters that should be further explored and comparison of first order similarities is given in the next paragraphs. In Chapter 2.2, the structures of subduction zones as seen in seismological images were reviewed. Slabs show different dips at depth, and the interaction with the lower mantle can be quite variable and related to the viscosity contrast between lower and upper mantle (Ringwood, 1991). In my models, the artificial transition zone of lithospheric material at 500 km depth decouples the subducting slab from anything below. Hence the dip of the slab is driven by slab pull, and all models show an almost vertical slab at depth. Only a positive OP velocity can induce a flatter slab in the pre-deformation phase. However, the flattened slab swings back into a vertical position during the deformation phase, which accelerates shortening in the OP plate. This mechanism is probably different in nature, when the the slab interacts with the lower mantle. High lower mantle viscosity could lead to slab anchoring in the lower mantle, slowing down OP shortening.

The seismic tomography cross section through the contractional central Japanese subduction zone (Fig. 4 (B)(15)) shows a relatively shallow dipping slab, which is laying down in the lower mantel transition zone. Hence slab interaction with the lower mantle transition zone might indeed counter-act swing-back of the slab during shortening of the OP. Slab interaction with the lower mantle is also important for slab roll-back as slab-anchoring might counteract the backwards movement of the trench. Hence our model results have to be seen in light of these considerations and it will be useful to compare our model results with future models including a lower mantle.

Figure 5 shows that subduction zones have diverse structures in the uppermost 200 km, ranging from flat slab subduction (e.g. Central Mexico; Fig. 5g) to relatively steep dipping slabs (e.g. Central America, Fig. 5f). Espurt et al. (2008) show, with geodynamic analogue models, that flat subduction is only possible when a buoyant oceanic or continental plateau is subducted, as for instance the Carnegie and Iquique ridges at the Chilean subduction zone.

In all my models, the general geometries at the plate interface are the same with a steeply dipping, almost vertical slab. Flat subduction is never created. The thermal setup of the slab is thus probably too cold to induce buoyant rise and flat slab subduction. However, the models with terranes did not show any significant change in slab dip either. Flat slab subduction was not produced by models of terrane subduction by Tetreault and Buiter (2012) and Vogt and Gerya (2014). Fig. 13 shows that the slab is comparably strong and stiff, and keeps the structure inherited from the subduction interface also at depth. Hence a buoyant slab might not be enough to induce flat slab subduction, but the slab also needs to be considerably weakened. Possible

weakening mechanisms can be metamorphic reactions (e.g. eclogitisation) and (coupled) fluid flow (e.g. Faccenda et al., 2012). This shows that the rheology of the slab is in my subduction models possibly too homogeneous and strong, in comparison to what would be expected in nature. Integration of fluid flow induced weakening would be a useful next step to gain a more realistic slab rheology.

The models with an extending OP show that corner flow can create a weak lithosphere in the vicinity of the slab. This weak area focusses subsequent deformation, and leads to rupture of the continental crust and rifting of a 150 to 200 km wide contentinal block. The distance between spreading centre and the trench subsequently grows and is also dependent on the OP movement. The distances between trench and active back-arc spreading-centres in the Tonga-Kermadec, Mariana, Ryukyu and Tonga subduction zones range between 100 to 400 km (see Fig. 1 B, Fig. 2). This is approximately the same as produced in the models. Hence it is most likely that corner flow induced weakening occurs on earth and is an important factor for slab rollback and back-arc spreading. The fact that above-named subduction zones are ocean-ocean subduction zones additionally shows that corner flow weakening is important, independent of the subduction setting. However, this relationship needs further and more detailed investigation.

A contractional OP strain regime is in my models dominated by ablative subduction. This restricts the width of the resulting orogen to <250 km. The style can be modified by extensional inheritance (two thrust sheets), and the timing of deformation is modified by eclogitisation of the lower continental crust. Yet those factors do not influence the width of the orogen. Accordingly, my models never produced a wide, plateau-like orogen, like the central Andes with a lateral extent of up to 600 km. These results are in contradiction to modelling results by Pope and Willett (1998), who propose that ablative subduction is the driving force for crustal thickening creating an Andes-style mountain belt. However, their model is driven by a S-point approach and not fully dynamic. So do they for instance not account for a frictional subduction interface. This has shown to be an important factor, as discussed in chapter 5.1.3, and a reduction of the friction in the subduction channel is reasonable and might lead to a wider orogen.

The fast, ablative subduction drags down the temperature contour lines, and a relatively cold orogen forms with heat flow values below the initial values ($< \sim 50\,\mathrm{mW/m^2}$). However, heat flow measurements show an average surface heat flow of 75 ± 15 for the plateau region of the Central Andes (Currie and Hyndman, 2006). Geochemical signatures of Cordilleran arc magmas show that the majority of magma is derived through melting of the overriding continental crust (Ducea and Barton, 2007). This requires high temperatures at the thickened continental Moho and supports the high heat flow values. For future modelling studies, it would be interesting to investigate, whether reduced friction in the subduction channel is enough to slow down shortening to allow the thickened crust to radioactively heat up, or whether magmatism and associated temperature advection processes are necessary to match heat flow measurements and build a wide orogen. This could also shed light on whether the pyroxenite formation of lower crustal restite and their delamination are necessary to build an Andean style mountain range. Additionally the influence of a weaker crust needs to be explored (as discussed in chapter 5.3).

Geological cross sections through active or formerly active subduction margins at the Western coast of North America, show that terrane accretion is a viable mechanism for crustal thickening and that accreted terranes can stay at the margin (Fig. 9; Monger et al., 1982; Hammer et al., 2010). In my models, terrane accretion is also happening, but subsequent subduction removes the terrane material through downwards drag in the subduction channel. As the downward drag is dependent on the friction of the subduction channel, further models with a weaker subduction channel might be interesting here as well. Additionally a stratified terrane rheology, as used by Tetreault and Buiter (2012), might help to detach the terrane in a pre-defined detachment zone and leave it else frictionally strong.

The last three paragraphs show that the shortening mode in our models needs to be further explored until a comparison with real structures is possible. Thereby friction in the subduction channel, coupling with the lower mantle, rheology of the overriding crust and fluid/magma flow coupling are probably the most important factors, and need to be addressed in the next modelling phase.

6 Conclusion

Through numerical ocean-continent subduction models, I could extract a modular set of parameters whose combinations determine the overriding plate strain regime in subduction zones. The main determining parameters are return flow, overriding plate velocity and subduction velocity. Return flow leads to trench retreat and back-arc opening, and thus an extensional OP strain regime. A similar behaviour can be invoked by overriding plate movement away from the trench. Overriding plate movement towards the trench is the only possibility to induce overriding plate shortening, and only when the movement rules out trench retreat through return flow. All deformation of the OP is preceded by corner flow induced removal of the lithospheric mantle of the overriding plate. Hence corner flow induced thinning is the link between the different factors determining OP deformation. As subduction of the oceanic plate drives corner flow, the subduction velocity has a timing influence on the OP deformation. Modelling results from Schellart et al. (2007) show that the return flow intensity is decreasing with increasing slab edge distance in a subduction zone. If one applies this relationship to our model results, we find that the centres of wide subduction zones are less prone to trench retreat, while small subduction zones or subduction segments near slab edges are more likely to retreat. Additionally, if the OP moves towards the trench, centres of wide subduction zones are more likely to shorten than small subduction zones or segments near slab edges. This coincides with statistical a analysis of subduction zones on Earth (Schellart, 2008), and shows that the models can reproduce the first order features of subduction zones on earth.

A first attempt to compare my extending models to nature shows that they produce reasonable results and that corner flow weakening is probably also an important factor on earth.

All the models showing shortening of the overriding plate are strongly dominated by ablative subduction, and the structures do not properly reproduce orogenic characteristics as for instance found in the Andes. Models investigating the influence of lower continental crustal metamorphism on mountain building show that a heavy, metamorphosed lower crust can induce, and has influence on, the timing of shortening. However, the influence is overprinted by ablative subduction, and the models can neither validate nor reject the idea that delamination of a heavy lower crustal eclogite is the driver for orogenesis in Cordilleran systems, as proposed by DeCelles et al. (2009). Models with an extensional pre-shortening phase are also dominated by ablative subduction, and show only little structural differences. Hence, further modelling is necessary to produce more realistic shortening structures, and I propose that the most important factors to investigate are friction in the subduction channel, coupled fluid flow and interactions of the slab with the lower mantle.

The lower continental crust is still enigmatic in its composition and rheology (Hacker et al., 2015). A first attempt to investigate the influence of a weaker lower crust has shown that a weaker lower continental crust leads to earlier shortening, but later extension of the OP. However, the structures are very similar, and a proper investigation with even weaker continental rheologies is necessary.

Additionally I investigated the long term evolution of terrane accretion at a subduction margin. I could reproduce frontal accretion of a weak terrane, as shown by Vogt and Gerya (2014), but further subduction viscously removes all the accreted material. This in turn accelerates removal of the lithospheric mantle of the overriding plate. Here as well the high friction in the subduction channel dominated the system. Further studies should focus on the rheological difference between the accreted material and the subduction channel.

References

Arcay, D., Doin, M. P., Tric, E., Bousquet, R., and Capitani, C. de (2006). Overriding plate thinning in subduction zones: Localized convection induced by slab dehydration. *Geochemistry Geophysics Geosystems* 7.

Arcay, D., Tric, E., and Doin, M. P. (2005). Numerical simulations of subduction zones - Effect of slab dehydration on the mantle wedge dynamics. *Physics of the Earth and Planetary Interiors* 149, pp. 133–153.

Argus, D. F. and Gordon, R. G. (1991). No-Net-Rotation Model of Current Plate Velocities Incorporating Plate Motion Model Nuvel-1. *Geophysical Research Letters* 18, pp. 2039–2042.

Arriagada, C., Roperch, P., Mpodozis, C., and Cobbold, P. R. (2008). Paleogene building of the Bolivian Orocline: Tectonic restoration of the central Andes in 2-D map view. *Tectonics* 27.

Beaumont, C., Nguyen, M. H., Jamieson, R. A.., and Ellis, S. (2006). Crustal flow modes in large hot orogens. *Geological Society, London, Special Publications* 268, pp. 91–145.

Bird, P. (2003). An updated digital model of plate boundaries. *Geochemistry Geophysics Geosystems* 4.

Bostock, M. G. (2013). The Moho in subduction zones. *Tectonophysics* 609, pp. 547–557.

Braun, J., Thieulot, C., Fullsack, P., DeKool, M., Beaumont, C., and Huismans, R. (2008). DOUAR: A new three-dimensional creeping flow numerical model for the solution of geological problems. *Physics of the Earth and Planetary Interiors* 171, pp. 76–91.

Buiter, S. J. H., Govers, R., and Wortel, M. J. R. (2001). A modelling study of vertical surface displacements at convergent plate margins. *Geophysical Journal International* 147, pp. 415–427.

Butler, J. P., Beaumont, C., and Jamieson, R. A. (2013). The Alps 1: A working geodynamic model for burial and exhumation of (ultra)high-pressure rocks in Alpine-type orogens. *Earth and Planetary Science Letters* 377, pp. 114–131.

Chudinovskikh, L. and Boehler, R. (2001). High-pressure polymorphs of olivine and the 660-km seismic discontinuity. *Nature* 411, pp. 574–577.

Cruciani, C., Carminati, E., and Doglioni, C. (2005). Slab dip vs. lithosphere age: No direct function. *Earth and Planetary Science Letters* 238, pp. 298–310.

Currie, C. A., Beaumont, C., and Huismans, R. S. (2007). The fate of subducted sediments: A case for backarc intrusion and underplating. *Geology* 35, pp. 1111–1114.

Currie, C. A., Huismans, R. S., and Beaumont, C. (2008). Thinning of continental backarc lithosphere by flow-induced gravitational instability. *Earth and Planetary Science Letters* 269, pp. 435–446.

Currie, C. A. and Hyndman, R. D. (2006). The thermal structure of subduction zone back arcs. *Journal of Geophysical Research-Solid Earth* 111.

DeCelles, P. G., Ducea, M. N., Kapp, P., and Zandt, G. (2009). Cyclicity in Cordilleran orogenic systems. *Nature Geoscience* 2, pp. 251–257.

DeMets, C., Gordon, R. G., Argus, D. F., and Stein, S. (1994). Effect of Recent Revisions to the Geomagnetic Reversal Time-Scale on Estimates of Current Plate Motions. *Geophysical Research Letters* 21, pp. 2191–2194.

Dewey, J. F. and Bird, J. M. (1970). Mountain Belts and New Global Tectonics. *Journal of Geophysical Research* 75, pp. 2625–&.

Ducea, M. N. and Barton, M. D. (2007). Igniting flare-up events in Cordilleran arcs. *Geology* 35, pp. 1047–1050.

England, P. C. and Thompson, A. B. (1984). Pressure Temperature Time Paths of Regional Metamorphism .1. Heat-Transfer during the Evolution of Regions of Thickened Continental-Crust. *Journal of Petrology* 25, pp. 894–928.

Espurt, N., Funiciello, F., Martinod, J., Guillaume, B., Regard, V., Faccenna, C., and Brusset, S. (2008). Flat subduction dynamics and deformation of the South American plate: Insights from analog modeling. *Tectonics* 27.

Faccenda, M. (2014). Water in the slab: A trilogy. *Tectonophysics* 614, pp. 1–30.

Faccenda, M., Gerya, T. V., and Burlini, L. (2009). Deep slab hydration induced by bending-related variations in tectonic pressure. *Nature Geoscience* 2, pp. 790–793.

Faccenda, M., Gerya, T. V., Mancktelow, N. S., and Moresi, L. (2012). Fluid flow during slab unbending and dehydration: Implications for intermediate-depth seismicity, slab weakening and deep water recycling. *Geochemistry Geophysics Geosystems* 13.

Ferris, A., Abers, G. A., Christensen, D. H., and Veenstra, E. (2003). High resolution image of the subducted Pacific (?) plate beneath central Alaska, 50-150 km depth. *Earth and Planetary Science Letters* 214, pp. 575–588.

Fischer, K. M., Ford, H. A., Abt, D. L., and Rychert, C. A. (2010). The Lithosphere-Asthenosphere Boundary. *Annual Review of Earth and Planetary Sciences, Vol 38* 38, pp. 551–575.

Forsyth, D. and Uyeda, S. (1975). Relative Importance of Driving Forces of Plate Motion. *Geophysical Journal of the Royal Astronomical Society* 43, pp. 163–200.

Fullsack, P. (1995). An arbitrary Lagrangian-Eulerian formulation for creeping flows and its application in tectonic models. *Geophysical Journal Interational* 120, pp. 1–23.

Funiciello, F., Faccenna, C., and Giardini, D. (2004). Role of lateral mantle flow in the evolution of subduction systems: insights from laboratory experiments. *Geophysical Journal International* 157, pp. 1393–1406.

Funiciello, F., Faccenna, C., Giardini, D., and Regenauer-Lieb, K. (2003). Dynamics of retreating slabs: 2. Insights from three-dimensional laboratory experiments. *Journal of Geophysical Research-Solid Earth* 108.

Gerya, T. V. (2010). *Numerical Geodynamic Modelling*. Cambridge University Press.

Gerya, T. V. and Yuen, D. A. (2007). Robust characteristics method for modelling multiphase visco-elasto-plastic thermo-mechanical problems. *Physics of the Earth and Planetary Interiors* 163. 210vh Times Cited:98 Cited References Count:45, pp. 83–105.

Gleason, G. C. and Tullis, J. (1995). A Flow Law for Dislocation Creep of Quartz Aggregates Determined with the Molten-Salt Cell. *Tectonophysics* 247, pp. 1–23.

Gripp, A. E. and Gordon, R. G. (1990). Current Plate Velocities Relative to the Hotspots Incorporating the Nuvel-1 Global Plate Motion Model. *Geophysical Research Letters* 17, pp. 1109–1112.

– (2002). Young tracks of hotspots and current plate velocities. *Geophysical Journal International* 150, pp. 321–361.

Grool, A. (2012). Determining important factors in the occurrence of subduction rollback through numerical modelling. MA thesis. University of Bergen.

Hacker, B. R., Kelemen, P. B., and Behn, M. D. (2011). Differentiation of the continental crust by relamination. *Earth and Planetary Science Letters* 307, pp. 501–516.

– (2015). Continental Lower Crust. *Annual Review of Earth and Planetary Sciences* 43.

Hacker, Bradley R. (1996). Eclogite formation and the rheology, buoyancy, seismicity, and H2O content of oceanic crust. 96, pp. 337–346.

Hammer, P. T. C., Clowes, R. M., Cook, F. A., Velden, A. J. van der, and Vasudevan, K. (2010). The Lithoprobe trans-continental lithospheric cross sections: imaging the internal structure of the North American continent. *Canadian Journal of Earth Sciences* 47, pp. 821–857.

Hampel, A. and Pfiffner, A. (2006). Relative importance of trenchward upper plate motion and friction along the plate interface for the topographic evolution of subduction-related mountain belts. *Geological Society, London, Special Publications* 253, pp. 105–115.

Hansen, R. T. J., Bostock, M. G., and Christensen, N. I. (2012). Nature of the low velocity zone in Cascadia from receiver function waveform inversion. *Earth and Planetary Science Letters* 337, pp. 25–38.

Hetényi, G., Godard, V., Cattin, R., and Connolly, J. A. D. (2011). Incorporating metamorphism in geodynamic models: the mass conservation problem. *Geophysical Journal International* 186, pp. 6–10.

Heuret, A. and Lallemand, S. (2005). Plate motions, slab dynamics and back-arc deformation. *Physics of the Earth and Planetary Interiors* 149, pp. 31–51.

Hirth, G., Evans, R. L., and Chave, A. D. (2000). Comparison of continental and oceanic mantle electrical conductivity: Is the Archean lithosphere dry? *Geochemistry Geophysics Geosystems* 1.

Hirth, G. and Kohlstedt, D. L. (1996). Water in the oceanic upper mantle: Implications for rheology, melt extraction and the evolution of the lithosphere. *Earth and Planetary Science Letters* 144, pp. 93–108.

Huang, Y., Chubakov, V., Mantovani, F., Rudnick, R. L., and McDonough, W. F. (2013). A reference Earth model for the heat-producing elements and associated geoneutrino flux. *Geochemistry Geophysics Geosystems* 14, pp. 2003–2029.

Huismans, R. S. and Beaumont, C. (2003). Symmetric and asymmetric lithospheric extension: Relative effects of frictional-plastic and viscous strain softening. *Journal of Geophysical Research-Solid Earth* 108.

– (2011). Depth-dependent extension, two-stage breakup and cratonic underplating at rifted margins. *Nature* 473, pp. 74–8.

Huismans, R. S. and Beaumont, C. (2014). Rifted continental margins: The case for depth-dependent extension. *Earth and Planetary Science Letters* 407, pp. 148–162.

Hyndman, R. D., Currie, C. A., and Mazzotti, S. P. (2005). Subduction zone backarcs, mobile belts, and orogenic heat. *GSA Today* 15, pp. 4–10.

Jarrard, R. D. (1986). Relations among Subduction Parameters. *Reviews of Geophysics* 24, pp. 217–284.

Jones, D. L., Silberling, N. J., and Hillhouse, J. (1977). Wrangellia - Displaced Terrane in Northwestern North-America. *Canadian Journal of Earth Sciences* 14, pp. 2565–2577.

Karato, S. and Wu, P. (1993). Rheology of the Upper Mantle - a Synthesis. *Science* 260, pp. 771–778.

Katsura, T., Yoneda, A., Yamazaki, D., Yoshino, T., and Ito, E. (2010). Adiabatic temperature profile in the mantle. *Physics of the Earth and Planetary Interiors* 183, pp. 212–218.

Kim, Y.H., Miller, M. S., Pearce, F., and Clayton, R. W. (2012). Seismic imaging of the Cocos plate subduction zone system in central Mexico. *Geochemistry, Geophysics, Geosystems* 13.

Kreemer, C., Holt, W. E., and Haines, A. J. (2003). An integrated global model of present-day plate motions and plate boundary deformation. *Geophysical Journal International* 154, pp. 8–34.

Li, C., Hilst, R. D. van der, Engdahl, E. R., and Burdick, S. (2008). A new global model for P wave speed variations in Earth's mantle. *Geochemistry Geophysics Geosystems* 9.

Mackwell, S. J., Zimmerman, M. E., and Kohlstedt, D. L. (1998). High-temperature deformation of dry diabase with application to tectonics on Venus. *Journal of Geophysical Research-Solid Earth* 103, pp. 975–984.

Mann, P. and Taira, A. (2004). Global tectonic significance of the Solomon Islands and Ontong Java Plateau convergent zone. *Tectonophysics* 389, pp. 137–190.

McKenzie, D. P. (1969). Speculations on Consequences and Causes of Plate Motions. *Geophysical Journal of the Royal Astronomical Society* 18, pp. 1–32.

– (1978). Some Remarks on Development of Sedimentary Basins. *Earth and Planetary Science Letters* 40, pp. 25–32.

Minear, J. W. and Toksöz, M. N. (1970). Thermal Regime of a Downgoing Slab and New Global Tectonics. *Journal of Geophysical Research* 75, pp. 1397–1419.

Monger, J. W. H., Price, R. A., and Tempelmankluit, D. J. (1982). Tectonic Accretion and the Origin of the 2 Major Metamorphic and Plutonic Welts in the Canadian Cordillera. *Geology* 10, pp. 70–75.

Müller, R. D., Royer, J. Y., and Lawver, L. A. (1993). Revised Plate Motions Relative to the Hotspots from Combined Atlantic and Indian-Ocean Hotspot Tracks. *Geology* 21, pp. 275–278.

Müller, R. D., Sdrolias, M., Gaina, C., and Roest, W. R. (2008). Age, spreading rates, and spreading asymmetry of the world's ocean crust. *Geochemistry Geophysics Geosystems* 9.

Oncken, O., Hindle, D., Kley, J., Elger, K., Victor, P., and Schemmann, K. (2006). Deformation of the central Andean upper plate system - Facts, fiction, and constraints for plateau models. *The Andes*. Springer Berlin Heidelberg, pp. 3–27.

O'Neill, C., Muller, D., and Steinberger, B. (2005). On the uncertainties in hot spot reconstructions and the significance of moving hot spot reference frames. *Geochemistry Geophysics Geosystems* 6.

Pearce, F. D., Rondenay, S., Sachpazi, M., Charalampakis, M., and Royden, L. H. (2012). Seismic investigation of the transition from continental to oceanic subduction along the western Hellenic Subduction Zone. *Journal of Geophysical Research* 117.

Pelletier, J. D., DeCelles, P. G., and Zandt, G. (2010). Relationships among climate, erosion, topography, and delamination in the Andes: A numerical modeling investigation. *Geology* 38, pp. 259–262.

Pope, D. C. and Willett, S. D. (1998). Thermal-mechanical model for crustal thickening in the central Andes driven by ablative subduction. *Geology* 26, pp. 511–514.

Rapp, R. P. and Watson, E. B. (1995). Dehydration Melting of Metabasalt at 8-32-Kbar - Implications for Continental Growth and Crust-Mantle Recycling. *Journal of Petrology* 36, pp. 891–931.

Ringwood, A. E. (1991). Phase-Transformations and Their Bearing on the Constitution and Dynamics of the Mantle. *Geochimica Et Cosmochimica Acta* 55, pp. 2083–2110.

Rondenay, S., Abers, G. A., and Van Keken, P. E. (2008). Seismic imaging of subduction zone metamorphism. *Geology* 36, pp. 275–278.

Rudnick, R. L. and Fountain, D. M. (1995). Nature and Composition of the Continental-Crust - a Lower Crustal Perspective. *Reviews of Geophysics* 33, pp. 267–309.

Saleeby, J., Ducea, M., and Clemens-Knott, D. (2003). Production and loss of high-density batholithic root, southern Sierra Nevada, California. *Tectonics* 22.

Schellart, W. P. (2008). Overriding plate shortening and extension above subduction zones: A parametric study to explain formation of the Andes Mountains. *Geological Society of America Bulletin* 120, pp. 1441–1454.

Schellart, W. P., Freeman, J., Stegman, D. R., Moresi, L., and May, D. (2007). Evolution and diversity of subduction zones controlled by slab width. *Nature* 446, pp. 308–311.

Schellart, W. P., Stegman, D. R., Farrington, R. J., and Moresi, L. (2011). Influence of lateral slab edge distance on plate velocity, trench velocity, and subduction partitioning. *Journal of Geophysical Research-Solid Earth* 116.

Schellart, W. P., Stegman, D. R., and Freeman, J. (2008). Global trench migration velocities and slab migration induced upper mantle volume fluxes: Constraints to find an Earth reference frame based on minimizing viscous dissipation. *Earth-Science Reviews* 88, pp. 118–144.

Sibson, R. H. (1990). Conditions for fault-valve behaviour. *Geological Society, London, Special Publications* 54, pp. 15–28.

Sleep, N. H. (2005). Evolution of the continental lithosphere. *Annual Review of Earth and Planetary Sciences* 33, pp. 369–393.

Sobolev, S. V. and Babeyko, A. Y. (2005). What drives orogeny in the Andes? *Geology* 33, pp. 617–620.

Stadler, G., Gurnis, M., Burstedde, C., Wilcox, L. C., Alisic, L., and Ghattas, O. (2010). The Dynamics of Plate Tectonics and Mantle Flow: From Local to Global Scales. *Science* 329, pp. 1033–1038.

Stegman, D. R., Farrington, R., Capitanio, F. A., and Schellart, W. P. (2010). A regime diagram for subduction styles from 3-D numerical models of free subduction. *Tectonophysics* 483, pp. 29–45.

Stein, C. A. and Stein, S. (1992). A Model for the Global Variation in Oceanic Depth and Heat-Flow with Lithospheric Age. *Nature* 359, pp. 123–129.

Stern, R. J. (2004). Subduction initiation: spontaneous and induced. *Earth and Planetary Science Letters* 226, pp. 275–292.

Tao, W. C. and O'Connell, R. J. (1992). Ablative Subduction - a 2-Sided Alternative to the Conventional Subduction Model. *Journal of Geophysical Research-Solid Earth* 97, pp. 8877–8904.

Tetreault, J. L. and Buiter, S. J. H. (2012). Geodynamic models of terrane accretion: Testing the fate of island arcs, oceanic plateaus, and continental fragments in subduction zones. *Journal of Geophysical Research-Solid Earth* 117.

– (2014). Future accreted terranes: a compilation of island arcs, oceanic plateaus, submarine ridges, seamounts, and continental fragments. *Solid Earth* 5, pp. 1243–1275.

Thieulot, C. (2011). FANTOM: Two- and three-dimensional numerical modelling of creeping flows for the solution of geological problems. *Physics of the Earth and Planetary Interiors* 188, pp. 47–68.

Vogt, K. and Gerya, T. V. (2014). From oceanic plateaus to allochthonous terranes: Numerical modelling. *Gondwana Research* 25, pp. 494–508.

Warren, C. J., Beaumont, C., and Jamieson, R. A. (2008). Formation and exhumation of ultra-high-pressure rocks during continental collision: Role of detachment in the subduction channel. *Geochemistry Geophysics Geosystems* 9.

Wessel, P., Harada, Y., and Kroenke, L. W. (2006). Toward a self-consistent, high-resolution absolute plate motion model for the Pacific. *Geochemistry Geophysics Geosystems* 7.

White, R. S., Mckenzie, D., and Onions, R. K. (1992). Oceanic Crustal Thickness from Seismic Measurements and Rare-Earth Element Inversions. *Journal of Geophysical Research-Solid Earth* 97, pp. 19683–19715.

Wolf, M. B. and Wyllie, P. J. (1993). Garnet Growth during Amphibolite Anatexis - Implications of a Garnetiferous Restite. *Journal of Geology* 101, pp. 357–373.